

THE DIVERSITY OF VARIATIONS IN THE SPECTRA OF TYPE IA
SUPERNOVAE

A Thesis

by

ANDREW JAMES WAGERS

Submitted to the Office of Graduate Studies of
Texas A&M University
in partial fulfillment of the requirements for the degree of

DOCTOR OF PHILOSOPHY

August 2012

Major Subject: Physics

THE DIVERSITY OF VARIATIONS IN THE SPECTRA OF TYPE IA
SUPERNOVAE

A Thesis

by

ANDREW JAMES WAGERS

Submitted to the Office of Graduate Studies of
Texas A&M University
in partial fulfillment of the requirements for the degree of

DOCTOR OF PHILOSOPHY

Approved by:

Chair of Committee,	Lifan Wang
Committee Members,	Nicholas Suntzeff
	George Kattawar
	Sean McDeavitt
Head of Department,	George R. Welch

August 2012

Major Subject: Physics

ABSTRACT

The Diversity of Variations in the Spectra of Type Ia Supernovae. (August 2012)

Andrew James Wagers, B.A., Berea College; M.S., Stephen F. Austin State

University

Chair of Advisory Committee: Dr. Lifan Wang

Type Ia supernovae (SNe Ia) are currently the best probe of the expansion history of the universe. Their usefulness is due chiefly to their uniformity between supernovae (SNe). However, there are some slight variations amongst SNe that have yet to be understood and accounted for. The goal of this work is to uncover relationships between the spectral features and the light curve decline rate, Δm_{15} . Wavelet decomposition has been used to develop a new spectral index to measure spectral line strengths independent of the continuum and easily corrected for noise. This new method yields consistent results without the arbitrary uncertainties introduced by current methods and is particularly useful for spectra which do not have a clearly defined continuum. These techniques are applied to SN Ia spectra and correlations are found between the spectral features and light curve decline rate.

The wavelet spectral indexes are used to measure the evolution of spectral features which are characterized by 3 or 4 parameters for the most complicated evolution. The three absorption features studied here are associated with sulfur and silicon and all show a transition in strength between 1 to 2 weeks after B-band maximum. Pearson correlation coefficients between spectral features and Δm_{15} are found to be significant within a week of maximum brightness and 3 to 4 weeks post-maximum. These correlations are used to determine the principal components at each epoch among the set of SN spectra in this work. The variation contained in the first principal component (PC1) is found to be greater than 60% to 70% for most epochs

and reaching as high as 80% to 90% for epochs with the highest correlations. The same first principal component can be used to relate spectral feature strengths to the decline rate. These relations were used to estimate a SN light curve decline rate from a set of spectra taken over the course of the explosion, from a single spectrum, or from even a single spectral feature. These relationships could be used for future surveys to estimate spectral characteristics from light curve data, such as photometric redshift.

DEDICATION

This work is dedicated to my beautiful, loving, and patient wife, Kari. She encouraged me when I was discouraged, been my support when I needed it most, and pushed me when I thought I could do no more. Kari, you are a crown to your husband.

I also dedicate this work to my faithful son, Dillon, who has had to put up with many days and hours where Daddy was chained to his computer and not able to fight off evil knights and dragons. The completion of this work will hopefully inspire many new adventures.

ACKNOWLEDGMENTS

This project was initially given to me by Lifan Wang whom I would like to thank for direction, guidance, and the opportunity to work on this project. Without your guidance none of this would have been possible. I would also like to thank Steve Asztalos as a great help as I began this work. Others who have given helpful and encouraging feedback are Kevin Kriscuinus and Nicholas B. Suntzeff. I would also like to thank those of you who having willingly served on my committee: Lifan Wang, Nicholas B. Suntzeff, George W. Kattawar, and Sean McDeavitt.

Chapter 2 of this work was previously published as Wagers et al. (2010) and is used with the permission of the Astrophysical Journal.

TABLE OF CONTENTS

	Page
ABSTRACT	iii
DEDICATION	v
ACKNOWLEDGMENTS	vi
TABLE OF CONTENTS	vii
LIST OF TABLES	ix
LIST OF FIGURES	x
1. INTRODUCTION	1
1.1 A Brief History of Supernovae	1
1.2 The Cosmic Distance Ladder	3
1.3 Progenitor Models	7
1.4 Supernovae and Dark Energy	10
1.5 Supernovae Spectra	10
2. THE WAVELET SPECTRAL INDEX METHOD*	16
2.1 Wavelet Introduction	16
2.1.1 Wavelet Transform Algorithm	17
2.1.2 Normalization of Spectral Features	20
2.1.3 Normalization Spectral Features of SN Ia	23
2.2 Biases and Errors	24
2.2.1 Dependence of Spectral Features on Observational Noise	26
2.2.2 Bias Corrections	29
2.2.3 Error Estimates of the Spectral Indices	29
2.2.4 Procedure for Bias and Error Estimation	32
2.3 Applications to Type Ia Supernovae	33
2.3.1 Data Sample	35
2.3.2 X Versus the Epochs	35
2.3.3 X versus Δm_{15}	39
2.3.4 Extinction	50
3. APPLICATIONS OF WSIM	52
3.1 Type Ia SNe Subgroups: A Test	52

	Page
3.2 WSIM and Evolution	54
3.3 Correlation Evolution	70
3.4 PCA Evolution	72
3.5 Predicting Light Curve Decline Rate from Spectral Features Using WSIM	74
4. FUTURE WORK	83
4.1 WSIM in NIR and UV Spectra	83
4.2 Flux Ratios Applied to Wavelet Decomposed Spectra	83
4.3 Photometric Redshifts and Template Spectra	84
4.4 WSIM Applied to K-corrections	84
5. SUMMARY AND DISCUSSION	85
REFERENCES	89
APPENDIX A. INTRODUCTION TO PCA AND ICA	107
A.1 Principal Components Analysis	107
VITA	111

LIST OF TABLES

TABLE	Page
1.1 Effects of Spectral Luminosity Indicators on Hubble Dispersions	14
2.1 The Coefficients for the Dependence of X on Data Errors	27
2.2 The Coefficients for the Errors of X	27
2.3 The Spectroscopic Sample of SNe Ia	36
3.1 Evolution Fit Parameters for X_{4570}	55
3.2 Evolution Fit Parameters for X_{5150}	58
3.3 Evolution Fit Parameters for X_{5485}	61
3.4 Evolution Fit Parameters for X_{5750}	66
3.5 Evolution Fit Parameters for X_{6150}	69
3.6 Correlations between Spectral Indexes*	71
3.7 Estimates of $\Delta m_{15}(B)$ from WSIM and PCA	80

LIST OF FIGURES

FIGURE	Page
1.1 Expanding Envelope Model	11
2.1 Wavelet Decomposition of a Spectrum from SN 2001el	18
2.2 Spectrum Reconstructed by Sums of 3 Wavelet Scales	21
2.3 Spectral Features for Sums of Differing Scales	25
2.4 Monte Carlo Results for SQI	28
2.5 Monte Carlo Results of Noise Corrections	30
2.6 Monte Carlo Characterization of Uncorrected Errors	31
2.7 Temporal Evolution of the X Indexes	40
2.8 X_{6150} vs. Δm_{15} Correlation.	41
2.9 X_{5750} vs. Δm_{15} Correlation	43
2.10 X_{5485} vs. Δm_{15} Correlation	45
2.11 5150 Å Emission Peak vs. Δm_{15} Correlation	46
2.12 4570 Å Emission Peak vs. Δm_{15} Correlation	48
2.13 The Ratio of the Emission Peaks vs. Δm_{15} Correlation	49
2.14 Spectral Feature Evolution with Reddening	50
2.15 Spectral Index Correlation with Δm_{15} Adjusted for Reddening	51
3.1 Branch Plot Using Spectral Indexes	53
3.2 X_{4570} Evolution	57
3.3 X_{5150} Evolution	60

FIGURE	Page
3.4 X_{5485} Evolution	63
3.5 X_{5750} Evolution	65
3.6 X_{6150} Evolution	68
3.7 Δm_{15} Correlation Evolution	73
3.8 PC1 & PC2 Evolution	75
3.9 Percent Variation Evolution	76
3.10 Δm_{15} Prediction Examples	78
3.11 Δm_{15} Predictions for the Entire Dataset	79
A.1 3D Representation of Principal Components Analysis	109

1. INTRODUCTION

The current era of cosmology has been referred to as the era of precision cosmology. The current data sets have become big and robust enough to make fine distinctions in plausible cosmological models. This has not always been the case. Many strands of research have lead astronomers to this era. In the rest of this chapter we will discuss discoveries and events that have lead up to the present work. Chapter 2 introduces the Wavelet Spectral Index Method (WSIM) and Chapter 3 applies WSIM to SNe Ia subgroups, feature evolution, light curve shape estimates, and Hubble dispersions. Chapter 4 summarizes the results and Chapter 5 discusses possible future work that can be done with WSIM and the results presented here.

1.1 A Brief History of Supernovae

As the story is told, in 135 BC the Greek astronomer Hipparchus noticed what he believed to be a new star in the constellation Cassiopeia. This was an incredible event at the time because it was believed by many that the heavens were perfect and therefore could not change. In order to be sure when another new star appeared, Hipparchus created a catalog of over 1,000 stars and grouped them into 6 categories which became the basis of our modern magnitude scale (Marschall 1988; Stephenson & Green 2002). This “new star” was presumably a supernova. It was not until 185 AD that the Chinese made the first recorded observation of a supernova and it would be over 800 years until a supernova bright enough to be observed and recorded worldwide would occur. In 1572 and 1604, Tycho Brahe and Johannes Kepler respectively each observed a supernova. Tycho wrote a detailed account of his observations in a book entitled, *De Stella Nova*, meaning “the new star,” this was the first instance of the word “nova” being used to describe these objects (Stephenson & Green 2002).

This dissertation follows the style of the *Astrophysical Journal*.

I was not until the 1930's that the term “supernovae” was coined. Walter Baade and Fritz Zwicky wrote a series of papers in 1933 and 1934 that laid the foundations for supernova astronomy (Baade & Zwicky 1934a,b; Koenig 2005). Using the distance to M31, Baade and Zwicky were able to estimate the peak magnitude of the supernova that occurred in that galaxy in 1885. From this astronomers realized that the nova in M31 was several magnitudes higher than other novae. Much like Hipparchus, Zwicky was inspired to begin a systematic search for more supernovae. Before Zwicky's survey began in 1934, only 20 SNe had been recorded, by the time he died in 1974 over 400 had been discovered (more than 120 of those by Zwicky himself). In conjunction with Baade and Zwicky, Rudolph Minkowski took spectra with the 100-inch telescope at Mount Wilson (Marschall 1988). It was this ambitious work that laid the foundations for today's supernova research.

The first supernova spectrum observed was for SN 1885A in M31 but it was much later before astronomers understood supernova spectra. The broad spectral lines were difficult to identify. After more spectra were taken in the early twentieth century, astronomers began to understand that the broad spectral lines were due to rapidly expanding gaseous shells (Baade 1936; Branch 1990; Humason 1936).

It was Minkowski who laid the foundations for supernova types in his 1939 and 1941 papers, the former involving a detailed study of the spectra from SN 1937C and SN 1937D (Minkowski 1939, 1941). SN 1937C was the original prototype for Type I supernovae and later SN 1972E was added to define the Type I SNe (Kirshner et al. 1973; Minkowski 1939; Oke & Searle 1974). Type I supernovae are characterized by a lack of Hydrogen in their spectra while Type II show Hydrogen. The Type I supernovae proved to be a very heterogeneous group, while the Type II supernovae had much more variety which led Zwicky to suggest adding Types III, IV, and V (Zwicky 1965), but the distinctions were not convincing to most astronomers and Minkowski's classification held (Marschall 1988; Oke & Searle 1974). A major endeavour to identify spectral lines in SNe I spectra was undertaken by Payne-Gaposchkin and Whipple

(Payne-Gaposchkin & Whipple 1940). By 1965, astronomers were not much closer to understanding SNe spectra than they were 2 decades previously as Zwicky himself attested (Zwicky 1965).

Work done by McLaughlin suggested that there were strong He I lines in the spectra of SN 1954A and this was confirmed by Branch (Branch 1972; McLaughlin 1963). The He I lines would later be used to identify the subclass of SNe known as Type Ib. The line identifications that are most widely accepted today had their origins in Pskovskii (1969) who identified the P-Cygni profiles of the Type I spectra to be caused by low-excitation absorption. The sub-classification of Type I SNe did not occur until the spectra of SN 1983N and SN 1984L were seen to be significantly different than most other Type I SNe. Strong He I lines were found in both SNe by Harkness et al. (1987). Elias et al. (1985) first applied the designation Type Ib to these two SNe along with 1985F when all three showed similar nebular phase spectra to those of Type II SNe. Yet another subclass, Ic, was proposed by Wheeler & Harkness (1986) for SNe that show no signs of silicon or hydrogen and very weak signs of helium. It is thought that SNe Ib and SNe Ic are physically similar events distinguished only by the amount of helium present at the time of explosion (Wheeler et al. 1987; Wheeler & Harkness 1990). More will be discussed about Type Ia SNe spectra in Section 1.5.

1.2 The Cosmic Distance Ladder

Before Hipparchus was born, Aristarchus of Samos had proposed that the Sun, rather than the Earth, was the center of the universe. His critics, however, pointed out that the stars should show parallax — a shift of position in relation to background objects — if the earth moved about the sun. Almost 2,000 years later, similar reasoning led Tycho Brahe to believe that the earth was stationary, the sun orbited the earth, and all other planets orbited the sun. Their reasoning was logical but they had underestimated the vast distance between our sun and the nearest stars.

It was not until the observations of Friedrich Bessel in 1838 that parallax of a star was observed. Parallax distances are only reasonably obtainable out to a distance of ~ 100 parsecs (~ 250 parsecs with adaptive optics) and so it is not useful for measuring distances outside of our galaxy.

The next major rung on the cosmic distance ladder is based on Cepheid variable stars. Cepheid variable stars are stars that periodically vary in brightness over the course of a few days to several weeks. The relationship between the period and the luminosity of Cepheids was first discovered by Henrietta Leavitt in 1912 (Leavitt & Pickering 1912). Shapley & Hearn (1952) (and related works) used Leavitt’s period/luminosity relation to determine the distance to clusters in the Milky Way. It was through the distribution of these clusters that Shapley determined the approximate location of the center of our galaxy (Marschall 1988). It was these same variable stars that allowed Edwin P. Hubble to determine the distance to the Andromeda Galaxy, M31, and prove that the mysterious “spiral nebulae” were, in fact, located far beyond the edge of our galaxy and that our Milky Way was one galaxy among many (Hubble 1929b). Cepheids allow us to measure distances to nearby galaxies, some of which have had SNe Ia occur within them (Hubble 1929a; Macri et al. 2001; Riess et al. 2012). Since we can use the Cepheid variables to measure the distance to the host galaxy, we can then calibrate the SNe Ia. So far, SNe Ia are one of the brightest and most promising rungs on the cosmic distance ladder.

Zwicky and Baade were the first to suggest that supernovae might be used as a “standard candle.” A standard candle is an object with a known intrinsic luminosity. With the intrinsic luminosity known we can estimate its luminosity distance from the measured flux as shown in Eq. 1.1.

$$F = \frac{L}{4\pi d_L^2} \quad (1.1)$$

where F is the measured flux, L is the intrinsic luminosity, and d_L is the luminosity distance. Another way to parametrize the luminosity distance is by comparing the

absolute and apparent magnitudes as shown in Eq. 1.2 with M as the absolute magnitude and m being the apparent magnitude.

$$M = m - 5(\log_{10}d_L - 1) \quad (1.2)$$

The first to publish a Hubble Diagram using SNe I was Kowal (1968) with a dispersion of magnitudes around the Hubble Law of ~ 0.6 magnitudes. Branch and Patches introduced a method analogous to Baade’s variable star standard candle method for Type I supernovae, “on the assumptions that the light curve is due to thermal emission from an expanding, optically thick photosphere and that the temperature may be derived from the normal stellar colour-temperature relation,” (Baade 1926; Branch & Patchett 1973). The figure on page 12 shows a simple model of how a SN’s expanding envelope is treated.

As more SNe Ia were observed it became clear that they could not be used as true standard candles. Almost 20% of SNe Ia were found to be peculiar by Branch et al. (1993). The intrinsic scatter in the Hubble Diagram for SNe Ia was much larger than those expected from measurement errors and the scatter became worse when they were corrected for reddening under the assumption the SNe Ia were uniformly blue at maximum (Sandage & Tammann 1993; van den Bergh & Pazder 1992). More evidence that SNe were not as uniform as was thought became apparent when two peculiar SNe were observed in 1991. SN 1991T was more luminous than the average SNe Ia and it had a peculiar spectrum that exhibited very shallow silicon absorption (Filippenko et al. 1992b; Phillips et al. 1992). The other peculiar SNe was SN 1991bg, which was 2.5 magnitudes dimmer in the B-band and it also faded much faster than its normal counterparts (Filippenko et al. 1992a; Leibundgut et al. 1993; Turatto et al. 1996). It had become clear that SNe Ia were much more diverse than previously anticipated.

Phillips (1993) found that the decline rate of the B-band magnitude from B-band maximum until 15 days past maximum, parametrized as Δm_{15} correlated strongly

with the B-band peak magnitude. Expanding on Phillips's effort, Hamuy et al. (1995, 1996a), using the data from the Calan/Tololo Supernova Search (CTSS), were able to confirm and refine Phillips' relation. Hamuy was able to reduce the scatter in the Hubble Diagram to 0.17 magnitudes in the B-band. Other refinements of the Phillips' relation have been done by Phillips et al. (1999); Prieto et al. (2006).

A known way in which SNe Ia maximum magnitudes can be affected through reddening. Reddening can be something intrinsic within the supernova itself or produced through scattering by interstellar gas and dust. There are two ways of approaching the problem of correcting for reddening, the first is to assume that these two types of reddening cannot be distinguished and the second is to find a parameter to distinguish the two. The first approach is taken by the SALT and SALT2 light curve fitters (Guy et al. 2005, 2007). The SALT2 fitter parametrizes reddening as, c , and uses Equation 1.3 to correct the maximum magnitude of SNe Ia. The second approach to reddening corrections was taken by the Multicolor Light Curve Shape (MLCS) method, later updated to the MLCS2k2 method (Jha et al. 2007; Riess et al. 1996). The MLCS2k2 method used model reddening to compare the true reddening to the observed reddening as the evolve during the explosion and was able to bring dispersion down to 0.15 and even 0.12 magnitudes (Riess et al. 1996, 1999). Equation 1.4 describes the corrections for magnitude in filter X . Unfortunately, these two methods applied to recent data sets have given rise to a slight disparity between values for cosmological parameters, which has been explained as differences in extinction priors and U-band discrepancies between nearby and high- z samples (Foley et al. 2012; Hicken et al. 2009b; Kessler et al. 2009).

$$\mu_B = m_B^{MAX} - M + \alpha_x \times x_1 - \beta c \quad (1.3)$$

$$\mathbf{m}_X(t - t_0) = \mathbf{M}_X^0 + \mu_0 + \zeta_X(\alpha_X + \frac{\beta_X}{R_V})A_V^0 + \mathbf{P}_X\Delta + \mathbf{Q}_X\Delta^2 \quad (1.4)$$

It has been shown that host galaxy properties correlate with some properties of SNe Ia. This is important when constraining biases in the data. Shaw (1979) showed that the radial position of SNe within the host galaxies is biased at higher redshift, this is important if SNe luminosities are affected by metallicity since metallicity varies with radius in galaxies. Some later studies confirmed this radial bias (Hatano et al. 1998; Wang, L. et al. 1997b), while others did not (Howell et al. 2009; Ivanov et al. 2000). Relationships have been sought between SNe Ia properties (particularly peak luminosity and Hubble residuals) and global galaxy properties such as host galaxy mass (Kelly et al. 2010; Lampeitl et al. 2010; Sullivan et al. 2006, 2010), luminosity (Gallagher et al. 2005), morphology (Bronder et al. 2008; Hicken et al. 2009b; Lampeitl et al. 2010; Sullivan et al. 2003), metallicity (Gallagher et al. 2005, 2008; Hamuy et al. 2000, 2001; Howell et al. 2009; Kelly et al. 2010; Prieto et al. 2008), age (Gallagher et al. 2008; Hamuy et al. 1995, 2000; Howell et al. 2009; Ivanov et al. 2000; Kelly et al. 2010; Neill et al. 2009; Sullivan et al. 2006), size (Kelly et al. 2010), star formation rate (Gallagher et al. 2005; Neill et al. 2009; Sullivan et al. 2006, 2010), and dust (Commins 2004; Pennypacker et al. 2004; Sullivan et al. 2003). The main correlations have been shown to relate the diversity of SNe Ia properties with host galaxy mass, host galaxy metallicity, and host galaxy age (see previous references). However, these galactic properties are not independent of each other. Consequently, there is some debate on the validity of some of these relations, particularly host galaxy metallicity (see previous references). Only a few studies have looked at the effect of host galaxy morphology and SNe Ia spectra. These studies have found a link between only the Si II $\lambda 6355$ feature and morphology (Branch & van den Bergh 1993; Branch et al. 1996; Bronder et al. 2008).

1.3 Progenitor Models

It is generally believed that SNe Ia result from a runaway thermonuclear explosion within a white dwarf, however the complete process is not understood (Pakmor

et al. 2010b). The most widely accepted progenitor models are the single-degenerate (Whelan & Iben 1973), double-degenerate (Iben & Tutukov 1984; Webbink 1984), and the sub-Chandrasekhar mass models (Woosley & Weaver 1986). In the single degenerate (SD) model, a white dwarf (WD) accretes matter from its giant companion until the mass of the WD approaches the Chandrasekhar limit ($\sim 1.4M_{\odot}$). As the WD nears this limit, conditions become such that nuclear fusion begins and propagates through the star below the sound speed (deflagration) and later will presumably begin to propagate supersonically (detonation) (Hoefflich & Khokhlov 1996; Khokhlov 1991; Seitenzahl et al. 2011). This model is called the delayed detonation model. One problem is the need for the accretion rate to be neither too slow or too fast. It is expected that during the accretion process, SD progenitors should produce significant amounts of X-rays prior to the explosion, this is not seen (Di Stefano 2010; Gilfanov & Bogdán 2010; Lepo & van Kerkwijk 2011).

The double-degenerate (DD) model begins with two WD's orbiting about each other. Eventually these two coalesce with a mutual mass greater than the Chandrasekhar limit after which the thermonuclear explosion progresses much like it does in the single-degenerate system. The DD model of SNe Ia do not duplicate the observed light curves and spectra as naturally as SD model (Saio & Nomoto 1985). However, some recent models have shown the DD model to be more likely (Pakmor et al. 2010a,b; van Kerkwijk et al. 2010), but the conditions necessary for this channel of producing SNe Ia are not common enough to explain the entire SNe Ia rate.

The third likely channel for SNe Ia is a sub-Chandrasekhar mass WD where He detonation occurs on the surface in an accreted He shell, this causes a shock-wave to travel through the WD and detonate the core. There are many advantages to this model including the fact that very few C-O WD are near the Chandrasekhar limit as is needed for a SD progenitor, the range of ^{56}Ni masses produced are also more readily explained by the heterogeneous nature of initial masses (Pakmor et al. 2010b), it avoids the deflagration to detonation transition which is not well characterized by

other models (Pakmor et al. 2010a). Past work has shown that the sub-Chandrasakar models give ^{56}Ni masses that are consistently too low to reproduce SNe Ia data (Nugent et al. 1997; Stritzinger et al. 2006). However, recent work has shown that this problem can be overcome if the shell is thin enough but it requires a very narrow mass window (Pakmor et al. 2010b; Shen et al. 2010; Sim et al. 2010). Another short-coming of the sub-Chandrasakar models is that they show the production of high-velocity iron-group elements which are not observed in SNe Ia spectra (Pakmor et al. 2010b).

There are three possible channels to reach a SC WD: 1) a rapidly spinning WD can reach masses higher than $1.4M_{\odot}$ (Di Stefano et al. 2011; Hachisu et al. 2012; Yoon & Langer 2005), 2) two WD merge into a single massive object (Howell 2001; Raskin et al. 2010; Tutukov & Yungelson 1994), and 3) asymmetric effects could mimic a SC explosion (Hillebrandt et al. 2007; Maeda & Iwamoto 2009). Over the last decade, only a handful of the super-Chandrasekhar-mass (SC) progenitors have been observed. The first of these was SN 2003fg (SNLS-03D3bb) observed by the SuperNova Legacy Survey (SNLS) and it was determined to be super-luminous by Howell et al. (2006). The light curve of SN 2003fg did not hold to the Phillip’s relation, its decline rate was slow ($\Delta m_{15} = 0.84$ converted from a stretch factor of $s = 1.13$ using the equation from Perlmutter et al. 1997) compared to its luminosity (2.2 times higher than a typical supernovae). The ^{56}N mass required for this luminosity implied that the progenitor was significantly above the Chandrasekhar limit ($\sim 2.1M_{\odot}$). Since SN 2003fg, a few more examples of SC SNe Ia have been observed including: SN 2006gz (Hicken et al. 2007), SN 2007if (Scalzo et al. 2010; Yuan et al. 2010), and SN 2009dc (Silverman et al. 2011; Tanaka et al. 2010; Taubenberger et al. 2011; Yamanaka et al. 2009). Some other common factors of this subclass of SNe Ia are the presence of C II lines and low photosphere velocities as measured from the Si II line blueshifts. The presence of carbon in the outer layers of the SNe suggests a large amount of unburned material which is not seen in typical SNe Ia (Branch et al. 2003b; Khokhlov et al. 1993; Marion

et al. 2006; Tanaka et al. 2008; Thomas et al. 2007). The slower photospheric velocity runs contrary to the typical Chandrasekhar mass theory but can be explained by higher binding energy in SC progenitors (Howell et al. 2006). It is difficult to speak too dogmatically about SC SNe Ia until more examples are observed. Only one SC SNe Ia is used in this work (SN 2006gz).

1.4 Supernovae and Dark Energy

The 2011 Nobel Prize in physics was awarded for the discovery of “dark energy” (DE). Riess et al. (1998a) and Perlmutter et al. (1999) found that distant supernovae were dimmer than was previously expected. The most widely accepted explanation for the dimness is that there is a previously unknown force causing the universe to accelerate its expansion. Two main physical explanations are being explored either modifying current cosmological models, typically by adding back in Einstein’s cosmological constant, or by modifying the force of gravity.

The most direct probe of DE is studying its equation of state, w . According to current data and models, $w \sim -1$ but it may vary as a function of redshift. In order to measure w or $w(z)$ an expansion history of the universe must be determined. SNe Ia as standardizeable candles are currently one of the best tools available for making a determination of the expansion history of the universe.

1.5 Supernovae Spectra

As discussed in Section 1.1, SNe spectra remained mysterious for sometime. Much has been done in the past several decades to observe and interpret SNe Ia spectra. SNe spectra are the most detailed probe of the chemical composition and structure of the explosion and can provide many clues to the explosion mechanism. Line identifications are generally made by simulating the output spectra of an underlying explosion model. By using the density structure and composition from the model,

approximations can be made of the relative strength of spectral lines. The spectra of Type Ia supernovae prior to maximum show broad P-Cygni spectral lines superimposed on a star-like blackbody continuum. The P-Cygni lines are produced by the interaction of different regions of the expanding envelope moving at different velocities. Figure 1.1 shows a simple model of a SN's expanding envelope. It is desirable to speak of this period as the “photospheric epoch” where the physical origin of the blackbody continuum is called the “photosphere” of the supernova. At latter times, ~ 1 month after maximum, the spectra no longer have a continuum component and are dominated by emission lines. This is referred to as the “nebular phase.” It is widely agreed upon that the main contributors to SNe Ia spectra are intermediate mass elements (IME) such as O, Mg, Si, S, Ca, and iron group elements, mainly Fe and Co.

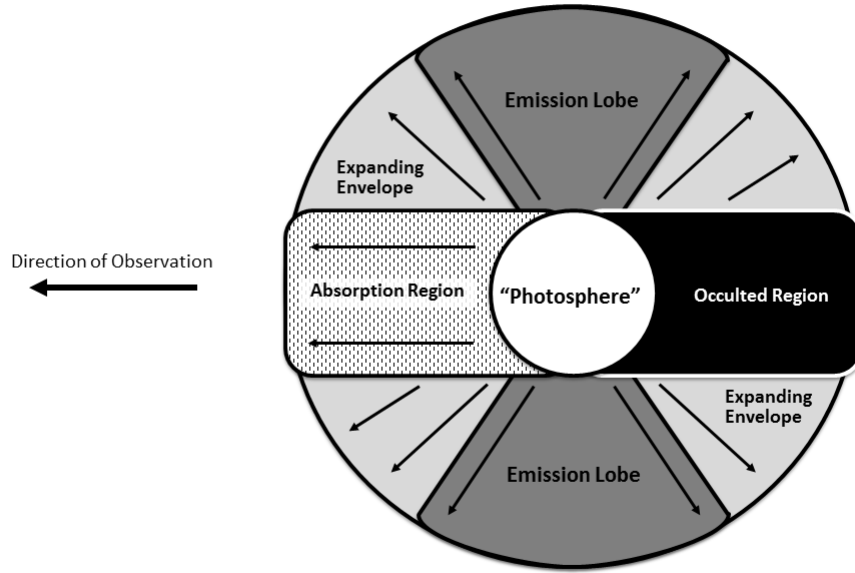


Fig. 1.1. Expanding Envelope Model. This figure shows a simple model of the expanding envelope of a SNe explosion. This figure is adapted from Fisher (2000) and Mihalas (1978).

The synthetic spectral code, SYNOW had earlier incarnations in the works of Branch et al. (1983, 1985) and then presented in Fisher (2000). Similar methods were also used by Mazzali et al. (1993). The PHOENIX code was developed by Hauschildt and collaborators (see Baron & Hauschildt 1998; Hauschildt 1992, and references therein) as a model of an expanding spherical atmosphere without the use of the Sobolev approximation which is used in the previously mentioned methods. These codes have been instrumental in making line identifications in SNe Ia spectra.

The spectral classification of supernovae was discussed in Section 1.1. Many recent developments have been made in the study of Type Ia SNe spectra. One such development is the establishment of sub-groupings of Type Ia SNe. Branch et al. (2006) defined 4 sub-groupings of SNe based on line depths and shapes of the Si II $\lambda 6355$ line near maximum and the location of the SNe on the W(5750) vs. W(6100) plot (see Figure 1 in Branch et al. 2006). Branch et al. (2009) revisited these subgroups with a larger sample. The groups were still a valid sub-grouping but the larger sample shows that the subgroups are not discrete.

An alternative sub-grouping was presented by Benetti et al. (2005) based on the velocity evolution of the spectral lines. The supernovae were characterized as being in one of three groups — FAINT, LVG, and HVG — by using clustering analysis on five measured parameters: M_B , Δm_{15} , $\mathcal{R}(\text{Si II})$, v_{10} , and \dot{v} . The velocity gradient, \dot{v} , is defined as the average daily decrease in the expansion velocity. The low velocity gradient (LVG) group is defined as those SNe with $\dot{v} < 60 - 70 \text{ km s}^{-1} \text{ day}^{-1}$. As their name implies, the FAINT subgroup is composed of fainter SNe and consequently this group has on average a larger Δm_{15} . The high velocity gradient (HVG) group consists of normal SNe with larger \dot{v} . Tanaka et al. (2008) gives some possible explanations for the differences between LVG and HVG SNe in differences in temperature and possibly asphericity. These two sub-groupings are complementary to one another since they are based on different measurements. The Core Normal and Shallow Silicon

subgroups from Branch et al. (2006) correspond well with the LVG, while the Broad Line and Cool subgroups correspond to HVG and FAINT subgroups respectively.

A third subgrouping was set forth by Wang, X. et al. (2009) which classified SNe as “Normal” or “HV” where the second grouping have Si II absorption velocities $\simeq 11,800 \frac{km}{s}$. It was found that a separate reddening law could be applied to the two subgroups which yielded a Hubble dispersion ~ 0.136 . The discrepancy between the two groups could be due to intrinsic color differences between the groups or circumstellar dust.

Another use of spectral data is to constrain the extent of spherical symmetry in the explosion through spectrapolarimetry. McCall (1985) originally made the case that an increase in polarization should be seen near the minimum of P-Cygni spectral features since the absorption would block some of the light from the unpolarized continuum. The emission peak would be due to the emission of unpolarized light and would therefore lower the overall polarization near the peak of the P-Cygni profile. These effects were not seen, however, until in the mid-1990’s more concerted efforts were made to observe SNe with spectrapolarimetry. Polarization in SNe Ia is weak near maximum but can be observed pre-maximum. Also, the continuum polarization is weak which suggests that SNe Ia are nearly spherical. Observations of SN 2001el suggested that the polarizations of SNe Ia come from the outer layers implying that the exterior layers are asymmetric but the inner layers are more symmetric (Wang, L. et al. 2003). This asymmetry is re-enforced by the apparent clumpiness of Ca II in the outer, high-velocity layers of the SN (Kasen et al. 2003; Leonard et al. 2005; Wang, L. et al. 2003). The Si II $\lambda 6355 \text{ \AA}$ line is one of the most strongly polarized lines in SNe Ia and was observed in 17 SNe by Wang, L. et al. (2007). The polarization of the 17 SNe was shown to correlate with Δm_{15} . For a more thorough treatment of spectrapolarimetry of supernovae see Wang, L. & Wheeler (2008).

There have been many efforts to find spectral luminosity indicators (some examples are compared in Table 1.1). Nugent et al. (1995) defined two line ratios that

Table 1.1. Effects of Spectral Luminosity Indicators on Hubble Dispersions

Paper	Method	# of SNe	σ
Riess et al. (1998b)	Snapshot	7	0.18
Bongard et al. (2006)	\mathcal{R}_{Ca}	8	0.1 (0.25)
"	\mathcal{R}_{CaS}	8	0.1 (0.19)
"	\mathcal{R}_{Si}	8	0.07 (0.07)
"	\mathcal{R}_{SiS}	8	0.09 (0.04)
"	\mathcal{R}_{SiSS}	8	0.09 (0.05)
Foley et al. (2008)	UV spectra	16	0.090 (0.140)
Bailey et al. (2009)	$\mathcal{R}_{\frac{642}{443}}$	58	0.12-0.13
Wang, X. et al. (2009)	v_{SiII} subgrouping	158	0.125
Foley & Kasen (2011)	v_{SiII} subgrouping	121	0.13

correlated with Δm_{15} , $\mathcal{R}(SiIII)$ and $\mathcal{R}(CaII)$. In order to improve on the spectral ratios, Bongard et al. (2006, 2008) suggested the $\mathcal{R}(SiS)$ as an alternative that should be more sensitive to the underlying continuum level and therefore more sensitive to temperature fluctuations. Hachinger et al. (2006) studied a wide variety of spectral features and the ratios of their pseudo-equivalent widths. They showed that the $\mathcal{R}(SiIII)$ correlation with Δm_{15} was driven mainly by the $\lambda 5972$ Å feature from Si II. Other spectral ratios were studied but these were all related to the same Si II $\lambda 5972$ Å feature. Taking spectral ratios even further, Bailey et al. (2009) made a systematic search for the best correlation between spectral ratios and peak magnitude. The best flux ratio was found to be $\mathcal{R}_{\frac{642}{443}}$, the ratio of fluxes at 6420 Å and 4430 Å. This particular ratio performed as well, if not better than SALT2 corrections using x_1 and c .

Clearly, spectral data contains much information about the explosion and its progenitor. One important piece of information for cosmology is the redshift of each SNe. This is typically found through follow-up on the host galaxy spectra or by fitting the spectra of the SNe itself. However, this type of follow-up will no longer be

feasible when large surveys like the LSST begin to discover $\sim 200,000$ SNe per year (LSST Science Collaborations et al. 2009). Photometric redshift estimates will need to be employed in order to make maximal use of the SNe data that will come out of these surveys. Photometric redshift estimates of galaxies are commonly used. There are two main methods of determining photometric redshifts for galaxies: empirical methods using training sets and template fitting methods (see Budavári 2009, for a more detailed discussion about different photo- z methods). These will be easily modified for use with SNe Ia. The first method is to define redshift as a function of multiple filter magnitudes and colors (an example for galaxies can be seen in Connolly et al. 1995; Li & Yee 2008). A similar method was applied to SNe Ia by Wang, Y. (2007); Wang, Y. et al. (2007), redshift was estimated from a function of *griz* light curves focused on the flux at *i*-band maximum. The second method for determining photometric redshift estimates involves using templates to fit the data in question. Asztalos et al. (2010) presented a method using templates based on the “Branch normal” set of template spectra from Nugent et al. (2002). One of the motivations for the current work was to explore the relationships between spectral features and other SNe Ia characteristics in order to create a heterogeneous set of template spectra or a template spectra generator so that SNe Ia photo- z methods could be tested more robustly.

2. THE WAVELET SPECTRAL INDEX METHOD*

2.1 Wavelet Introduction

A major difficulty in analyzing spectroscopic data with highly blended atomic lines is to quantify the strength of certain spectral features. These spectral features are superimposed on a continuum so line blending can make it difficult to reliably define the continuum level. In the case of supernova spectra, the pre-nebular phase spectra typically show P-Cygni profiles with both emission and absorption components whereas the nebular phase spectra are dominated by broad overlapping emission lines. The spectral features are therefore of various widths and strengths, and neighboring features are heavily blended. Further, the data typically contain observational noise, flux calibrations errors and uncertainties in the amount of dust extinction. The noise makes the definition of a continuum very uncertain and accordingly the calculation of equivalent width becomes unreliable. In many observations, in particular those at high redshift, the observed supernova spectra are heavily contaminated by host galaxy spectra. This affects severely the definition of line depth.

For Type Ia supernovae, it is known that certain spectral line ratios such as the Si II 5972/Si II 6355, and the Ca II H&K lines are sensitive to the intrinsic brightness of the supernova Nugent et al. (1995). The measurement of the line strength is, however, not trivial. For instance, to measure the Si II 5972/Si II 6355, and the Ca II ratio, Nugent et al. (1995) employed a simple approach by drawing straight lines at the local peaks of the spectral features and measure the depth of the absorption minima from the straight line. However, the location of the straight line and the position of the line minimum are not easy to define in the presence of observational errors. It is for this reason the ratio is derived only for a number of very well observed local supernovae. Pseudo-equivalent widths are typically estimated to measure the

*Reprinted with permission from “QUANTIFYING SPECTRAL FEATURES OF TYPE Ia SUPERNOVAE” by Wagers, A., Wang, L., and Asztalos, S., 2010. *Astrophysical Journal*, 711, 711-730, Copyright 2010 by The American Astronomical Society.

strengths of spectral features . The continuum level is estimated by finding the maxima on either side of the feature and a straight line is used to connect the two maxima and then is used as the continuum level. In the past the maxima have been found either by eye (Branch et al. 2006; Nugent et al. 1995) or by a simple algorithm (Garavini et al. 2007a; Hachinger et al. 2006). Then the equivalent width is calculated by finding the area and depth of the chosen region using the estimated continuum level.

In this paper, the spectral features of Type Ia supernovae will be analyzed instead through wavelet transformations. This technique avoids many of the challenges mentioned above associated with identifying line strengths. Here wavelet transformations are applied to Type Ia supernovae spectra with the purpose to quantify the spectral features for cosmological applications.

2.1.1 Wavelet Transform Algorithm

Wavelet decomposition, like Fourier decomposition, expresses a given function in terms of the superposition of a set of simple basis functions. Unlike Fourier decomposition, individual wavelet functions are localized in the spatial domain on a scale that is variable. The transform is carried out in direct space so artifacts related to periodicity are avoided. The reconstruction is trivial and again, unlike the Fourier decomposition, there are a finite number of wavelets scales so that the original function can be restored without distortion. The evolution of the transform from one scale to the next is easy to follow and the interpretation of the spectrum at each scale is straightforward.

There are a large number of functions that can be used for the wavelet transform. It has been previously demonstrated that the à trous algorithm is a particularly useful tool for studying spectral features (Holschneider et al. 1989; Shensa 1992; Starck et al. 1995, 1997) and is thus adopted for our purposes. Taken literally, the French term à trous is interpreted as “with holes”, expressing the fact that convolution is

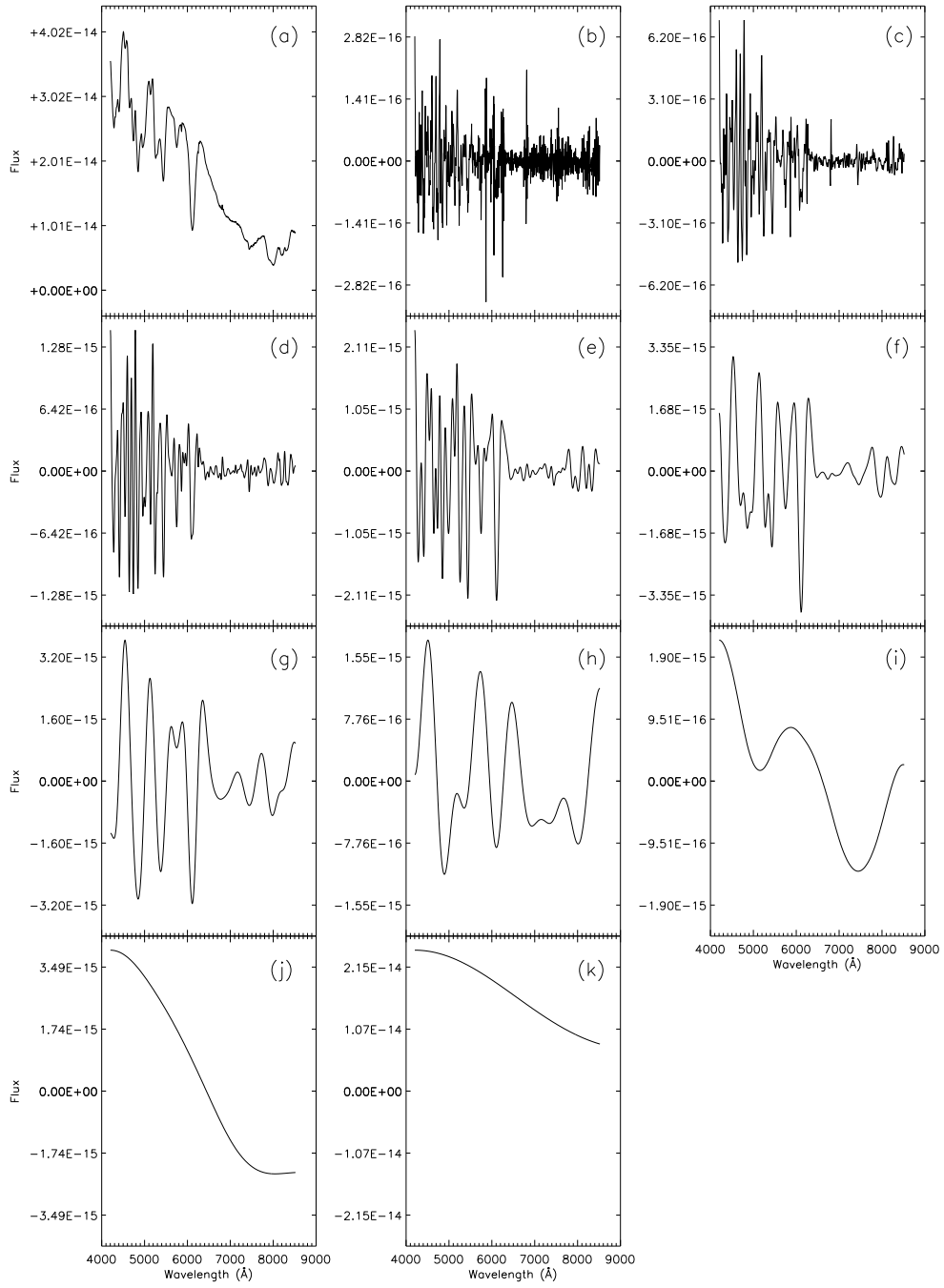


Fig. 2.1. Wavelet Decomposition of a Spectrum from SN 2001el. (a) The spectrum of SN 2001el, (b-j) the wavelet scales 1 to 9, and (k) the smoothed array c_p of the SN 2001el from top left to lower right. A sum of of scales (b) to (k) recovers the original spectrum (a). The mean fluxes of each of the wavelet scales (b) to (j) are identically zero.

interlaced. That is, the convolution mask retains the same number of points but increases in scale as the decomposition is performed, resulting in holes within the convolution mask. More technically, the à trous wavelet uses a dyadic wavelet to merge non-dyadic data in a simple and efficient procedure. Assuming a scaling function $\phi(x)$ (which corresponds to a low pass filter also called the convolution mask), the first filtering is performed on the original data $c_0(k)$ by a twice magnified scale leading to the $c_1(k)$ set. This convolution mask for à trous wavelet is usually a triangle function or a cubic spline function which amounts to a weighted average of a small number of data points. The signal difference $c_0(k) - c_1(k)$ is the wavelet scale $w_1(k)$ and contains the information between these two scales (in this case the point-to-point variation within the data). The result, $w_1(k)$, is the discrete set associated with the wavelet transform corresponding to $\phi(x)$. The operation is performed successively to obtain the wavelet scale $w_j(k)$ at each scale j until scale J is reached where 2^J is equal to the number of data points. The original spectrum c_0 can be expressed as the sum of all the wavelet scales and the last smoothed array c_p :

$$c_0(k) = c_p(k) + \sum_{j=1}^p w_j(k)$$

To demonstrate the basic features of the à trous wavelet transformation, we show in Figure 2.1 the wavelet transformation of a well observed supernova SN 2001el. The data were obtained through the spectropolarimetry program at the Very Large Telescope of the European Southern Observatory (Wang, L. et al. 2003). The sampling step of the data is binned to 5Å. The signal to noise ratio (SNR) of the data is everywhere above 150 - this unusually high SNR is a result of the spectropolarimetry observations. The original data is show in Figure 2.1a, and the consecutive wavelet scales for $j = 1, 9$ are shown in Figure 2.1b to 2.1j.

Figure 2.1k represents the smoothed array c_p . The number of 5 Å bins in the SN 2001el spectrum taken 1 day after B-band maximum is 864. In order to use the à trous algorithm the data must have 2^J data points, to meet this requirement the

spectrum was padded at the red end with a decaying exponential so that the data has 2^{10} data points giving $J = 10$ and allowing only 10 wavelet scales. Further note that each of the individual wavelet scales have zero mean. It can be seen that at small scales the wavelet is dominated by observational noise and the supernova signal starts to become significant only for $j \geq 3$, and the broad spectral wiggles associated with the supernova dominate the wavelet scales of $j = 5, 6$, and 7 . The supernova spectral features are typically a few hundred Å wide and are effectively isolated in the decomposed spectra.

The spectral features of a supernova can be better described by a blend of several wavelet scales. For this reason, we can calculate the sum of more than one scales to reflect the existence of features of various width:

$$W_{\{l\}} = \sum_{j \in \{l\}} w_j,$$

where $\{l\}$ is a subset of wavelet scales. Examples of these spectra are shown in Figure 2.2 for SN 2001el.

2.1.2 Normalization of Spectral Features

The wavelet scales, having the units of the original flux spectrum, need to be normalized to construct quantities that measure the strength of the spectral features that do not depend on the absolute flux level of the spectrum. There undoubtedly is more than one way to normalize the scales. The simplest approach is to normalize all the wavelet scales by dividing them by the smoothed array c_p . This approach is simple and will certainly work fine for data without host galaxy contamination. For data with host galaxy contamination, or those with poor background subtraction, this approach introduces systematic errors to the normalized scales.

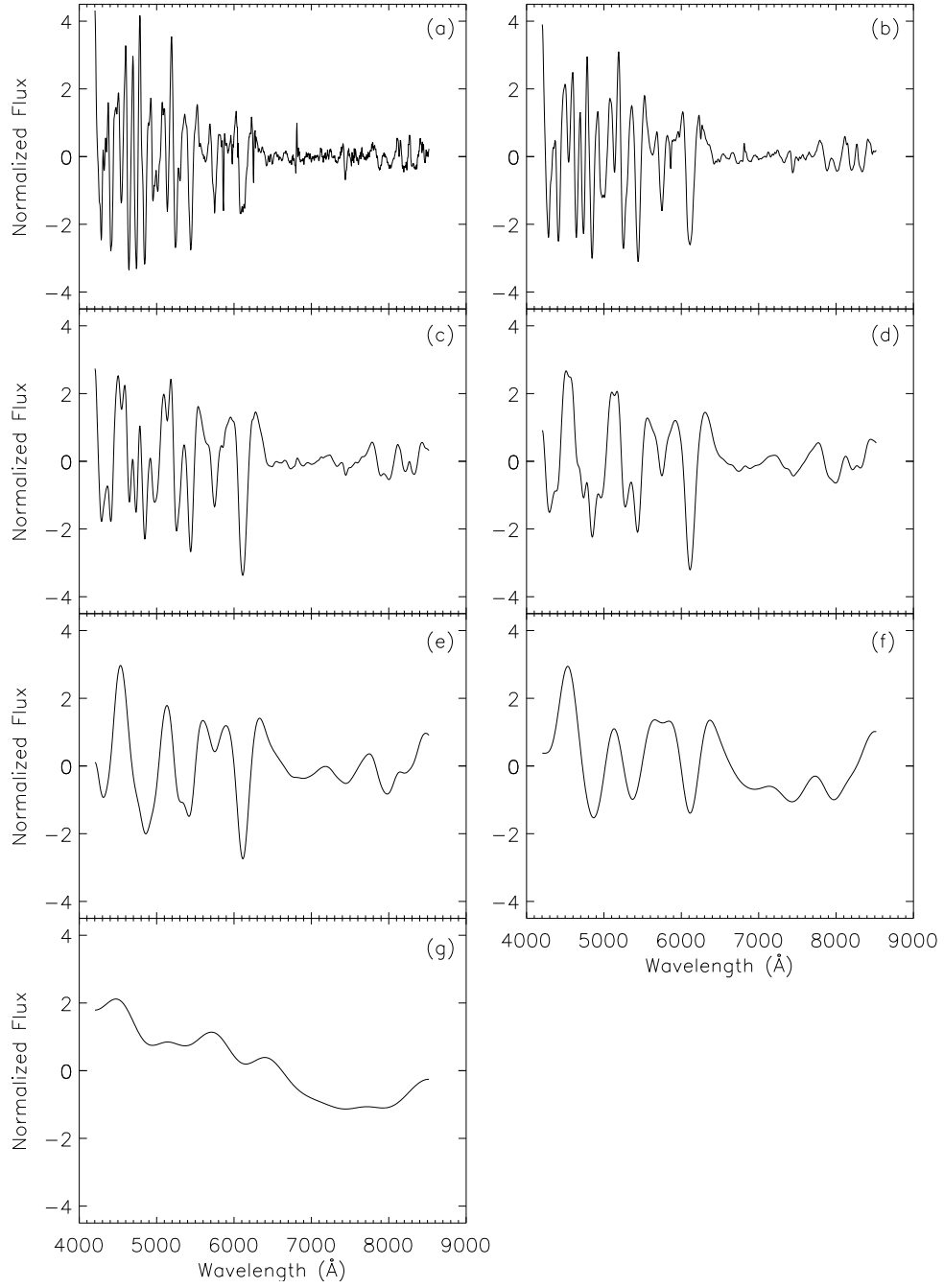


Fig. 2.2. Spectrum Reconstructed by Sums of 3 Wavelet Scales. Wavelet sums for SN 2001el over (a) scales 1 to 3, (b) 2 to 4, (c) 3 to 5, (d) 4 to 6, (e) 5 to 7, (f) 6 to 8 and (g) 7 to 9. Running combinations of the different scales captures features of varying width.

In our approach, the normalized wavelet scale is defined using the standard deviations of the spectral features from any given wavelet scale:

$$\hat{W}_{\{l\}}(\lambda) = W_{\{l\}}(\lambda) / \sqrt{\Sigma_{\lambda_1}^{\lambda_2} W_{\{l\}}^2(\lambda) / N_{12}} \quad (2.1)$$

$$= W_{\{l\}}(\lambda) / \sigma_{\{l\}}, \quad (2.2)$$

where N_{12} is the number of data points between λ_1 and λ_2 . The mean and standard deviation of $\hat{W}_{\{l\}}$ are zero and 1, respectively. This is effectively a self-normalization that exploits only the intrinsic properties of the wavelet scales involved. Host galaxy contamination (which does strongly affect c_p) would not have a significant effect in this context.

The spectral index X_j of any feature between λ_a and λ_b at a given scale j is defined by averaging the normalized wavelet scale \hat{W}_j :

$$X_{\{l\}} = \Sigma_{\lambda_a}^{\lambda_b} \hat{W}_{\{l\}}(\lambda) / N_{ab},$$

with N_{ab} being the bin size in the wavelength region λ_a and λ_b . X_j defines a normalized number which measures the strength of the spectral features in the normalized wavelet scale \hat{W}_j between λ_a and λ_b . Alternatively, one can also calculate the power P_j between λ_a and λ_b for wavelet scale j :

$$P_{\{l\}} = \Sigma_{\lambda_a}^{\lambda_b} \hat{W}_{\{l\}}^2(\lambda) / N_{ab}.$$

$P_{\{l\}}$ and $X_{\{l\}}$ contain the same information. In this study, we will focus on $X_{\{l\}}$.

One obvious advantage to using wavelet scales to estimate spectral feature strengths is that they do not depend on the definition of the spectral continua. Furthermore, since they can be estimated locally around a spectral feature, spectral indices are useful in minimizing uncertainties due to errors in spectral flux calibrations. Similarly, the spectral indices as defined here are less sensitive to errors of background

subtraction, which is usually one of the dominate sources of uncertainty, especially in the studies of high redshift supernovae.

2.1.3 Normalization Spectral Features of SN Ia

The wavelet technique is particularly well-suited for studying scattering-dominated spectra of expanding atmospheres with P-Cygni spectral features: the net flux of the P-Cygni feature is usually close to zero. Wavelet decomposition is consistent with this as the mean flux is zero for the various wavelet scales. Wavelet transforms thus makes it easy to separate emission and absorption components of a spectrum in a mathematically robust way.

In this study, the supernova spectra are first decomposed into various scales as described in the above section. In addition, to reflect the fact the spectral features are a blend of different scales, the sum of the wavelet scales 3, 4, and 5 are used as the primary spectrum for the analysis of spectral features (though other scales have also been analyzed). All the decomposed spectra are normalized in a similar way as given in Equation 2.2. To derive quantities that are less sensitive to errors of flux calibration, we need to restrict calculation of the normalization factor to a small wavelength region and yet to have large enough spectral coverage so that the feature strengths will not be affected by boundary. In this study, the spectra are divided into four regions: (A) 5500 to 6500 Å, (B) 4985 to 5985 Å, (C) 4850 to 5450 Å, and (D) 4250 to 5200 Å; the variance in each of these sections of spectra is calculated and used as the normalization factor. These regions are arbitrarily chosen to contain the features listed below and are large enough to characterize the variance in that spectrum around each feature. Interesting features include the Silicon II lines at 6355 and 5972 Å in region (A), the Sulfur II lines at 5433 Å and 5459 Å in region (B), and the two strong peaks chosen because they are strong, clean peaks at 5150 Å and 4570 Å, in region (C) and (D), respectively. The two emission peaks arise in part from P Cygni profiles of Si II at 5041 Å and Mg II at 4471 Å and are chosen as clean

examples of emission features. The five spectral features are shown in Figure 2.3 and are the main focus of subsequent analyses.

2.2 Biases and Errors

In practice, the observed data contain noise and estimates of X_j can be biased. The noise affects X_j in two ways: First, when the noise is large, its effect can propagate to all the wavelet scales and become a significant component at the wavelet scale of interest. Secondly, it changes the normalization factor when calculating \hat{W}_j - data with larger noise can be systematically biased to give a larger normalization factor because the additional power from shot noise. This bias is usually not a problem for high SNR data, but can be significant for data with a low SNR. The correction factor $\Pi(j)$ for scale j is defined as:

$$\sigma_0(j) = \sigma(j)\Pi_{1j}, \quad (2.3)$$

where $\sigma_0(j)$ is the variance at the j th scale in the ideal case of no photon shot noise.

Typically, published spectroscopic data do not have associated noise spectra. One instead has to rely on the flux spectrum to estimate the noise levels. A major advantage of wavelet transformation is that it allows estimates of the noise characteristics based on the spectral data itself. If we assume that all the continuum or spectral features are much broader than the data sampling step, the spectral fluctuations of the wavelet scale with $j = 1$ should then represent mostly shot noise. This is generally reasonable as can be seen in Figure 2.1 (b) for the spectrum of Type Ia supernova 2001el.

Recognizing that smaller wavelet scales contain more information of the noise property than larger wavelet scales, we can define the spectral quality index (SQI)

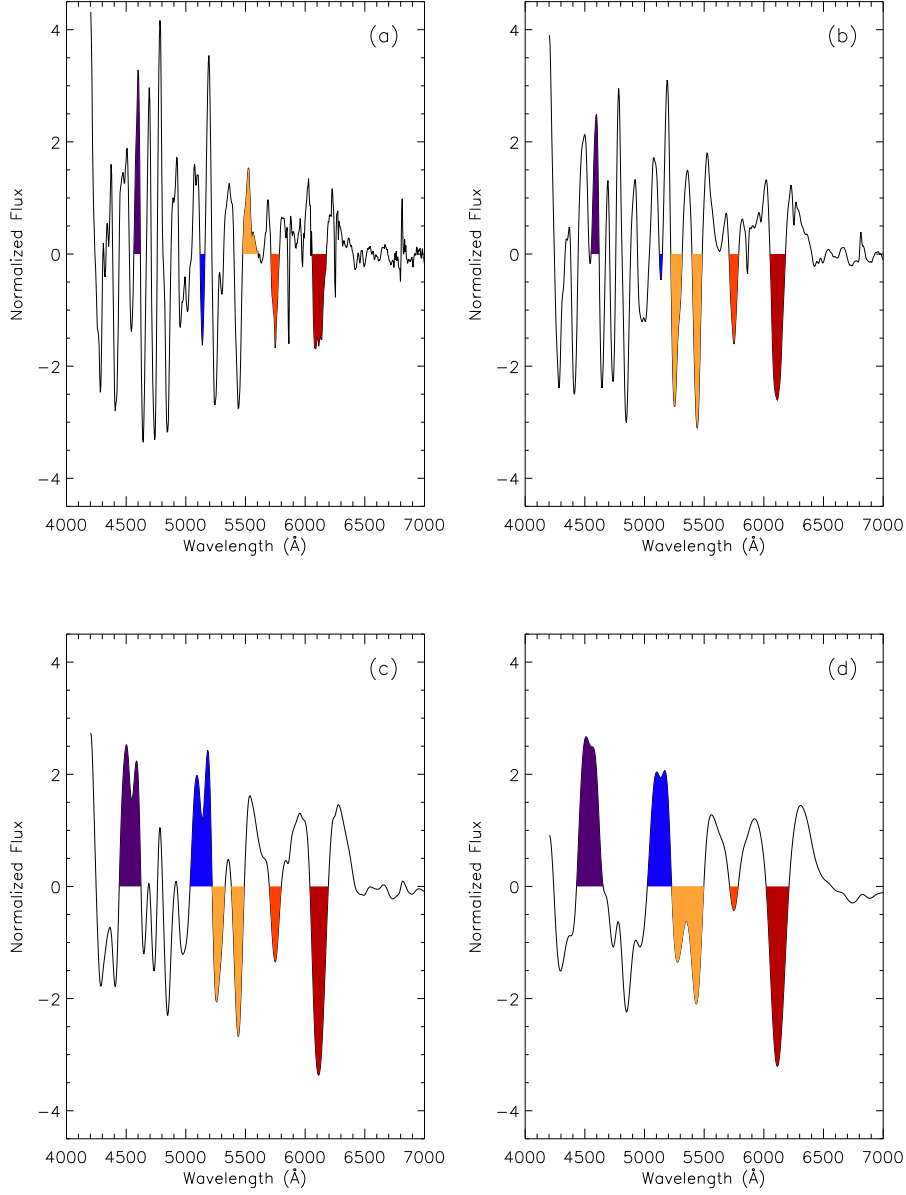


Fig. 2.3. Spectral Features for Sums of Differing Scales. Spectral features for Type Ia supernovae. (a): $l = 1, 2, 3$. (b): $l = 2, 3, 4$, (c) $l = 3, 4, 5$, and (d) $l = 4, 5, 6$. The spectral features are well resolved in (c) and (d).

of the normalized wavelet scale $\{l\}$ as the variance ratio of normalized scale $\{l\}$ and the lowest normalized scale $\{1\}$:

$$\rho_{\{l\}\{1\}} = \Sigma_{\lambda 1}^{\lambda 2} \hat{W}_{\{l\}}^2 / \Sigma_{\lambda 1}^{\lambda 2} \hat{W}_{\{1\}}^2, \quad (2.4)$$

where the braces $\{\}$ reflect that the various quantities are actually sums of various wavelet scales. Specifically, $\hat{W}_{\{1\}}$ is the normalized sum of three wavelet scales, where $\{l\} = 1, 2, 3$ in this instance. The SQI measures the relative importance of noise levels in estimating of the spectral feature index. It can be calculated directly from the decomposed spectra without an error spectrum. Note that SQI is a quantity that can be localized to certain wavelength intervals.

For a given spectrum $\{c_i\}$, the dependence of the wavelet spectral indices $X_{\{l\}}$ and the correction factor Π on SQI can be estimated through Monte-Carlo simulations.

2.2.1 Dependence of Spectral Features on Observational Noise

Monte Carlo simulations are required to quantify the dependence of X indices on observational noise. The characteristic parameter of the noise is the SQI defined in Equation 2.4 - the ratio of spectral variance of combined wavelet scales $l = 3, 4, 5$ to that of the combined scales $l = 1, 2, 3$. To perform such these simulations one needs a series of noise free spectra of supernova spectra. The spectropolarimetry program at the ESO VLT has acquired several high quality spectra of SN Ia with SNRs around 150 (Wang, L. et al. 2003). Spectra of SN 2001V and SN 2001el from the spectropolarimetry program will be used in this simulation to quantify the relations between X and SQI.

In the example shown in Figure 2.4, various levels of Poisson noises were added to the spectrum of SN 2001el at day +1. The noise is added to the spectra, which are then transformed to various wavelet scales and the various X indices are calculated. The top panel in Figure 2.4 shows the relation between ρ and the assumed SNR with

Table 2.1 The Coefficients for the Dependence of X on Data Errors

SN	Day	$\gamma_{31}(A)$	$\gamma_{31}(B)$	$\gamma_{31}(C)$	$\gamma_{31}(D)$	mean	$\gamma_{41}(A)$	$\gamma_{41}(B)$	$\gamma_{41}(C)$	$\gamma_{41}(D)$	mean
01V	-8	0.1132	0.1116	0.1183	0.1144	0.1144	0.0263	0.0240	0.0273	0.0259	0.0258
01el	-4	0.1220	0.1236	0.1229	0.1224	0.1227	0.0567	0.0587	0.0566	0.0573	0.0573
01el	+1	0.1220	0.1236	0.1229	0.1224	0.1227	0.0581	0.0583	0.0552	0.0551	0.0567
01el	+9	0.1251	0.1273	0.1250	0.1240	0.1254	0.0585	0.0607	0.0599	0.0577	0.0592

the addition of Poisson noise. The SQI is calculated in the wavelength intervals of 550.0 nm to 650.0 nm, 498.5nm to 598.5 nm, and 425.0 to 520.0 nm. It can be seen that ρ is correlates well with the SNR of the input data: reducing the SNR decreases ρ . This confirms that the SQI can effectively capture effect the photon shot noise, and can be used to quantify the noise level of the data.

The variances used to normalized the spectra at the various wavelet scales are clearly correlated. This is shown in the middle panel of Figure 2.4, where the data exhibit nearly identical slopes over the different wavelength regions. A linear relationship between $\sigma^2(1)$ and $\sigma^2(3)$, and between $\sigma^2(1)$ and $\sigma^2(4)$ is assumed for the fits. The slopes γ_{1j} extracted from these fits are given in Table 2.1.

The bottom panel in Figure 2.4 clearly demonstrates how the correction factor Π increases dramatically for ρ approaching 2.82 (which corresponds to a SNR of below 1 per 0.5 nm bin). This implies that the spectral features are dominated by the noise, hence it becomes impossible to extract the spectral indices reliably.

The correction factor for ρ can be fit well with a function

$$\Pi_{1j} = \sqrt{(1 - \gamma_{1j}\rho_{1j}^2)}, \quad (2.5)$$

with the relevant coefficients taken from Table 2.2 for the various lines.

Table 2.2 The Coefficients for the Errors of X

SN	Date	$\eta(6150)$	$\psi(6150)$	$\eta(5750)$	$\psi(5750)$	$\eta(5485)$	$\psi(5485)$	$\eta(5150)$	$\psi(5150)$	$\eta(4570)$	$\psi(4570)$
2001V	-8	-0.02486	0.0469	-0.0156	0.0293	-0.0203	0.0601	-0.0373	0.0545	-0.0179	0.0453
2001el	-4	-0.00625	0.0367	-0.00628	0.05429	-0.02449	0.05892	-0.01626	0.06382	-0.01165	0.05248
2001el	+1	0.133	1.248	0.212	1.188	0.160	1.412	0.176	1.533	0.157	1.531
2001el	+9	0.159	1.276	0.194	1.282	0.234	1.279	0.203	1.442	0.177	1.672
2001el	+1	0.145	1.194	0.265	1.322	0.175	1.295	0.181	1.500	0.216	1.408

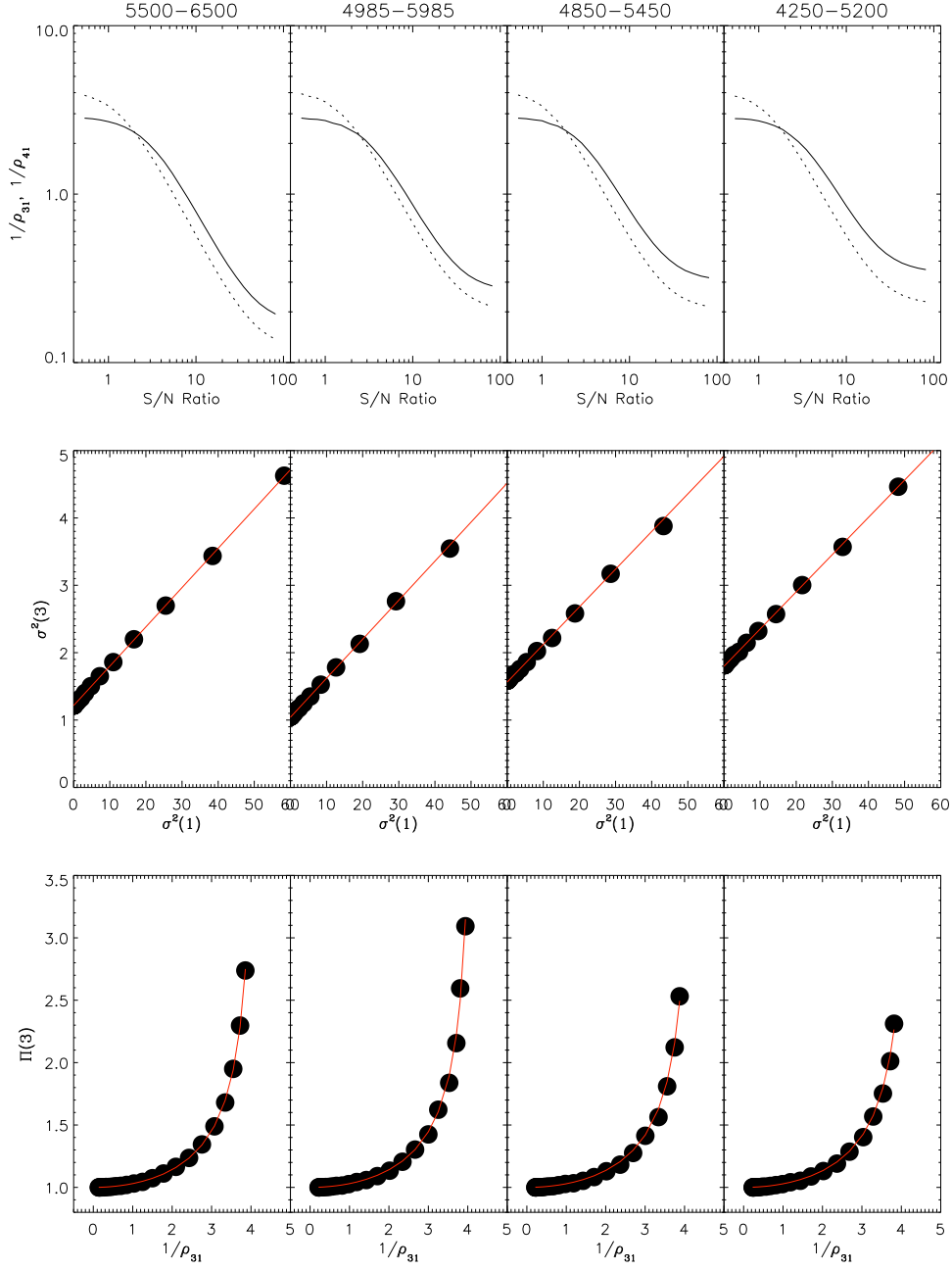


Fig. 2.4. Monte Carlo Results for SQI. (Top) The relation between the SQI and the input SNR ratios. The solid lines show SQI of fourth wavelet scale and the dashed line the third. (Middle) The relation between the variance of the third and first wavelet scales. The effect of a large $\sigma(1)$ propagates linearly to larger wavelet scales. (Bottom) The correlation of the bias correction factor and SQI for the third wavelet scale. The SNR was varied in all cases via the addition of noise in the Monte Carlo simulations.

2.2.2 Bias Corrections

The various X indices for the spectral features are derived from the Monte-Carlo simulation of data with different SQI. As shown in Figure 2.5, the X indices (shown as open squares apparently suffer strong bias when the data are noisy. The various X indices after Π corrections are shown in Figure 2.5. The effect is generally small for high SNR data, but becomes important for data with low SNR. In any case the bias is effectively removed by applying the correction factor Π .

2.2.3 Error Estimates of the Spectral Indices

Assuming photon shot noise, the Monte Carlo simulations also give error estimates for the X indices. The errors as a function of ρ are shown in Figure 2.6. These errors are fitted with a function of the form:

$$\sigma_X = \eta \rho^\psi, \quad (2.6)$$

and the relevant coefficients η and ψ are shown in Table 2.2. Simulations were performed for all of the SN 2001V and SN 2001el spectra and it was found that in all cases the bias can be well corrected. Note that due to the lack of a completely noise-free SN Ia spectrum, at extremely high SNR (such as those that are higher than or comparable with the signal to noise ratio of the SN 2001el spectra as used in the simulation) the Monte Carlo simulations do not give correct estimates of the errors. Such cases are unlikely to be relevant as in such situations, the errors are likely to be dominated by calibration systematics rather than shot noise. The error function given above will be used for all cases here. As can be seen in Figure 2.6, the above expression gives an excellent description of the dependence when the errors are described by ρ .

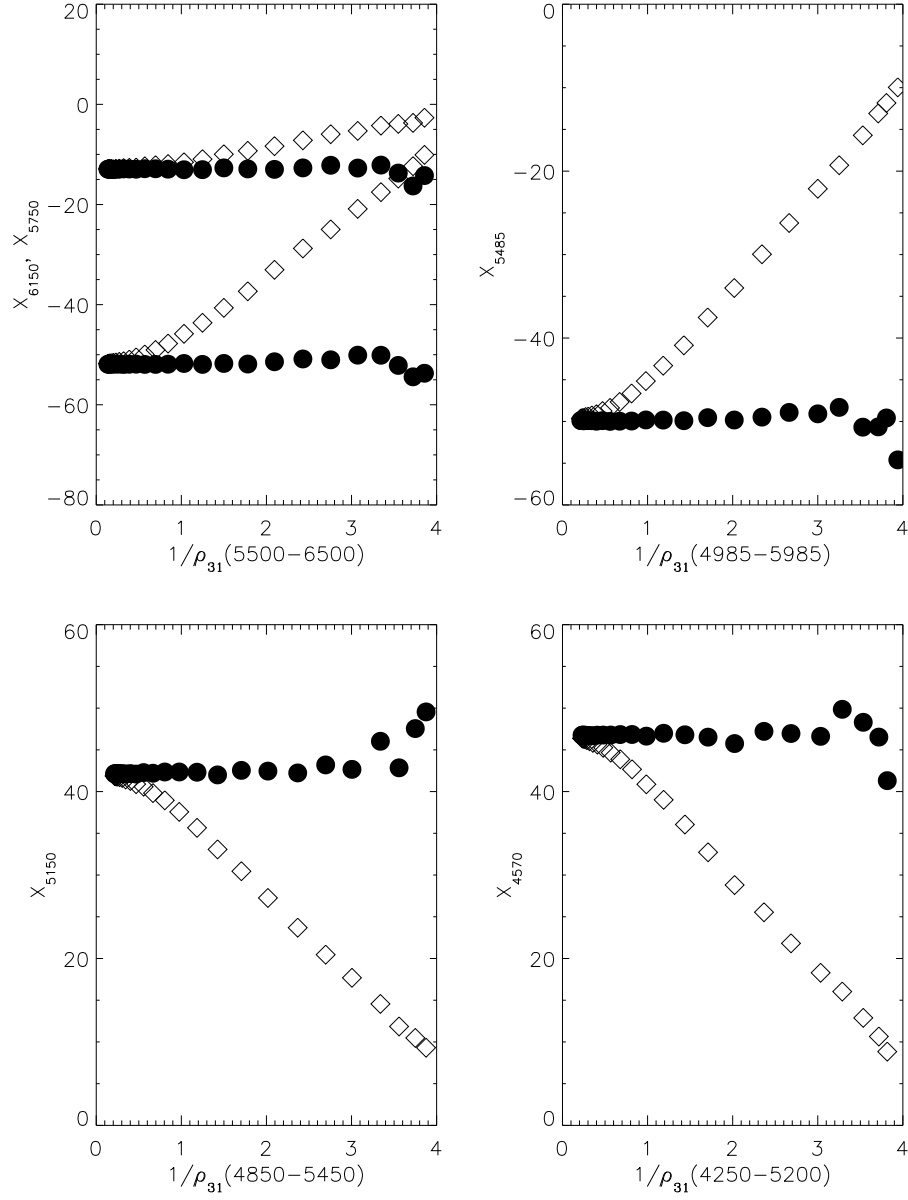


Fig. 2.5. Monte Carlo Results of Noise Corrections. Line indices corrected for ρ dependence for important SN Type 1a spectral features. The X indices are derived from the sum of wavelets 3,4,5 of SN 2001el 1 day past optical maximum.

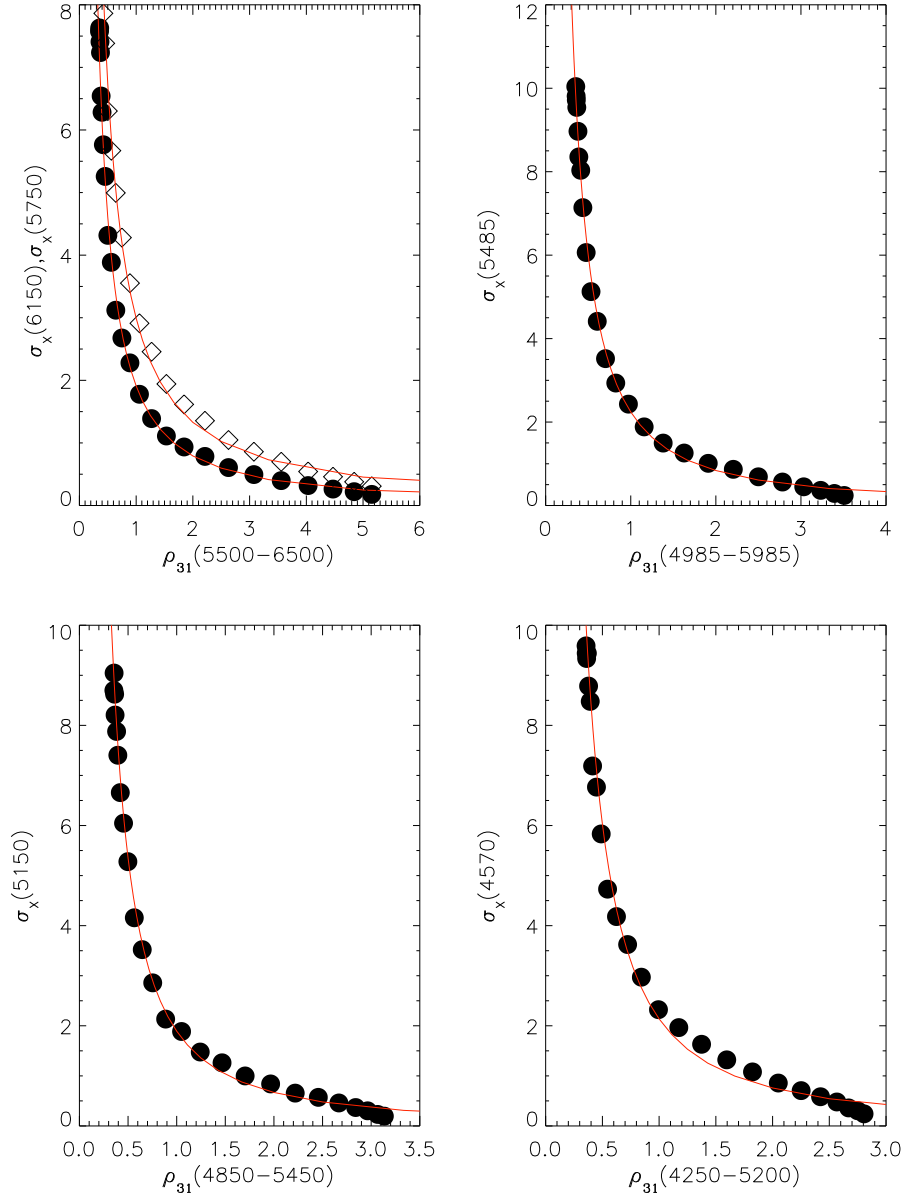


Fig. 2.6. Monte Carlo Characterization of Uncorrected Errors. Errors of the X indices as functions of ρ for SN 2001el at optical maximum.

The ρ dependence of the X indices and their errors have a weak dependence among the different varieties of supernovae and the epoch of the supernovae.

2.2.4 Procedure for Bias and Error Estimation

The procedure for removing bias and estimating errors from noisy supernovae spectra is premised on extracting correction factors from a supernova with a large SNR. Here we enumerate a correction recipe using wavelet scales $l = 3, 4, 5$ with SN 2001 el as our reference spectrum.

1. Compute the ratio of the sum of the squares of wavelet scales 3,4,5 and 1,2,3 (ρ_{31} in Equation 2.4) for SN 2001el

$$\rho_{31} = \frac{\hat{W}_{\{3,4,5\}}^2}{\hat{W}_{\{1,2,3\}}^2}.$$

2. Degrade the SNR of SN 2001 el in multiple steps with the addition of Poisson noise. Compute $\sigma_{\{1,2,3\}}^2$ and $\sigma_{\{3,4,5\}}^2$ at each step.
3. Extract γ_{31} by assuming a linear relationship between $\sigma_{\{1,2,3\}}^2$ and $\sigma_{\{3,4,5\}}^2$ (see middle panel of Figure 2.4).

$$\sigma_{\{3,4,5\}}^2 = \beta + \gamma_{31} * \sigma_{\{1,2,3\}}^2$$

,

where $\sigma_{\{l\}}$ is defined in Equation 2.3.

4. Repeat each of the above steps over all regions of interest to extract a mean value for γ_{31} . Equivalently, use the values for γ_{31} by consulting Table 2.1.
5. Using Equation 2.5, compute ρ_{31} values for each SNe having typical values of the SNR.

6. Compute the correction factor Π_{31} using this value of ρ_{31} and the value of γ_{31} computed for SN 2001el

$$\Pi_{31} = \sqrt{1 - \gamma_{31}\rho_{31}^2}$$

.

7. The spectral index of any supernovae feature can be corrected for bias by dividing the uncorrected value by Π_{31} as in Equation 2.3.

$$X_{corr} = \frac{X}{\Pi_{31}}$$

.

8. The error bars are determined from the same set of simulations. With σ_X defined as in Equation 2.6 with parameters defined as in 2.2 construct the relationship

$$\log_{10}(\sigma_X) = \eta + \psi \log_{10}(\rho_{31})$$

, where all quantities refer to a SNe with a large SNR (e.g. SN 2001 el). Equivalently, use the values for η and ψ from Table 2.2.

9. With these values η and ψ compute the variance in the spectral index for a SN with a typical value of SNR as

$$\sigma_X = 10^\eta \rho_{31}^\psi$$

.

2.3 Applications to Type Ia Supernovae

Spectral indexes lend themselves to a quantitative analysis of the temporal and magnitude evolution of the spectral lines. Nugent et al. (1995) measured the *ratio*

of the depths of the SiII 6355 Å and 5972 Å features and established correlations with Δm_{15} . Other studies of these and other spectral features have adopted slightly more elaborate procedures based on equivalent (Hachinger et al. 2006) and pseudo equivalent widths (EW) (Altavilla et al. 2009; Branch et al. 2009; Garavini et al. 2007a; Hachinger et al. 2006) to study these and other absorption features. Recently, Arsenijevic et al. (2008); Stanishev et al. (2007) have used wavelets coupled with the pseudo-EW technique to study a Si II absorption feature. Emission features have received less attention than absorption features and usually involve a distinct procedure from the absorption features Bongard et al. (2006); Nugent et al. (1995). Recently, Bailey et al. (2009) described a variance of the above methods wherein absorption and emission features in a training set of spectra are studied to extract the optimal flux ratio to Δm_{15} correlation. This ratio is then applied to correct the magnitudes of other supernovae within a validation set.

The wavelet technique developed here differs in several important respects from those described in the preceding paragraph. Our methodology is premised on the existence of one (or more) very high SNR spectra. Spectral line strengths are first extracted for this high SNR spectrum from a combination of intermediate wavelet scales. Excluding the lowest and highest reduces the effects of noise and the continuum, respectively. Working with wavelets from a high SNR spectrum allows corrections to be made to lower SNR spectra. Perhaps the most salient difference is that performing our analysis entirely in wavelet space permits us to avoid definition of the continuum (the mean of the wavelet scales is zero and integration is performed from one zero on the leading to the next zero on the trailing edge of a feature). Consequently, we are able to work directly with line strengths of the features themselves, not their ratios. Lastly, this technique permits absorption and emission lines to be treated democratically. It is our expectation that the wavelet method gives to a more robust measure of line strength. In Sections 2.3.2 and 2.3.3 we apply this technique to data described in the subsequent section.

2.3.1 Data Sample

The supernovae included in this study are given in Table 2.3. A large number of low- z spectra ($z < 0.1$) were collected from libraries that are publicly available, such as the SUSPECT Supernova Database^a and the Center for Astrophysics Supernova Archive^b, as well as other SNe that are available in the literature. The spectra are corrected by the host galaxy redshift but no dust extinction correction is applied. The original wavelength coverages, step sizes and SNRs of these spectra are vastly different. In our analysis, all the spectra are first rebinned to 5 Å sampling step for convenience. After wavelet decomposition was performed the spectra were checked for edge effects that would distort calculations, the affected spectra were removed.

2.3.2 X Versus the Epochs

The evolution of spectral features in Type Ia SNe has been a topic of much study but due to the limitations of the pseudo-equivalent width method and small sample sizes it has been mainly a qualitative study (for some more recent examples see Branch et al. 2005; Garavini et al. 2007b; Matheson et al. 2008; Pastorello et al. 2007; Quimby et al. 2007; Wang, X. et al. 2008). However some Mg II, Fe II, and Ca II features have been studied quantitatively by Folatelli (2004) and Garavini et al. (2007a) using the pseudo-equivalent method. It is the hope of the authors that the wavelet spectral indexes described here will facilitate more quantitative studies of SNe Ia spectra.

An example of the time evolution of X indices is shown in Figure 2.7 for SN 2005cf - a normal Type Ia supernova with $\Delta m_{15} = 1.16$. For a spectroscopically normal supernovae like SN 2005cf, X_{6150} and X_{5750} exhibit little evolution in line strength for roughly ± 8 days around maximum. These two spectral indexes are associated

^a<http://bruford.nhn.ou.edu/suspect/index1.html>

^b<http://www.cfa.harvard.edu/supernova/SNarchive.html>

Table 2.3: The Spectroscopic Sample of SNe Ia

SN	Δm_{15}^a	Branch Subtype ^b	X_{6150}	X_{5750}	X_{5485}	X_{5150}	X_{4570}	Spectra Source ^o
1981B	1.125(0.010)	BL	-56.645(0.157)	-10.339(0.298)	-48.941(0.245)	42.956(0.175)	43.306(0.184)	1
1983G	1.37(0.01) ^b	...	-59.818(0.649)	-13.890(3.411)	... ^k	49.532(0.483)	... ^k	2
1984A	1.294(0.063)	BL	-63.615(0.974)	-5.166(1.167)	-39.319(0.489)	45.827(0.573)	43.895(0.781)	3
1986G	1.643(0.022)	CL	-49.109(0.295)	-20.165(0.534)	-32.227(0.456)	40.231(0.386)	51.494(0.521)	4
1989B	1.262(0.017)	CL	-54.202(0.486)	-13.218(0.428)	-47.078(0.424)	41.870(0.216)	46.161(0.318)	5,6
1990N	1.138(0.024)	CN	-53.751(0.112)	-9.683(1.763)	... ^k	39.630(0.312)	... ^k	7,8
1991T	0.986(0.009)	SS	-52.505(0.274)	-2.976(0.499)	-29.806(0.829)	34.860(0.159)	21.783(0.474)	9,10,11
1991bg	1.857(0.125)	CL	-46.461(0.324)	-25.588(0.582)	-22.972(0.382)	24.081(0.436)	51.622(0.367)	12,13,14
1992A	1.320(0.015)	BL	-54.040(0.242)	-16.239(0.517)	-46.671(0.447)	41.067(0.300)	36.031(0.336)	15
1993H	1.70(0.10) ^c	...	-46.790(6.947)	-21.166(3.053)	-27.335(0.697)	35.324(0.093)	51.183(1.020)	16
1994D	1.558(0.013)	CN	-53.234(0.212)	-14.450(0.182)	-48.604(0.216)	37.600(0.114)	35.566(0.207)	17,18
1996X	1.299(0.009)	CN	-53.837(0.216)	-9.917(0.400)	-51.935(0.309)	41.193(0.271)	43.070(0.317)	19,20
1997bp	1.231(0.013)	...	-64.847(1.884)	-3.015(1.935)	... ^k	42.951(0.729)	... ^k	21
1997br	1.141(0.021)	SS	-43.186(4.832)	-21.652(3.106)	... ^k	40.701(0.171)	... ^k	22
1997do	1.099(0.237)	BL	-57.978(0.878)	-11.934(0.186)	... ^k	43.880(0.995)	... ^k	23
1997dt	1.04(0.15) ^d	CN	-56.255(0.148)	-8.051(0.475)	-50.003(0.632)	41.675(0.655)	47.482(0.538)	23
1998V	1.150(0.025)	CN	-52.756(0.285)	-10.737(0.517)	-47.976(0.406)	42.455(0.300)	35.278(0.390)	23
1998aq	1.185(0.008)	CN	-53.695(0.218)	-9.824(0.404)	-51.130(0.322)	39.259(0.262)	31.908(0.403)	23,24
1998bp	1.903(0.013)	CL	-45.839(0.215)	-28.182(0.399)	-33.504(0.312)	27.849(0.458)	48.179(0.449)	23
1998bu	1.014(0.008)	CN	-53.743(0.137)	-10.060(0.255)	-48.582(1.067)	40.477(0.177)	32.800(1.149)	23,25,26,27
1998de	1.881(0.066)	CL	-48.672(0.294)	-28.202(0.533)	-21.675(0.329)	38.392(0.564)	56.127(0.232)	23
1998dh	1.258(0.038)	BL	-55.895(0.209)	-10.240(0.388)	-47.762(0.285)	43.403(0.257)	45.766(0.205)	23
1998dm	0.983(0.339)	...	-53.027(0.094)	-12.198(3.126)	... ^k	47.453(0.919)	... ^k	23
1998ec	1.074(0.028)	BL	-62.305(0.121)	-4.422(0.232)	-47.332(0.591)	43.144(0.037)	42.297(0.887)	23
1998eg	1.15(0.09) ^e	CN	-53.627(0.317)	-11.681(0.570)	-52.964(0.531)	37.920(0.349)	39.311(0.394)	23
1998es	0.745(0.013)	SS	-52.360(0.668)	-4.399(0.549)	-45.227(0.306)	42.884(0.086)	31.574(0.194)	23
1999aa	0.811(0.014)	SS	-51.631(0.885)	-5.908(0.408)	-44.397(0.210)	43.020(0.087)	30.685(0.214)	23,28
1999ac	1.241(0.036)	SS	-56.123(0.280)	-9.354(0.509)	-44.465(0.327)	42.953(0.272)	44.159(0.183)	23,29
1999aw	0.814(0.018)	SS	-52.965(4.726)	-1.590(0.431)	... ^l	... ^l	... ^l	30
1999by	1.796(0.008)	CL	-46.242(0.484)	-27.599(0.338)	-23.743(0.369)	34.528(0.282)	56.148(0.363)	23
1999cc	1.567(0.102)	BL	-54.551(0.368)	-17.619(0.654)	-46.891(0.486)	40.408(0.439)	41.747(0.363)	23
1999cl	1.243(0.043)	BL	-59.260(0.397)	-6.847(0.703)	-38.325(0.538)	43.409(0.161)	46.195(0.193)	23
1999dq	0.973(0.030)	SS	-50.336(0.623)	-6.492(0.359)	-43.249(0.249)	43.592(0.086)	33.746(0.162)	23
1999ee	0.944(0.006)	SS	-52.461(0.418)	-9.313(0.737)	-48.746(0.446)	43.475(0.215)	39.278(0.177)	31

Continued on Next Page...

^c Δm_{15} from Hachinger et al. (2006)

Table 2.3 – Continued

SN	Δm_{15}^a	Branch Subtype ^b	X_{6150}	X_{5750}	X_{5485}	X_{5150}	X_{4570}	Spectra Source ^o
1999ej	1.446(0.018)	BL	-51.523(0.241)	-21.127(0.443)	-43.869(0.384)	36.897(0.338)	41.707(0.383)	23
1999gh	1.721(0.008)	BL	-53.856(2.065)	-21.929(0.901)	... k	39.822(3.692)	... k	23
1999gp	1.029(0.186)	SS	-54.055(0.844)	-3.634(1.409)	-46.510(0.863)	41.516(0.449)	37.941(0.408)	23
2000E	1.079(0.021)	SS	-51.938(0.250)	-7.507(0.493)	-46.913(0.479)	42.393(0.248)	33.210(0.667)	32
2000cf	1.364(0.043)	...	-51.376(1.230)	-13.827(0.031)	-48.438(0.101)	41.395(0.424)	47.646(0.232)	23
2000cn	1.675(0.027)	CL	-51.405(0.250)	-23.634(0.078)	... k	38.841(1.773)	... k	23
2000cx	0.971(0.006)	SS	-52.441(0.429)	-4.527(0.755)	-41.327(0.525)	44.369(0.285)	29.687(0.418)	23,33
2000dk	1.457(0.033)	CL	-50.096(0.017)	-23.257(0.389)	-39.544(0.354)	34.195(0.406)	38.875(0.413)	23
2000fa	1.140(0.027)	CN	-54.210(0.551)	-9.293(1.827)	-44.606(1.594)	40.845(1.452)	33.094(1.348)	23
2001V	0.743(0.034)	SS	-52.006(1.813)	-5.376(2.106)	-35.152(3.846)	39.213(4.099)	29.718(0.170)	23
2001ay	0.543(0.006)	BL	-63.993(0.203)	-2.843(0.378)	-30.552(0.265)	39.397(0.309)	59.731(0.666)	34
2001el	1.166(0.004)	CN	-52.317(0.744)	-12.737(0.230)	-50.087(0.342)	40.832(0.272)	... m	35
2002bo	1.260(0.007)	BL	-61.527(0.322)	-5.877(0.821)	-41.535(0.730)	45.575(0.464)	41.272(0.458)	36
2002cx	1.145(0.016)	SS	-32.952(3.231)	-19.216(6.785)	-28.614(6.820)	20.330(2.847)	27.516(2.514)	37
2002dj	1.08(0.05) ^f	BL	-63.346(0.267)	-2.519(2.441)	-46.720(0.321)	46.987(1.460)	38.889(0.614)	38
2002el	1.423(0.018)	...	-54.749(0.349)	-15.368(0.904)	-45.108(0.855)	37.251(0.296)	37.339(0.567)	39
2002er	1.301(0.009)	BL	-56.853(0.227)	-10.436(0.420)	-49.949(0.369)	41.584(0.248)	45.197(0.332)	40
2003cg	1.25(0.05)	CN	-52.901(0.295)	-8.980(0.506)	-43.235(0.634)	38.695(0.223)	36.871(0.400)	41
2003du	1.151(0.037)	CN	-54.388(0.192)	-7.664(0.360)	-53.238(0.300)	40.229(0.287)	39.471(0.283)	42,43
2004S	1.210(0.016)	CN	-48.235(3.103)	-18.474(5.782)	... k	40.250(2.452)	... k	45
2004dt	1.299(0.002)	BL	-64.706(0.662)	-3.370(0.231)	-41.069(0.266)	34.912(0.214)	45.159(0.400)	46
2004eo	1.417(0.004)	CL	-49.673(1.001)	-20.883(0.351)	-40.903(0.220)	41.306(0.303)	49.330(4.384)	47
2005bl	1.93(0.10)	CL	-45.532(3.327)	-25.784(3.759)	-17.737(3.337)	27.149(0.361)	40.669(1.949)	48
2005cf	1.161(0.006)	CN	-52.758(0.249)	-11.505(0.457)	-52.686(0.316)	40.237(0.356)	43.805(0.364)	49
2005cg	0.942(0.048) ^g	SS	-55.780(0.292)	-6.463(0.528)	... n	... n	... n	50
2005df	1.116(0.013)	...	-53.024(0.064)	-9.486(3.441)	-51.371(0.514)	46.312(2.108)	37.292(2.676)	51
2005hj	0.743(0.165) ^h	SS	-51.129(0.542)	-4.260(0.935)	-41.942(0.423)	49.066(0.336)	38.596(0.529)	52
2005hk	1.56(0.09) ^e	SS	-42.299(6.056)	-27.804(1.861)	-16.555(1.580)	31.749(0.302)	30.752(14.932)	53
2006gz	0.69(0.04) ⁱ	SS	-52.610(0.032)	-7.209(0.217)	... k	33.375(0.492)	... k	54
2006X	1.17(0.04) ^j	BL	-66.111(0.252)	-0.616(0.195)	-25.726(0.209)	42.110(0.088)	38.500(0.186)	55

^a Δm_{15} values were calculated by the super-stretch method from Wang, L. et al. (2006a) unless otherwise noted.

^bDesignations from Branch et al. (2009)

^c Δm_{15} from Hachinger et al. (2006)

^d Δm_{15} from Jha et al. (1999)

^e Δm_{15} from Phillips et al. (2007)

^f Δm_{15} from Pignata et al. (2008)

^g Δm_{15} converted from stretch value, s , from Quimby et al. (2006) using the equation from Perlmutter et al. (1997)

^h Δm_{15} converted from stretch value, s , from Quimby et al. (2007) using the equation from Perlmutter et al. (1997)

ⁱ Δm_{15} from Hicken et al. (2007)

^j Δm_{15} from Wang, X. et al. (2008)

^kThe 5485 Å and 4570 Å features show much more variance in their evolution, therefore the epoch range over which these features were fit was smaller. These SNe are missing X_{5485} and X_{4570} values because they did not have enough spectra within the smaller epoch range.

^lDue to noise or mis-calibration of the spectra at +3 days, there is not enough data to fit X_{5485} , X_{5150} , and X_{4570}

^mThe spectra for SN 2001el did not cover the wavelength region for this feature.

ⁿNot enough of the spectra for SN 2005bl covered the wavelength regions for X_{5485} , X_{5150} , and X_{4570} for a good fit to be made.

^oSpectra Source References: (1) Branch et al. (1983); (2) Harris et al. (1983); (3) Barbon et al. (1989); (4) Phillips et al. (1987); (5) Barbon et al. (1990); (6) Wells et al. (1994); (7) Mazzali et al. (1993); (8) Leibundgut et al. (1991); (9) Filippenko et al. (1992a); (10) Phillips et al. (1992); (11) Ruiz-Lapuente et al. (1992); (12) Leibundgut et al. (1993); (13) Filippenko et al. (1992b); (14) Turatto et al. (1996); (15) Kirshner et al. (1993); (16) Wang unpublished; (17) Meikle et al. (1996); (18) Patat et al. (1996); (19) Wang, L. et al. (1997a); (20) Salvo et al. (2001); (21) Anupama (1997); (22) Li et al. (1999); (23) Matheson et al. (2008); (24) Branch et al. (2003a); (25) Jha et al. (1999); (26) Meikle & Hernandez (2000); (27) Hernandez et al. (2000); (28) Garavini et al. (2004); (29) Garavini et al. (2005); (30) Strolger et al. (2002); (31) Hamuy et al. (2002); (32) Valentini et al. (2003); (33) Li et al. (2001); (34) Branch et al. (2006); (35) Wang, L. et al. (2003); (36) Benetti et al. (2004); (37) Li et al. (2003); (38) Pignata et al. (2008); (39) Wang unpublished; (40) Kotak et al. (2005); (41) Elias-Rosa et al. (2006); (42) Anupama et al. (2005); (43) Stanishev et al. (2007); (44) Howell et al. (2006); (45) Krisciunas et al. (2007); (46) Altavilla et al. (2007); (47) Mazzali et al. (2008); (48) Taubenberger et al. (2008); (49) Garavini et al. (2007b); (50) Quimby et al. (2006); (51) Quain in progress; (52) Quimby et al. (2007); (53) Phillips et al. (2007); (54) Hicken et al. (2007); (55) Wang, X. et al. (2008)

at this epoch with the SiII 5972 and 6355 lines. After 8 days past maximum X_{5750} becomes stronger and X_{6150} weakens. Similarly, around 8 days past maximum X_{5485} , associated at maximum with the S II 5433/5459 Å “w” feature, begins to weaken until it is completely obscured by 18 days past maximum. The emission features at 4750 and 5150 Å for this same supernova, by contrast, show comparatively little time evolution. These two emission features can be associated with P-Cygni profiles of Mg II and Si II but are highly blended making identification difficult (Wang, L. et al. 2006b).

Analysis of the time evolution is complicated by occasional large gaps between epochs and the need to occasionally track spectral features manually due to the decreasing velocity of the expanding photosphere. Consequently, a full analysis of the temporal evolution of the remaining supernovae in Table 2.3 will be analyzed in a separate paper.

2.3.3 X versus Δm_{15}

Figures 2.8 to 2.12 show the correlations between X and Δm_{15} for the five spectral features that we have adopted for our study. The line strengths in these figures are those computed at maximum light. In instances where no spectrum at maximum light exists a simple quadratic fit was made of all spectra within 8 days of maximum (for features that are not a smoothly varying the fit was restricted to within 5 days of maximum). The fits were checked for consistency and for supernovae with only two spectra closely sampled in time, a mean was taken to avoid aberrant behavior in the fit. Any supernova having only a single spectrum within the specified time range was removed, unless that spectrum was taken at maximum.

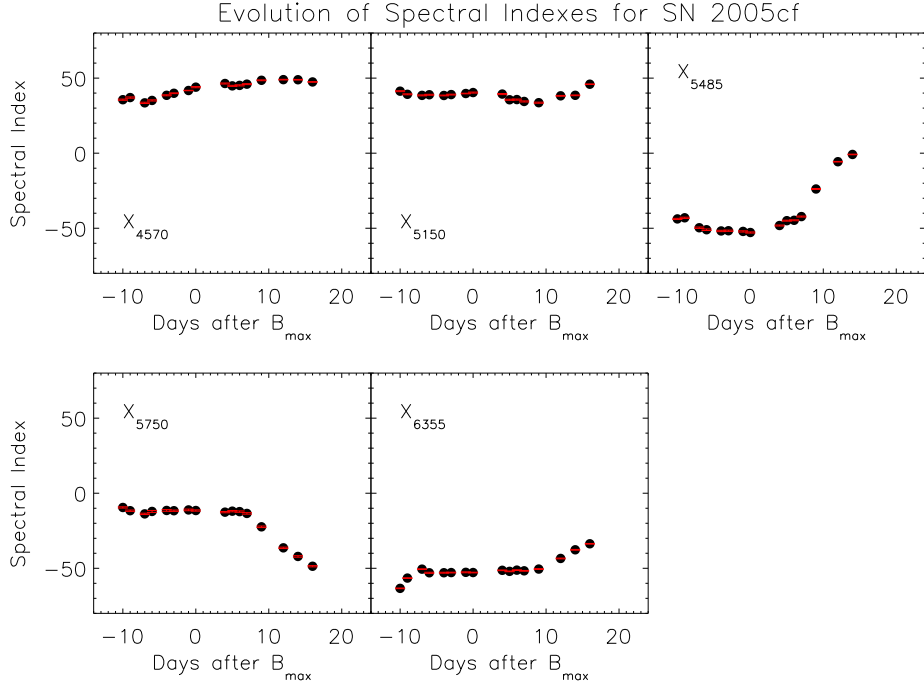
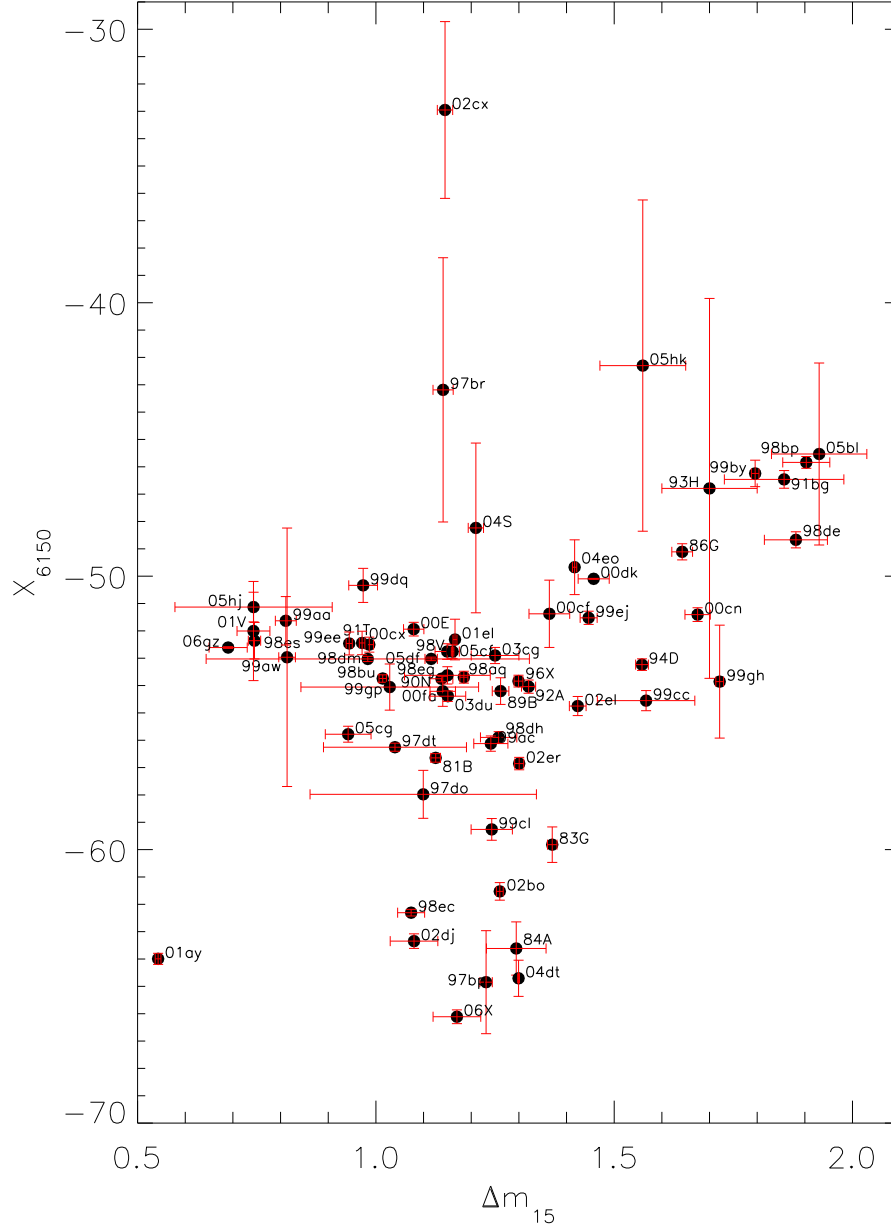


Fig. 2.7. Temporal Evolution of the X Indexes. The temporal evolution of the X indices of SN 2005cf. In order these are: (a) the emission feature at 4570 Å associated in part with the P Cygni profile of Mg II at 4471 Å, (b) the emission feature at 5150 Å associated in part with the P Cygni profile of Si II at 5041 Å, (c) the absorption “w” around 5485 Å associated around maximum with the S II 5433/5459 Å feature, (d) an absorption feature at 5750 Å associated around maximum with the Si II 5972 Å line, and (e) a strong absorption feature at 6150 Å associated around maximum with the Si II 6355 Å.



2.3.3.1 X_{6150}

It has been shown previously that the strength of the SiII 6355 Å line is not tightly correlated with the intrinsic brightness Hachinger et al. (2006). The spectral index associated with this feature is X_{6150} and Figure 2.8 confirms this observation in the main. However, the X_{6150} indexes do show a modest trend of weaker spectral strength for dimmer supernovae and supernovae with Δm_{15} less than 1.5 show large variations of the index strength. It merits mention that the several of these supernovae (e.g., SN 1997br, SN 2001ay, SN 2002cx, and SN 2005hk) are deviant with respect to the majority of the sample. It has been noted that these are all peculiar supernovae and it has been speculated that SN 1997br, SN 2002cx, and SN 2005hk may form a group distinct from most typical Type Ia supernovae (Branch et al. 2004, 2006, 2009; Howell & Nugent 2004; Jha et al. 2006b; Li et al. 1999, 2003; Phillips et al. 2007; Sahu et al. 2008).

2.3.3.2 X_{5750}

At maximum the X_{5750} index is a measure of the strength of the SiII absorption at 5972 Å. It has previously been shown that the ratio of the strength of this feature and that of the SiII 6355 Å line are well correlated with Δm_{15} Hachinger et al. (2006, 2008); Nugent et al. (1995). Using this correlation, a determination of the supernovae's maximum luminosity may be determined on the basis of a single spectra Riess et al. (1998b). These same two features have also been used to define Ia SNe subgroups Benetti et al. (2005); Branch et al. (2006, 2009).

Figure 2.9 shows the correlations with Δm_{15} . The X indexes for this line correlate tightly with Δm_{15} even without having been divided by the strength of the SiII 6355 Å line (X_{6150} at maximum). Note however, that the X index for this feature is normalized by the total variance of the wavelength scales from wavelength region between 5500 Å and 6500 Å, the variations due to SiII 6355 Å line are partially

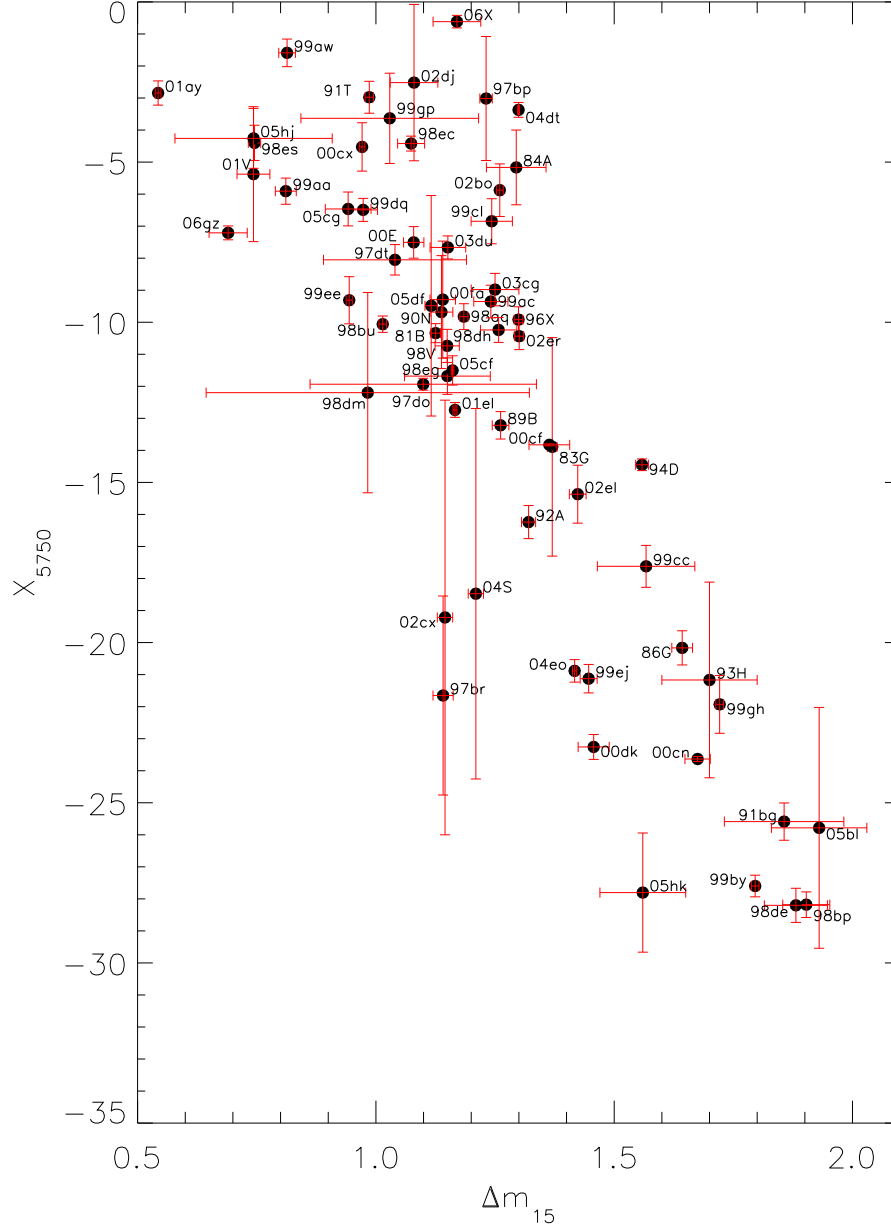


Fig. 2.9. X_{5750} vs. Δm_{15} Correlation. The correlation of the strength of X_{5750} (at maximum associated with SiII 5972) and Δm_{15} .

included in the derivations of the X indexes. The correlation between X and Δm_{15} can be well described by a linear relation. There has been some discussion as to what physical process causes this correlation (see Bongard et al. 2008; Branch et al. 2006; Garnavich et al. 2004; Hachinger et al. 2008, for some examples). We wish to emphasize that the X index of this feature measures the total strength of this feature and does not distinguish the physical origins of the feature.

2.3.3.3 X_{5485}

The “w” shaped spectral feature SII 5433/5459 Å is another important line that defines an SN Ia similar to the SiII 6355 lines (Bongard et al. 2006; Hachinger et al. 2006, 2008). The X_{5485} index is a measurement of this feature at maximum. Figure 2.10 suggests that the strength of this feature too may depend on Δm_{15} , though correlation is much weaker than that for X_{5750} . The deviant SNe are SN 1991T, SN 2001ay, SN 2005hk, SN 2006X, SN 2001V and SN 2002cx. SN 1997br has a similar spectral evolution to that of SN 1991T, but it has not been shown since it has only one spectrum within 5 days of maximum. However the X value (-30) for SN 1997br at 4 days before maximum is consistent with the X value for SN 1991T. Other 1991T-like SNe (SN 1998es, SN 1999aa, SN 1999dq, SN 2000cx) have more normal values but they still are on the upper edge of the distribution. There is apparently some diversity among slow declining SNe.

The SII line is generally much stronger than the SiII 5972 line and is thus much easier to measure. There is also much more evolution within this feature, consequently Figure 2.10 is restricted to spectra taken within 5 days of maximum.

2.3.3.4 X_{5150}

Figure 2.11 shows what might be interpreted as a slight dependence on Δm_{15} , though the trend is not as apparent as it is with the SII line or the SiII associated

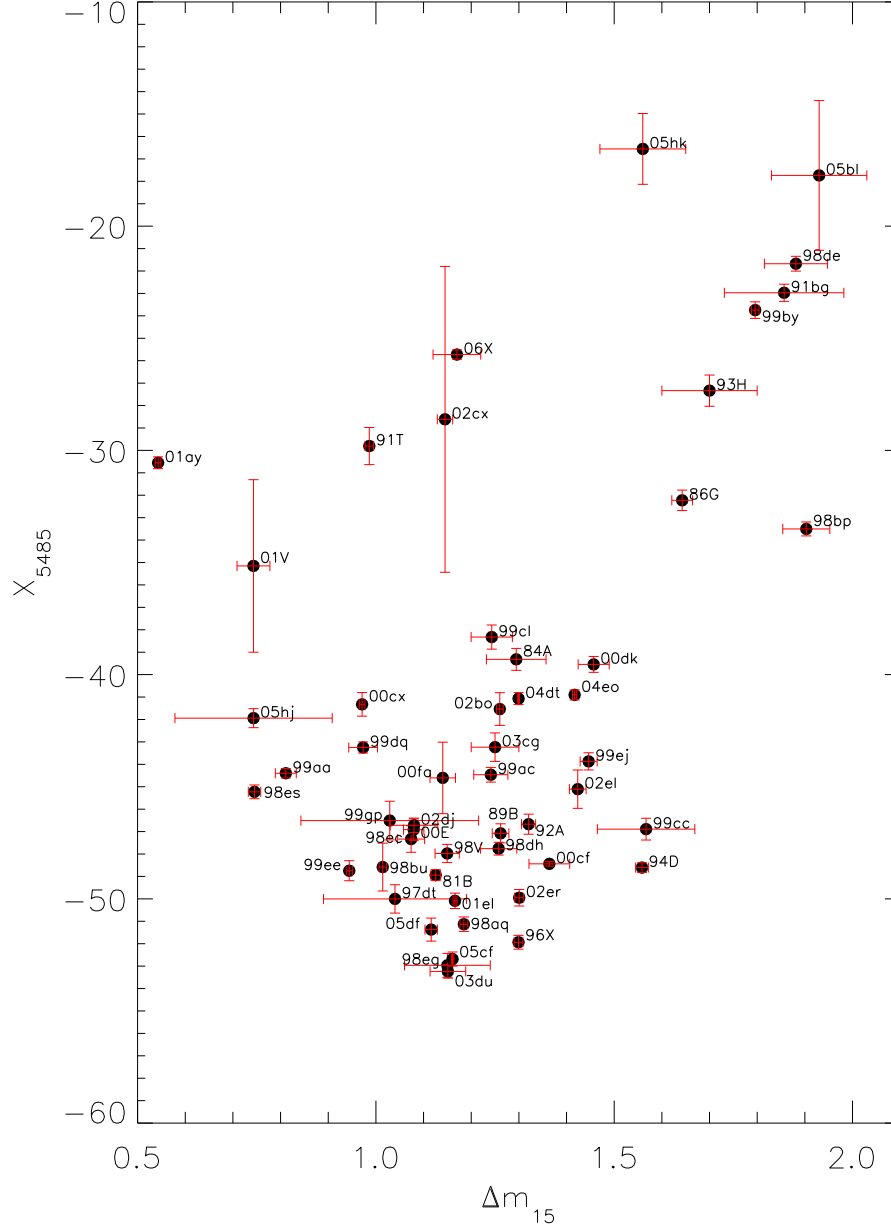


Fig. 2.10. X_{5485} vs. Δm_{15} Correlation. The correlation of the strength of X_{5485} (at maximum associated with SII 5433/5459 Å “w” feature) and Δm_{15} .

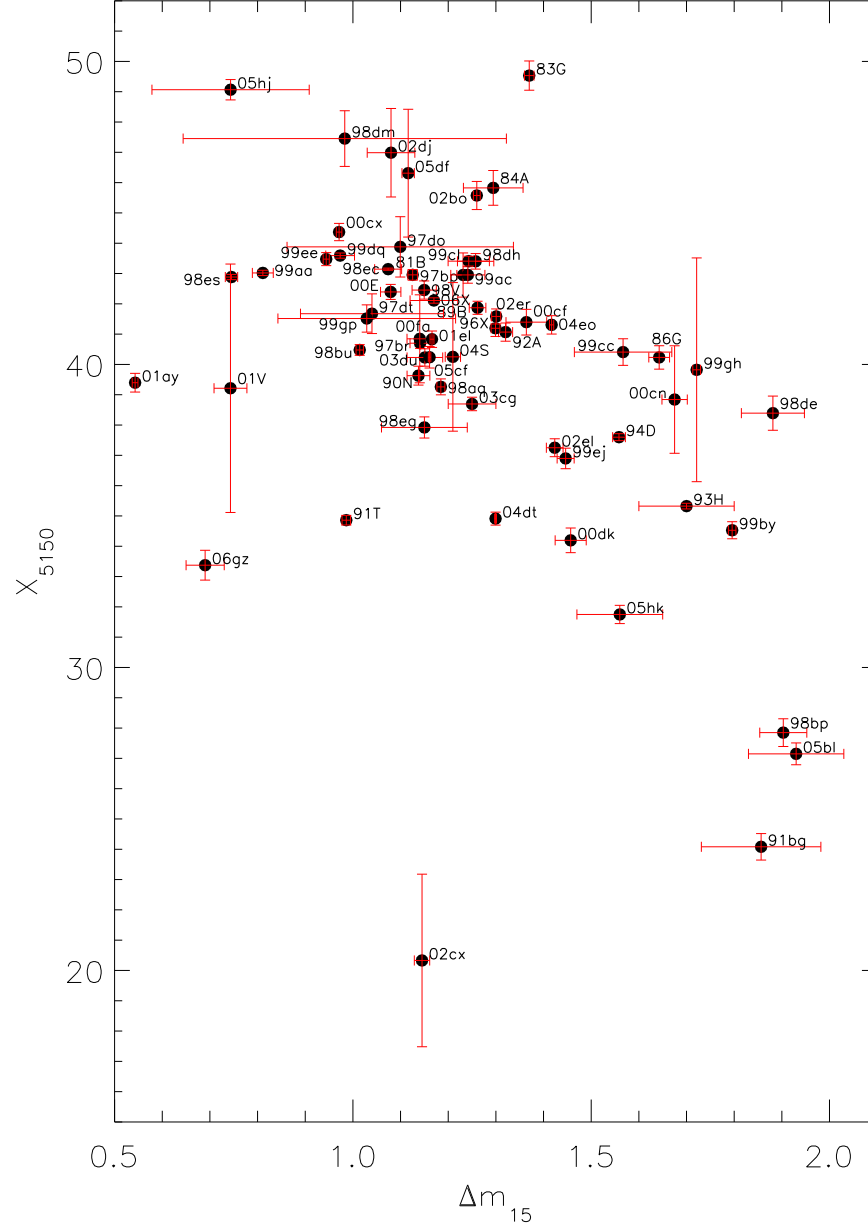


Fig. 2.11. 5150 Å Emission Peak vs. Δm_{15} Correlation. The correlation of the emission peak at 5150 Å and Δm_{15} .

indexes. The X values do decrease notably with Δm_{15} for the most sub-luminous supernovae. A majority of the data are clustered with a large amount of scatter. At maximum, X_{5150} is associated at least in part with the P Cygni profile of SiII at 5041 Å. The 5150 Å emission feature may not be a good indicator of decline rate.

2.3.3.5 X_{4570}

Similar to Figure 2.11, Figure 2.12 shows what appears to be weak dependence on Δm_{15} with the 4570 Å emission peak. This feature is partly associated with the MgII feature at 4471 Å at maximum. As with Figures 2.9 and 2.10 the more deviant SNe appear on the outer edges of the distribution. This tendency is somewhat stronger than that found for the 5150 Å feature and is in the opposite direction: the X value for 4570 Å is increasing with increasing Δm_{15} .

There is wide variation in early time evolution to this feature, consequently the data comprising Figure 2.12 is restricted to spectra taken within 5 days of maximum. Similar to the 5150 Å feature, the utility of the 4570 Å feature in specifying decline rate is uncertain.

2.3.3.6 Ratio Between the X_{4570} and X_{5150}

The suggestion of a correlation between Δm_{15} and the ratio of these two features appears in Figure 2.13, though it is also weak, particularly for the fast decliners. It appears that the 4570 Å feature has a stronger effect on this ratio than the 5150 Å feature.

Due to the restriction on the 4570 Å feature, the same restriction to spectra within 5 days of maximum is applied to Figure 2.13. This ratio may be a useful parameter for the slower decliners but not for fast decliners.

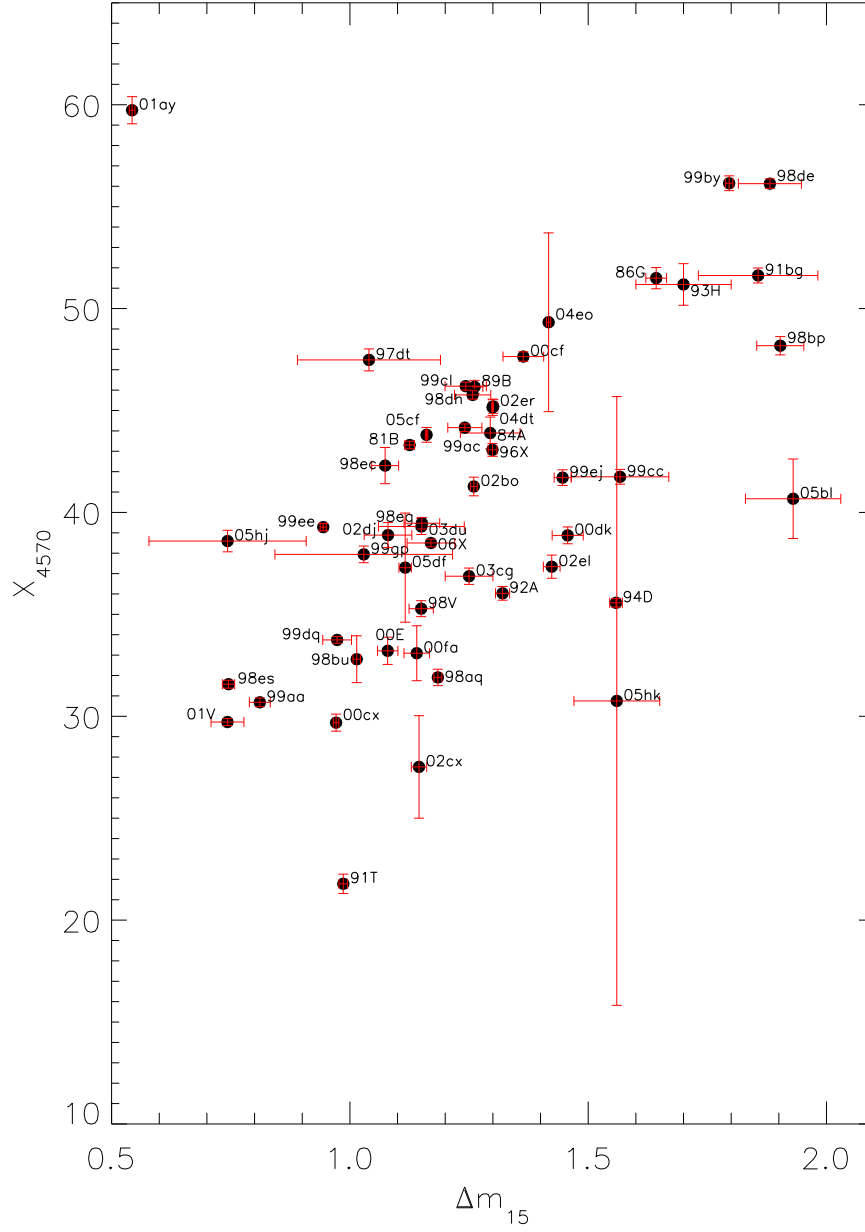


Fig. 2.12. 4570 Å Emission Peak vs. Δm_{15} Correlation. The correlation of the strength of the emission peak at 4570 Å and Δm_{15} .

Fig. 2.13. The Ratio of the Emission Peaks vs. Δm_{15} Correlation. The correlation of the ratio of the strength of the emission peak at 4570 Å and 5150 Å and Δm_{15} .

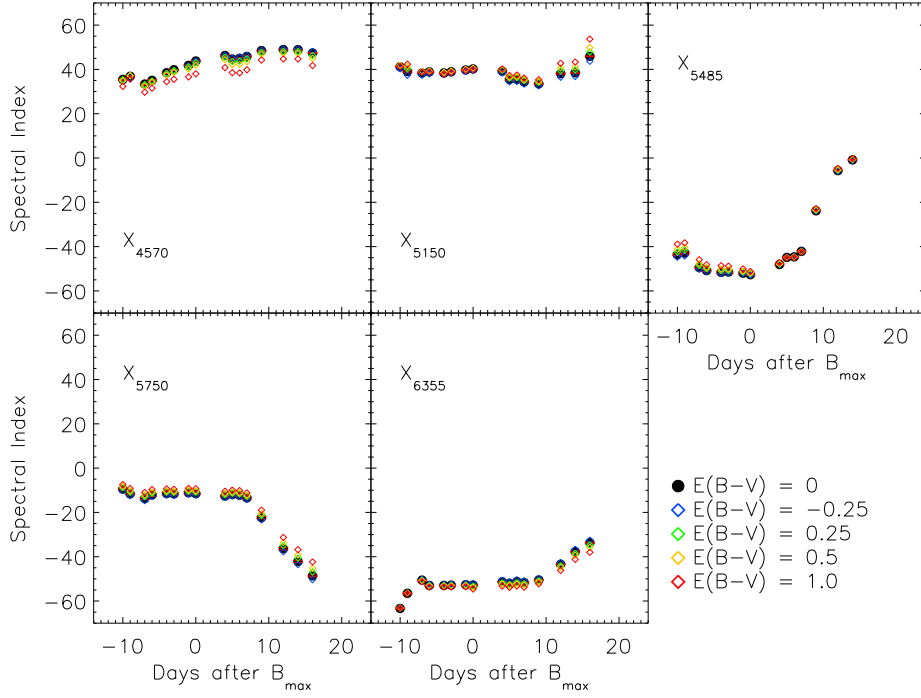


Fig. 2.14. Spectral Feature Evolution with Reddening. Same as Figure 2.7, but with the spectral indices recomputed separately for each of the 4 $E(B-V)$ values.

2.3.4 Extinction

To explore the impact of reddening on the spectral indices, each spectra in the supernova sample in Table 2.3 was reddened. Four values for $E(B-V)$ were chosen: -0.25, 0.25, 0.5, and 1.0. An identical procedure to that described in Section 2.2 was applied to these reddened spectra and spectral indexes were recalculated.

Figures 2.14 and 2.15 are similar to Figures 2.7 and 2.8, but now include the effects of various values of $E(B-V)$. Figures 2.14 and 2.15 together demonstrate that reddening has only a minor effect on spectral indices and is, in any event, an effect that can be corrected.

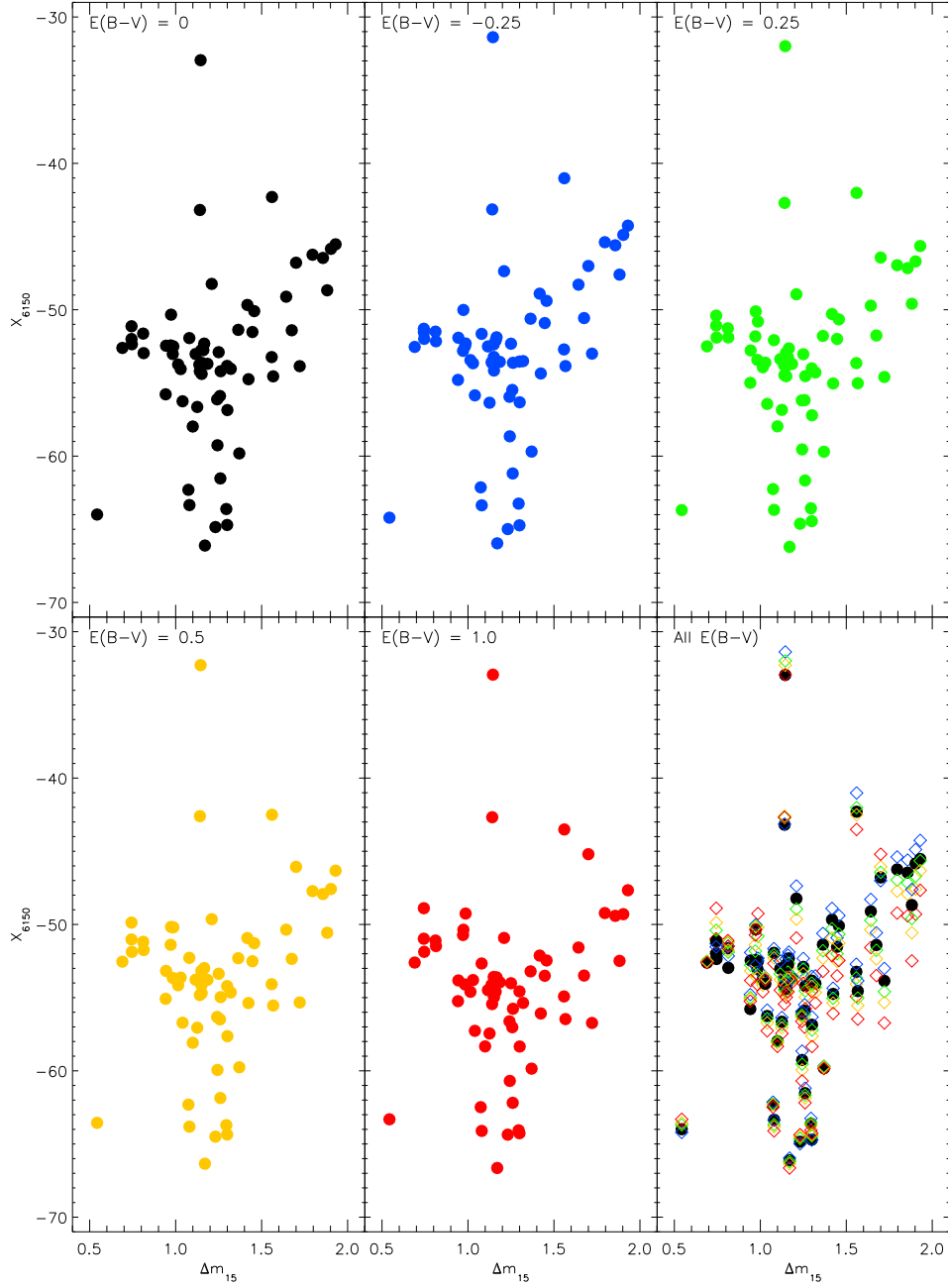


Fig. 2.15. Spectral Index Correlation with Δm_{15} Adjusted for Reddening. Same as Figure 2.8, but with the addition of four panels each displaying the spectral indices for four values of $E(B-V)$. The lower right panel overlays data from the first five panels.

3. APPLICATIONS OF WSIM

The previous chapter outlined the Wavelet Spectral Index Method (WSIM) and some preliminary applications. In this section WSIM is used to explore SNe subgroups near maximum, evolution of spectral features during the explosion, correlations between light curve shape and individual spectral features, and possible corrections for the Hubble diagram.

3.1 Type Ia SNe Subgroups: A Test

In a series of papers, David Branch and collaborators have used spectra to explore the existence of subgroups within Type Ia SNe. Branch et al. (2009) (from now on referred to as B5) divided Type Ia SNe into 4 subgroups using pseudo-equivalent widths (pEW's) and the appearance of SiII $\lambda 5750$ and $\lambda 6150$ features. These subgroups are: Core Normal (CN), Broadline (BL), Cool (CL), and Shallow Silicon (SS). A new category has been added in this work, "Known Peculiar," (KP). The SNe comprising this subgroup have been shown to be peculiar and include: SN 2001ay (Branch et al. 2006), SN 2002cx (Branch et al. 2004; Li et al. 2003), and SN 2005hk (Phillips et al. 2007). In B5, the 4 main subgroups were defined by where they lie on the $W(5750)$ - $W(6100)$ plane (Figure 2 in B5). The wavelet spectral index method and the pseudo equivalent-width method both measure the strength of individual spectral features therefore it is expected that they would show similar results. Figure 3.1 recreates Figure 2 from B5 using X_{5750} and X_{6150} values with our sample of SNe spectra. It should be noted that in Figure 3.1 the X_λ values for SNe without spectra at B-band maximum have been estimated through a simple fit as described in Chapter 2. There are two SNe with unpublished spectra, SN 1993H and SN 2005df (see Table 2.3 in Chapter 2 Wagers et al. 2010, and references therein for more information), included in this set.

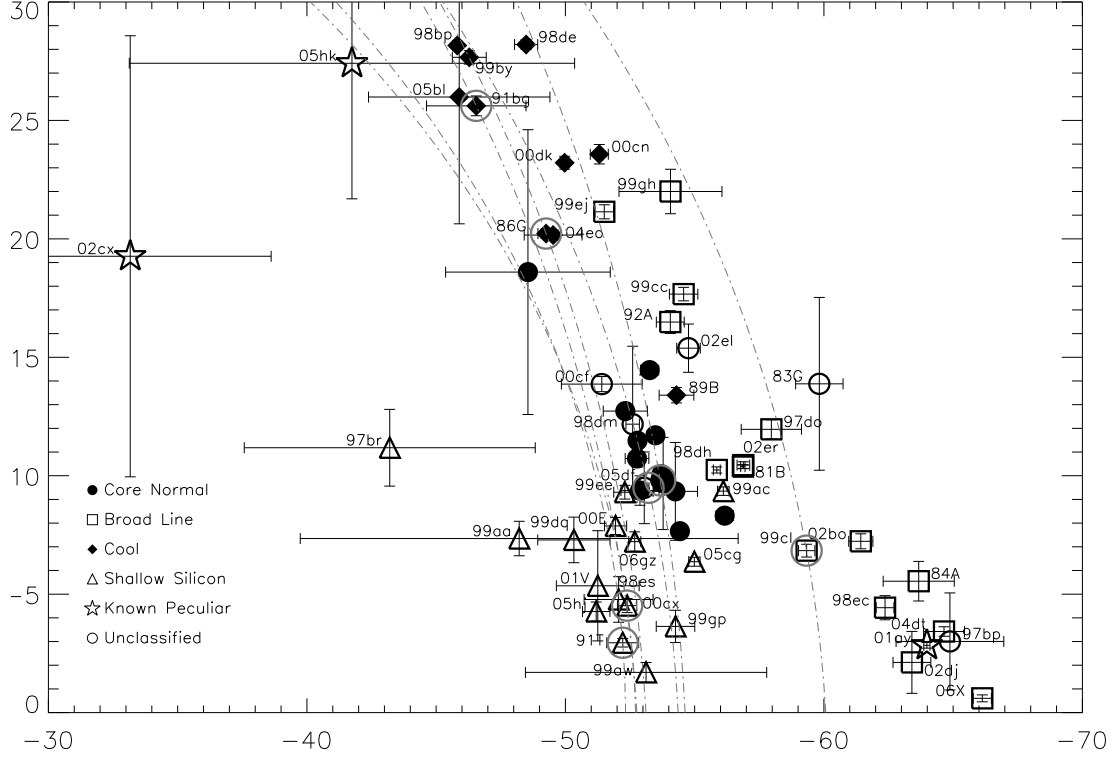


Fig. 3.1. Branch Plot Using Spectral Indexes. The subgroups of Type Ia SNe as defined by Branch et al. (2009) (referred to as B5) are indicated by the symbols. This plot has the same distinct upside-down “Y” shape as Figure 2 in B5 but now using the wavelet spectral index method as described in Chapter 2 (Wagers et al. 2010). The grouping is primarily the same as that in B5 with the addition of the “Known Peculiar” subgroup containing those SNe that have already been shown to be significantly divergent. The SNe designated by B5 as “Cool” appear weaker with respect to the other SNe due to a normalization effect. This is shown by the gray open circles and lines where the circle indicates the original position and the line illustrates the shift in both X_λ values when the 5750 SiII feature is strengthened or diminished artificially by a multiplicative constant across the feature.

WSIM does indeed show similar results to the pEW method used in B5 with a notable exception that the “Cool” SNe are measured to be weaker in X_{6150} . An explanation for this discrepancy may lie in the normalization used to calculate X_{5750} and X_{6150} . As described in Chapter 2, both X_{5750} and X_{6150} share a common normalization region ($5500 \text{ \AA} \leq \lambda \leq 6500 \text{ \AA}$). Since the normalization of each wavelet spectral index is based on the standard deviation within the region, the strength of both features will affect the normalization. To illustrate this, 6 SNe (SN 1986G, SN 1991T, SN 1991bg, SN 1998aq, SN 1999cl, SN 2000cx) with spectra taken at maximum and 1 SN (SN 2003cg) with a spectrum taken 1 day before maximum were modified to test this effect. The 5750 Si II feature was strengthened or weakened by a multiplicative constant applied to all pixels in the feature. Then the two spectral indexes in the deformed spectrum were recalculated. In Figure 3.1 the large open gray circles indicate the original position of the SNe that was used and the corresponding lines show how the measured strength of these features shifted as the 5750 \AA feature was varied.

3.2 WSIM and Evolution

Discussions concerning the feature strengths using WSIM are not limited to the time of maximum light. WSIM can also be used to study the evolution of the features during the course of the supernova explosion. The evolution of spectral indexes is shown in the figures that follow for all 64 SNe in our sample from 10 days before maximum to 25 days post-maximum. Chapter 2 introduced this use of WSIM, here simple fits to the wavelet spectral index evolution have been applied to quantitatively characterize the evolution. The evolutions of all 5 features studied are homogeneous for most SNe. Each one of these features can be fit with a simple function given by Equations 3.1 through 3.5, where t is days from B band maximum. The fits were preformed from $t = -10$ to $t = +25$ for X_{4570} , and X_{6150} ; from $t = -7$ to $t = +22$ for X_{5750} ; and from $t = -10$ to $t = +15$ for X_{5150} and X_{5485} . These ranges were chosen

due to high scatter outside of these epoch ranges. The scatter is due primarily to other lines encroaching on the spectral index region. The tables that follow give the fit parameters for each X_λ 's for each SNe and average fits for all SNe in each subgroup.

The most scatter is found in the evolution of the 4570 Å hump (see Figure 3.2), however the shape of this feature's evolution is nearly parabolic for all of the SNe studied. Equation 3.1 works well for epochs beyond a week after maximum. Earlier epochs show more complicated evolution. In particular the CN, BL, and CL SNe all show stronger emission than the parabolic fit for the CN SNe while the SS and KP SNe are weaker than the fit. At late time, 2 weeks past maximum, the CL SNe have consistently weaker X_{4570} values while the SS SNe seem to be slightly stronger implying a possible temporal (horizontal) shift and/or broadening in the parabolic behavior with the CL SNe peaking earlier and the SS SNe peaking later. This is not too surprising considering that CL SNe have a faster decline rate than CN and the SS have a slower decline rate.

$$X_{4570}(t) = A + B \times t + C \times t^2, \quad -10days \leq t \leq +25days \quad (3.1)$$

Table 3.1: Evolution Fit Parameters for X_{4570}

SN	Branch Subtype	A	B	C
1990N	CN	41.038(0.257)	1.001(0.034)	-0.040(0.002)
1994D	CN	42.607(0.082)	0.724(0.009)	-0.038(0.000)
1996X	CN	42.942(0.163)	0.810(0.035)	-0.040(0.001)
1997dt	CN	46.797(0.249)	0.618(0.080)	0.013(0.012)
1998V	CN	35.649(0.235)	2.236(0.100)	-0.095(0.007)
1998aq	CN	36.396(0.122)	1.033(0.023)	-0.030(0.001)
1998bu	CN	39.738(0.110)	1.391(0.018)	-0.060(0.001)
1998eg	CN	42.001(0.302)	1.111(0.064)	-0.047(0.003)
2000fa	CN	40.991(0.168)	1.205(0.029)	-0.043(0.002)
2001el	CN ^a
2003cg	CN	39.719(0.120)	1.104(0.019)	-0.062(0.001)
2003du	CN	40.301(0.081)	1.038(0.015)	-0.037(0.001)
2004S	CN	43.591(0.333)	1.337(0.080)	-0.060(0.004)
2005cf	CN	43.744(0.085)	0.733(0.010)	-0.033(0.001)

Table 3.1 – Continued

SN	Branch Subtype	A	B	C
Mean Values	CN	41.193(3.004)	1.103(0.413)	-0.044(0.024)
1981B	BL	43.358(0.166)	1.130(0.032)	-0.045(0.001)
1984A	BL	49.843(0.175)	0.458(0.023)	-0.019(0.002)
1991M	BL ^a
1992A	BL	40.479(0.136)	1.655(0.025)	-0.077(0.001)
1997do	BL	43.977(0.116)	0.675(0.012)	-0.027(0.001)
1998dh	BL	46.044(0.177)	1.091(0.104)	0.064(0.012)
1998ec	BL	44.197(0.173)	1.082(0.034)	-0.043(0.002)
1999cc	BL	42.099(0.154)	0.986(0.076)	-0.040(0.003)
1999cl	BL	45.938(0.078)	0.470(0.013)	0.027(0.002)
1999ej	BL	42.361(0.278)	1.931(0.110)	-0.112(0.008)
1999gd	BL ^a
1999gh	BL	52.751(0.742)	0.029(0.184)	-0.046(0.011)
2000B	BL ^a
2002bf	BL ^a
2002bo	BL	44.296(0.070)	-0.198(0.006)	0.056(0.001)
2002dj	BL	46.559(0.071)	0.599(0.006)	-0.026(0.001)
2002er	BL	47.127(0.058)	0.540(0.010)	-0.040(0.001)
2004dt	BL	42.911(0.133)	0.340(0.017)	-0.017(0.001)
Mean Values	BL	45.139(3.249)	0.771(0.586)	-0.025(0.047)
1986G	CL	48.472(0.202)	0.377(0.057)	-0.042(0.003)
1989B	CL	45.552(0.111)	1.192(0.019)	-0.070(0.001)
1991bg	CL	52.304(0.209)	-1.403(0.076)	0.036(0.003)
1998bp	CL	45.973(0.160)	0.139(0.036)	-0.018(0.002)
1998de	CL	56.416(0.205)	-0.035(0.049)	-0.062(0.017)
1999by	CL	52.864(0.099)	-0.164(0.021)	-0.013(0.001)
2000cn	CL	51.857(0.254)	0.470(0.020)	-0.059(0.002)
2000dk	CL	41.675(0.227)	1.873(0.054)	-0.107(0.007)
2004eo	CL	49.265(0.119)	0.474(0.020)	-0.045(0.001)
2005bl	CL	50.307(0.315)	-1.418(0.064)	0.035(0.003)
1997cn	CL ^a
Mean Values	CL	49.468(4.263)	0.151(1.017)	-0.035(0.045)
1991T	SS	36.803(0.075)	2.026(0.008)	-0.067(0.000)
1998ab	SS	56.563(20.539)	-0.145(2.025)	-0.015(0.050)
1998es	SS	33.295(0.091)	1.177(0.012)	-0.023(0.001)
1999aa	SS	34.562(0.087)	1.555(0.012)	-0.046(0.001)
1999ac	SS	44.042(0.075)	0.670(0.013)	-0.025(0.001)
1999aw	SS	28.456(0.702)	1.524(0.099)	-0.026(0.003)
1999dq	SS	35.219(0.078)	1.308(0.013)	-0.034(0.001)
1999ee	SS	41.755(0.065)	1.185(0.010)	-0.041(0.001)
1999gp	SS	37.897(0.146)	2.105(0.043)	-0.076(0.002)
2000E	SS	36.442(0.272)	1.283(0.036)	0.015(0.008)
2000cx	SS	28.034(0.115)	1.422(0.022)	-0.017(0.001)
2001V	SS	42.190(0.076)	1.466(0.009)	-0.059(0.000)
2005cg	SS ^a
2005hj	SS	39.192(0.295)	0.910(0.050)	0.195(0.014)
2006gz	SS	36.729(0.609)	0.733(0.035)	0.010(0.007)
Mean Values	SS	38.229(3.980)	1.451(0.494)	-0.049(0.024)
1997br	KP	37.963(0.086)	2.218(0.010)	-0.093(0.001)
2001ay	KP ^a
2002cx	KP	36.886(0.386)	1.453(0.047)	-0.066(0.002)
2004S	KP	43.591(0.333)	1.337(0.080)	-0.060(0.004)
2005hk	KP	35.631(0.173)	2.099(0.022)	-0.086(0.001)

^aThose SNe without fit parameters were not fit well by the function because the data was too sparse for a good fit.

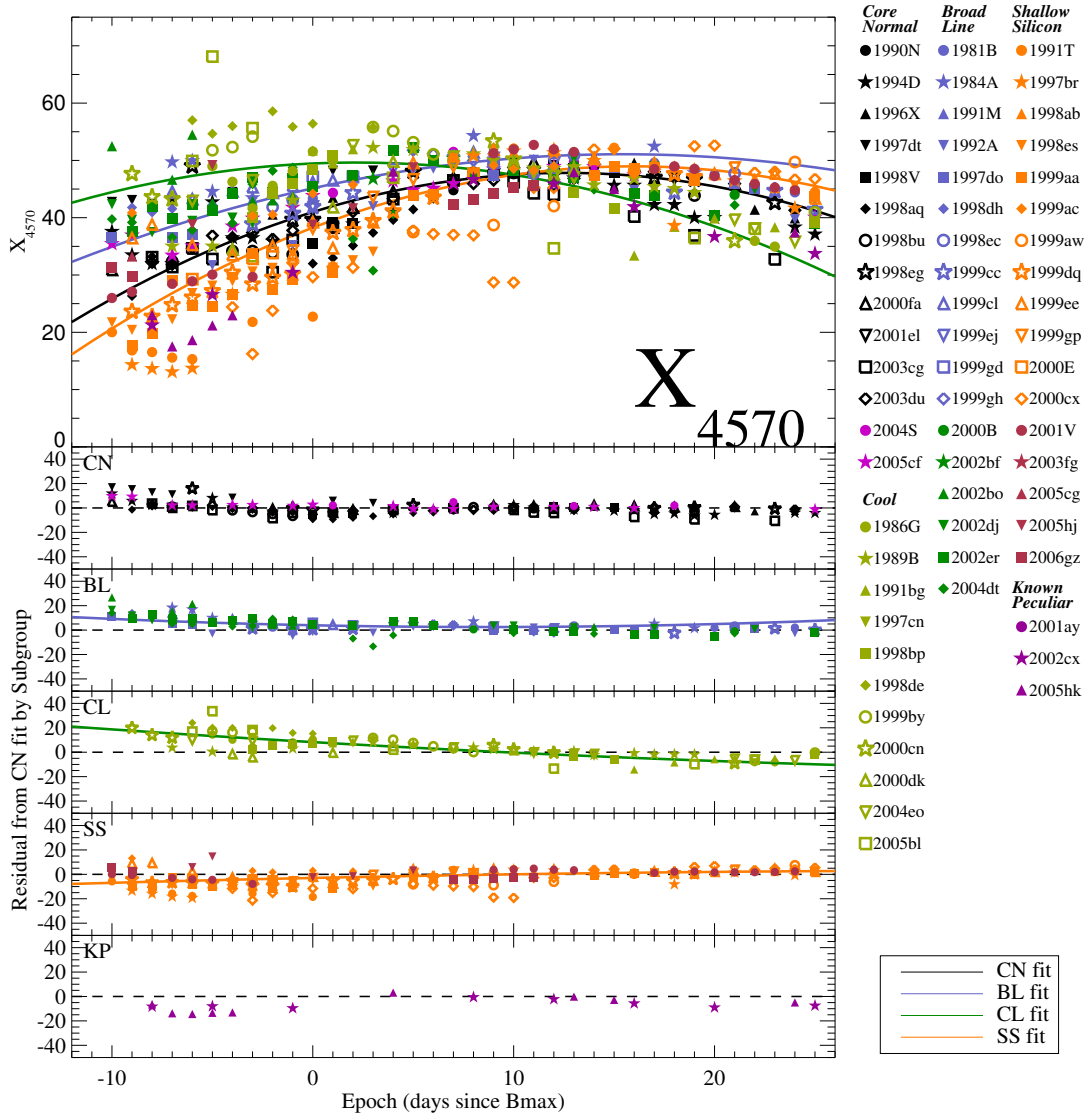


Fig. 3.2. X_{4570} Evolution. The evolution of the X_{4570} spectral index. The top panel shows measurements between 10 days before maximum to 25 days after maximum. The solid lines are average fits of each SNe subgroup as defined in Branch et al. (2009) using a simple quadratic fit (Equation 3.1) and the mean values given in Table 3.1. The mean values were determined by fitting each SNe with the defined function from 10 days pre-maximum to 25 days post-maximum. The 5 panels below show the residuals of the data with the fit. Each panel represents a different subgroup: “Core Normal” (CN), “Broad Line” (BL), “Cool” (CL), “Shallow Silicon” (SS), and “Known Peculiar” (KP) respectively.

The other emission hump (at 5150 Å) shows very subtle evolution (Figure 3.3) until about 1–2 weeks after maximum. Some SNe show a discontinuous break, this is due to an absorption feature which penetrates through the center of the emission hump far enough to split it into two separate emission features. A linear fit (Equation 3.2) is used to describe the evolution from 10 days before maximum to 15 days after maximum to avoid the discontinuity. The mean slope and mean intercept values for CN SNe are listed in Table 3.2. Comparing the other subgroups to the CN mean fit show that the BL SNe are stronger before maximum while the CL and SS SNe are weaker over the same epochs. After maximum all SNe follow closely the CN mean fit with the exception of the CL and KP SNe which are systematically weaker than the CN fit.

$$X_{5150}(t) = m \times t + b, \quad -10days \leq t \leq +15days \quad (3.2)$$

Table 3.2: Evolution Fit Parameters for X_{5150}

SN	Branch Subtype	b	m
1990N	CN	40.521(0.164)	0.140(0.016)
1994D	CN	41.328(0.058)	0.071(0.006)
1996X	CN	40.290(0.102)	0.123(0.017)
1997dt	CN	42.645(0.314)	0.293(0.056)
1998V	CN	42.209(0.173)	0.180(0.016)
1998aq	CN	39.565(0.085)	0.229(0.017)
1998bu	CN	39.549(0.081)	0.029(0.010)
1998eg	CN	38.630(0.292)	0.836(0.095)
2000fa	CN	41.338(0.183)	0.095(0.019)
2001el	CN	39.761(0.172)	-0.586(0.031)
2003cg	CN	38.169(0.089)	0.665(0.010)
2003du	CN	39.461(0.068)	0.007(0.011)
2004S	CN	35.169(0.305)	2.066(0.028)
2005cf	CN	38.564(0.072)	-0.132(0.009)
Mean Values	CN	39.800(1.893)	0.287(0.610)
1981B	BL ^a
1984A	BL	46.990(0.176)	-0.142(0.031)
1991M	BL ^a
1992A	BL	40.411(0.159)	0.039(0.022)
1997do	BL	43.019(0.113)	-0.169(0.009)
1998dh	BL	43.100(0.188)	0.254(0.032)
1998ec	BL ^a
1999cc	BL	41.034(0.194)	0.357(0.105)

Table 3.2 – Continued

SN	Branch Subtype	b	m
1999cl	BL	42.566(0.047)	0.555(0.010)
1999ej	BL	37.868(0.208)	0.089(0.026)
1999gd	BL ^a
1999gh	BL	64.895(0.200)	-3.855(0.022)
2000B	BL ^a
2002bf	BL ^a
2002bo	BL	45.455(0.035)	0.301(0.004)
2002dj	BL	43.270(0.058)	-0.060(0.006)
2002er	BL	40.963(0.058)	-0.150(0.008)
2004dt	BL	43.382(0.095)	-0.697(0.012)
Mean Values	BL	44.413(6.868)	-0.290(1.168)
1986G	CL	39.093(0.178)	0.923(0.049)
1989B	CL	38.124(0.104)	-0.289(0.012)
1991bg	CL	25.990(0.250)	-1.989(0.048)
1998bp	CL	26.975(0.169)	-1.514(0.019)
1998de	CL	35.908(0.220)	-0.545(0.060)
1999by	CL	27.991(0.149)	-2.118(0.027)
2000cn	CL	34.284(0.221)	-0.774(0.022)
2000dk	CL	33.779(0.164)	-0.407(0.026)
2004eo	CL	37.817(0.128)	-1.094(0.013)
2005bl	CL	28.672(0.574)	-1.896(0.085)
1997cn	CL ^a
Mean Values	CL	32.863(5.015)	-0.970(0.949)
1991T	SS	37.326(0.037)	0.699(0.005)
1998ab	SS ^a
1998es	SS	41.424(0.055)	0.293(0.009)
1999aa	SS	40.509(0.046)	0.302(0.006)
1999ac	SS	41.117(0.058)	-0.546(0.009)
1999aw	SS ^a
1999dq	SS	42.605(0.063)	0.487(0.012)
1999ee	SS	45.758(0.050)	0.002(0.006)
1999gp	SS	42.588(0.112)	0.508(0.029)
2000E	SS	40.605(0.114)	-0.315(0.023)
2000cx	SS	42.797(0.074)	0.882(0.008)
2001V	SS	40.496(0.052)	0.148(0.006)
2005cg	SS	...)	... ^a
2005hj	SS	44.969(0.178)	-0.840(0.038)
2006gz	SS	31.503(0.258)	-0.227(0.028)
Mean Values	SS	41.609(2.546)	0.186(0.532)
1997br	KP	39.090(0.049)	0.435(0.006)
2001ay	KP ^a
2002cx	KP	21.100(0.525)	-0.245(0.053)
2004S	KP ^a
2005hk	KP	22.573(0.129)	-0.201(0.018)

^aThose SNe without fit parameters were not fit well by the function because the data was too sparse for a good fit.

The three absorption features studied in this paper all show similar evolution. They all have relatively no evolution until 1 week post maximum where they make a rapid transition to another near constant strength (or disappear altogether as in

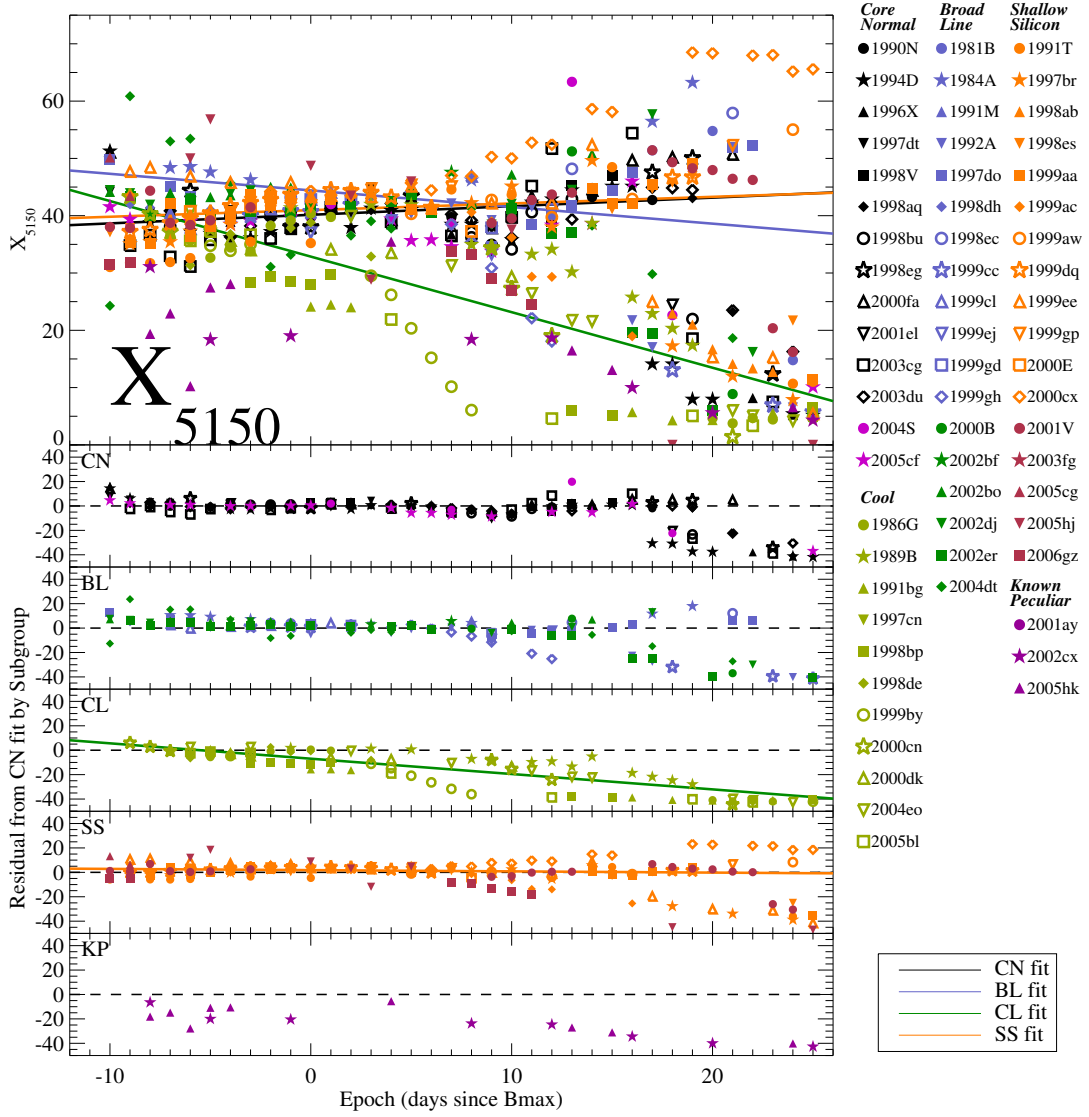


Fig. 3.3. X_{5150} Evolution. The evolution of the X_{5150} spectral index. The top panel shows measurements between 10 days before maximum to 25 days after maximum. The solid lines are average fits of each SNe subgroups as defined in Branch et al. (2009) using a simple linear fit (Equation 3.2) and the mean values given in Table 3.2. The mean values were determined by fitting each SNe with the defined function from 10 days pre-maximum to 15 days post-maximum. The 5 panels below show the residuals of the data with the fit. Each panel represents a different subgroup: “Core Normal” (CN), “Broad Line” (BL), “Cool” (CL), “Shallow Silicon” (SS), and “Known Peculiar” (KP) respectively.

the S II feature at 5485 Å see Figure 3.4). The S II feature measured by X_{5485} has much more scatter in its strength around maximum which was also seen in Chapter 2. In Figure 3.4 a fit to the CN SNe from 7 days before maximum to 20 days post-maximum is shown as a solid black line. The CN mean parameter values used in the fit are shown in Table 3.3. All SNe begin weaker than the fit at early time. The SS and CN SNe become stronger before making a transition while the BL and CL SNe stay relatively constant before the transition.

$$X_{5485}(t) = \alpha \left(\frac{1}{1 + e^{\frac{\beta-t}{\gamma}}} - 1 \right), \quad -7days \leq t \leq +20days \quad (3.3)$$

Table 3.3: Evolution Fit Parameters for X_{5485}

SN	Branch Subtype	α	β	γ
1990N	CN	48.476(0.420)	9.295(0.094)	1.237(0.037)
1994D	CN	49.490(0.103)	7.959(0.021)	1.461(0.017)
1996X	CN	51.500(0.133)	8.011(0.033)	1.491(0.028)
1997dt	CN ^a
1998V	CN	48.575(0.505)	5.287(0.700)	1.121(0.270)
1998aq	CN	50.675(0.146)	9.054(0.220)	1.133(0.113)
1998bu	CN	48.128(0.135)	8.105(0.022)	1.117(0.018)
1998eg	CN ^a
2000fa	CN	48.109(0.572)	7.168(0.106)	2.147(0.067)
2001el	CN	50.553(0.418)	8.345(0.154)	1.617(0.326)
2003cg	CN	40.070(0.259)	7.888(0.066)	1.300(0.051)
2003du	CN	52.582(0.106)	9.350(0.020)	1.691(0.019)
2004S	CN	51.860(0.385)	8.189(0.049)	1.336(0.033)
2005cf	CN	49.612(0.120)	9.021(0.026)	1.375(0.019)
Mean Values	CN	49.462(3.306)	7.925(1.317)	1.321(0.452)
1981B	BL ^a
1984A	BL ^a
1991M	BL ^a
1992A	BL	43.580(0.274)	8.335(0.036)	1.510(0.032)
1997do	BL	44.186(0.225)	7.519(0.066)	2.466(0.046)
1998dh	BL ^a
1998ec	BL ^a
1999cc	BL ^a
1999cl	BL	38.002(0.277)	5.066(0.209)	1.409(0.089)
1999ej	BL	43.659(0.183)	8.878(0.030)	1.009(0.047)
1999gd	BL ^a
1999gh	BL	31.483(0.622)	7.236(0.064)	1.232(0.042)
2000B	BL ^a
2002bf	BL ^a
2002bo	BL ^a
2002dj	BL	44.630(0.115)	8.289(0.038)	1.188(0.035)
2002er	BL	48.563(0.112)	8.621(0.034)	1.871(0.025)

Table 3.3 – Continued

SN	Branch Subtype	α	β	γ
2004dt	BL	38.792(0.109)	8.274(0.143)	1.068(0.077)
Mean Values	BL	42.014(3.858)	7.878(1.319)	1.299(0.686)
1986G	CL ^a
1989B	CL	45.980(0.212)	8.223(0.040)	1.456(0.040)
1991bg	CL ^a
1998bp	CL	33.778(0.192)	2.124(1.050)	0.389(0.370)
1998de	CL ^a
1999by	CL	43.000(8.737)	1.556(3.906)	9.113(2.237)
2000cn	CL ^a
2000dk	CL	38.188(0.211)	6.968(0.105)	1.233(0.042)
2004eo	CL	41.438(0.172)	6.985(0.033)	1.199(0.058)
2005bl	CL
1997cn	CL
Mean Values	CL	39.898(5.075)	7.615(0.737)	1.113(0.383)
1991T	SS	36.458(0.105)	9.744(0.028)	0.694(0.060)
1998ab	SS ^a
1998es	SS ^a
1999aa	SS	40.554(0.110)	6.944(0.121)	0.704(0.082)
1999ac	SS	40.529(0.120)	9.559(0.028)	1.196(0.029)
1999aw	SS	50.203(1.614)	12.891(0.218)	2.143(0.450)
1999dq	SS ^a
1999ee	SS	47.395(0.157)	7.493(0.051)	1.495(0.036)
1999gp	SS	44.267(0.264)	8.310(0.236)	0.923(0.163)
2000E	SS ^a
2000cx	SS	40.121(0.161)	8.956(0.028)	1.528(0.020)
2001V	SS	31.583(0.169)	9.072(0.045)	1.621(0.040)
2005cg	SS ^a
2005hj	SS	40.586(0.251)	8.632(0.084)	1.678(0.066)
2006gz	SS	49.456(0.706)	9.151(0.081)	2.295(0.082)
Mean Values	SS	38.661(4.476)	8.924(2.189)	1.064(0.586)
1997br	KP	32.807(0.167)	8.440(0.032)	1.387(0.043)
2001ay	KP ^a
2002cx	KP ^a
2004S	KP	51.860(0.385)	8.189(0.049)	1.336(0.033)
2005hk	KP ^a

^aThose SNe without fit parameters were not fit well by the function because the data was too sparse for a good fit.

The two X_λ 's measuring the Si II absorption have less scatter. Previously, Folatelli (2004) studied the evolution of the SiII features at 5750 Å and 6150 Å using equivalent widths. It was found that the 5750 Å feature had no evolution within 12 days of maximum and this is consistent with the results found here, however a gradual increase in the pEW of 6150 Å was found from 15 days before maximum to 60 days after maximum which is in disagreement with the results of this paper.

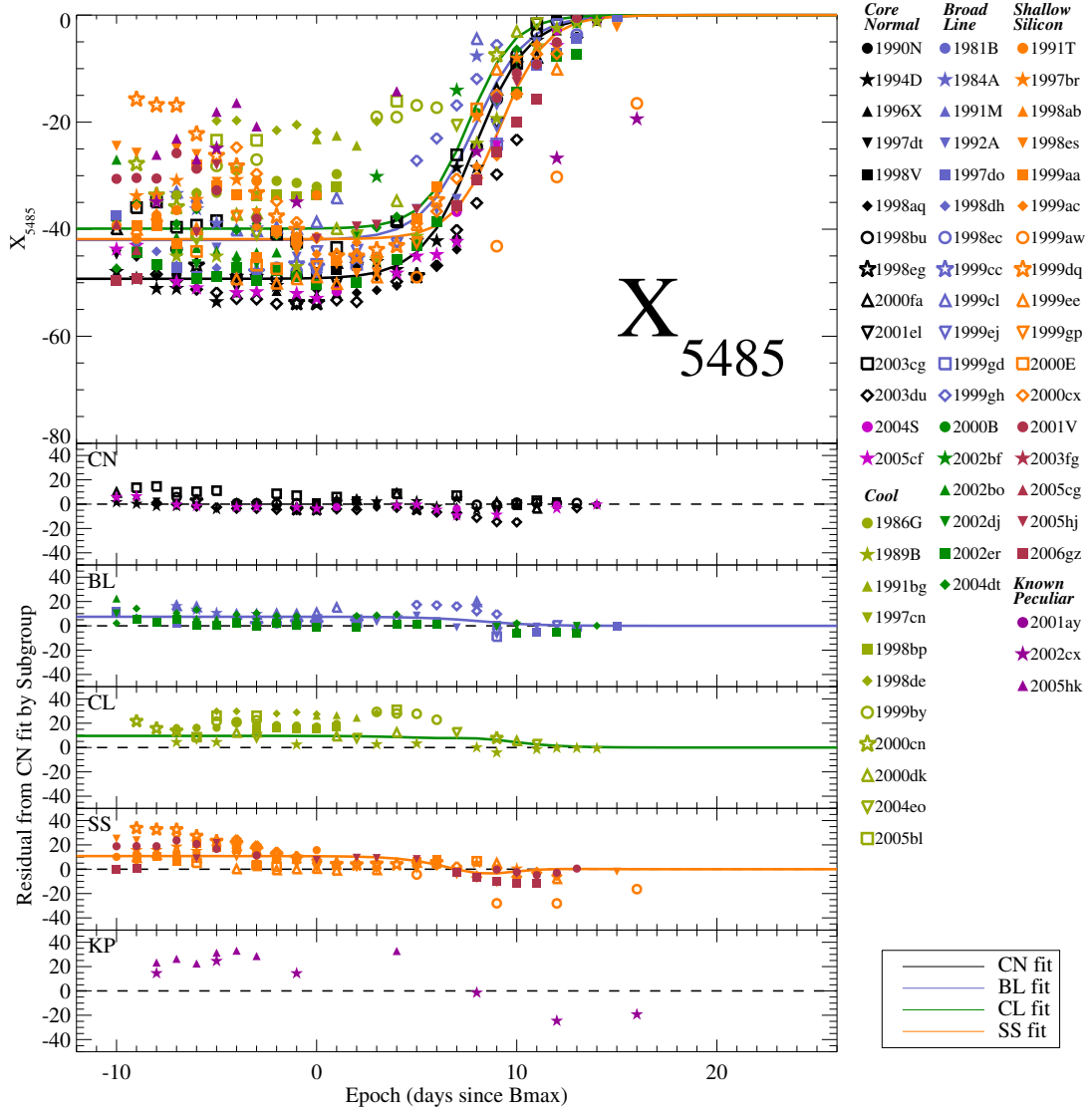


Fig. 3.4. X_{5485} Evolution. The evolution of the X_{5485} spectral index. The top panel shows measurements between 10 days before maximum to 25 days after maximum. The solid lines are average fits of each SNe subgroups as defined in Branch et al. (2009) using a simple fit given by Equation 3.3 and the mean values given in Table 3.3. The mean values were determined by fitting the function from 7 days pre-maximum to 20 days post-maximum. The 5 panels below show the residuals of the data with the fit. Each panel represents a different subgroup: “Core Normal” (CN), “Broad Line” (BL), “Cool” (CL), “Shallow Silicon” (SS), and “Known Peculiar” (KP) respectively.

Evolution of pEW for other spectral features has been found to be similar to the evolution here using X_λ , see Folatelli (2004) and Bronder et al. (2007, 2008).

Figure 3.5 shows the evolution of the X_{5750} as a black solid line showing the average fit for all CN SNe from 7 days before maximum and 20 days after maximum as given in Equation 3.4 using the CN mean values in Table 3.4. From the residual plots at the bottom of Figure 3.5 the BL SNe become weaker than the CN mean fit 1 week before maximum and then run parallel to the CN mean fit after that time. Before the transition the CL SNe have much stronger absorption than the CN mean fit but then they are weaker after the transition. This is due to the fact that the CL SNe have little to no transition from early to late time. As their name implies, the Shallow Silicon (SS) SNe start out much weaker than the rest of the sample but their X_{5750} becomes stronger and is comparable to the CN mean fit around 5 days after maximum. SS SNe are stronger after the transition due to a more drastic transition in this subgroup compared to the CN mean fit. The KP SNe have no noticeable transition which is evident in the residual plot where the KP SNe start stronger and end weaker than the CN mean fit.

$$X_{5750}(t) = \frac{\alpha}{1 + e^{\frac{\beta-t}{\gamma}}} + \epsilon, \quad -7days \leq t \leq +20days \quad (3.4)$$

The reason that X_{5750} becomes stronger by a week after maximum is likely due to contamination by Na ID which becomes progressively stronger after maximum. The best fitting synthetic spectra suggest this contamination and is most prominently seen in 1991bg-like SNe (Branch et al. 2005, 2006, 2008; Doull & Baron 2011; Filippenko et al. 1992b; Folatelli et al. 2012; Garnavich et al. 2004; Taubenberger et al. 2008). However, Mazzali et al. (1997) showed that the models do not naturally reproduce an appropriate absorption feature and the Na I distribution must be manually manipulated. Leibundgut et al. (1993) suggested that this feature could be a blend rather than Na ID. As the spectra evolve, this feature's shape changes which supports the idea that the feature is produced by a different element. The wavelet spectral

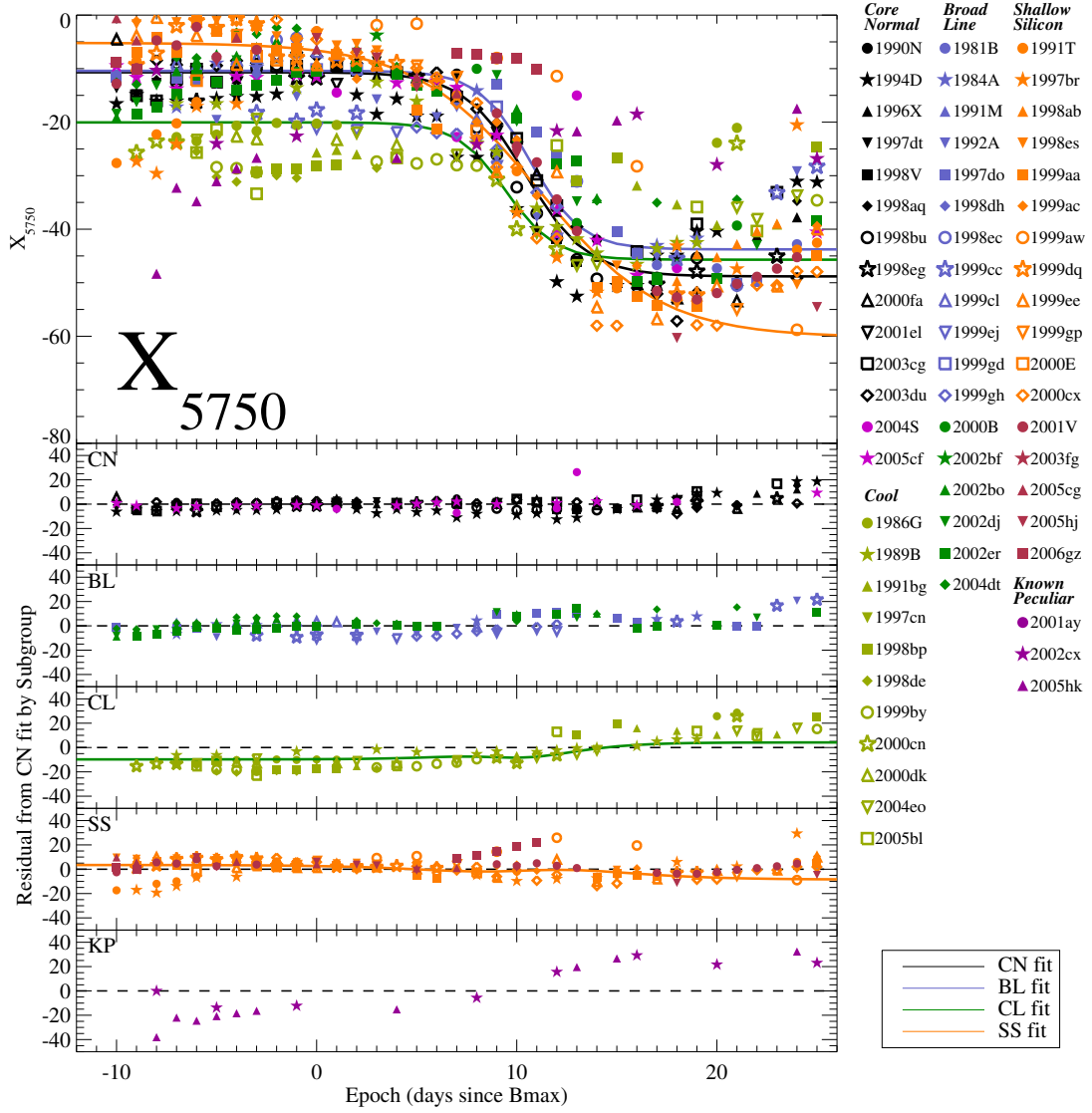


Fig. 3.5. X_{5485} Evolution. The evolution of the X_{5750} spectral index. The top panel shows measurements between 10 days before maximum to 25 days after maximum. The solid lines are average fits of each SNe subgroups as defined in Branch et al. (2009) using a simple fit given by Equation 3.4 and the mean values given in Table 3.4. The mean values were determined by fitting the function from 7 days pre-maximum to 20 days post-maximum. The 5 panels below show the residuals of the data with the fit. Each panel represents a different subgroup: “Core Normal” (CN), “Broad Line” (BL), “Cool” (CL), “Shallow Silicon” (SS), and “Known Peculiar” (KP) respectively.

indexes are defined only by their approximate wavelength and not the mechanism to produce their features. As a consequence, X_{5750} follows the absorption feature near 5750 Å and is insensitive to the origin of the feature.

Table 3.4: Evolution Fit Parameters for X_{5750}

SN	Branch Subtype	α	β	γ	ϵ
1990N	CN	-42.230(1.621)	11.723(0.258)	1.700(0.129)	-8.454(0.500)
1994D	CN	-31.032(0.195)	8.455(0.045)	1.264(0.035)	-15.715(0.125)
1996X	CN	-30.549(0.331)	9.606(0.125)	1.350(0.064)	-10.647(0.153)
1997dt	CN a
1998V	CN	-40.834(1.254)	10.411(0.376)	1.316(0.365)	-10.243(0.291)
1998aq	CN	-41.486(0.387)	9.699(0.539)	1.386(0.262)	-9.178(0.233)
1998bu	CN	-37.506(0.332)	9.497(0.045)	1.435(0.045)	-10.382(0.148)
1998eg	CN	-38.322(0.694)	10.985(0.000)	0.156(0.000)	-11.762(0.362)
2000fa	CN	-46.262(1.062)	11.152(0.131)	2.259(0.127)	-8.546(0.447)
2001el	CN	-35.130(3.646)	11.339(1.264)	2.258(1.003)	-12.544(0.405)
2003cg	CN	-31.517(0.940)	10.207(0.146)	1.541(0.122)	-10.648(0.291)
2003du	CN	-44.629(0.304)	11.162(0.061)	2.091(0.048)	-8.494(0.114)
2004S	CN	-56.908(11.259)	11.959(1.151)	6.307(1.496)	-5.768(3.760)
2005cf	CN	-38.204(0.632)	10.994(0.100)	1.728(0.068)	-11.485(0.151)
Mean Values	CN	-39.585(7.245)	10.553(1.015)	1.907(1.428)	-10.297(2.410)
1981B	BL a
1984A	BL	-31.736(0.701)	8.799(-0.000)	0.368(0.051)	-10.870(0.334)
1991M	BL a
1992A	BL	-27.422(0.378)	9.876(0.083)	1.181(0.109)	-17.899(0.259)
1997do	BL	-38.758(0.434)	12.926(0.056)	1.735(0.047)	-11.366(0.278)
1998dh	BL	-34.008(0.000)	21.197(0.000)	0.113(0.000)	-12.115(0.181)
1998ec	BL a
1999cc	BL	-36.254(0.000)	26.172(0.000)	0.267(0.000)	-19.164(0.259)
1999cl	BL a
1999ej	BL a
1999gd	BL a
1999gh	BL	-16.532(1.001)	10.147(0.155)	0.965(0.097)	-21.376(0.211)
2000B	BL a
2002bf	BL a
2002bo	BL a
2002dj	BL	-38.888(0.274)	11.705(0.043)	1.457(0.032)	-8.398(0.166)
2002er	BL	-38.970(0.368)	12.965(0.063)	1.559(0.052)	-12.445(0.124)
2004dt	BL	-30.987(0.371)	7.995(0.195)	2.115(0.104)	-4.472(0.171)
Mean Values	BL	-33.362(5.447)	10.643(1.953)	1.270(0.646)	-10.411(4.273)
1986G	CL a
1989B	CL	-29.201(0.591)	9.518(0.130)	1.503(0.112)	-15.174(0.247)
1991bg	CL a
1998bp	CL	-0.767(0.436)	6.857(0.000)	0.256(0.000)	-28.594(0.163)
1998de	CL a
1999by	CL a
2000cn	CL	-20.049(1.014)	9.302(0.089)	0.484(0.074)	-23.730(0.617)
2000dk	CL a
2004eo	CL	-27.682(1.160)	9.552(0.244)	1.676(0.149)	-21.238(0.194)
2005bl	CL a
1997cn	CL a
Mean Values	CL	-25.644(4.904)	9.457(0.136)	1.221(0.644)	-20.048(4.400)
1991T	SS	-48.959(1.467)	10.299(0.163)	2.053(0.145)	-6.580(0.536)
1997br	SS	-27.590(0.870)	9.341(0.093)	0.853(0.066)	-18.325(0.774)

Table 3.4 – Continued

SN	Branch Subtype	α	β	γ	ϵ
1998ab	SS ^a
1998es	SS	-56.498(1.277)	10.566(0.295)	3.197(0.176)	-2.041(0.529)
1999aa	SS	-50.388(0.664)	7.961(0.134)	2.714(0.116)	-4.699(0.306)
1999ac	SS	-76.194(12.472)	14.724(1.505)	5.152(0.625)	-4.579(0.898)
1999aw	SS ^a
1999dq	SS	-56.530(5.148)	12.396(1.111)	3.681(0.484)	-4.797(0.600)
1999ee	SS	-49.187(0.871)	10.518(0.128)	2.598(0.119)	-7.251(0.340)
1999gp	SS ^a
2000E	SS	-50.441(-0.000)	8.447(-0.000)	0.413(0.019)	-8.841(0.229)
2000cx	SS	-56.639(0.621)	10.151(0.056)	2.015(0.050)	-4.957(0.269)
2001V	SS	-47.499(0.563)	11.202(0.066)	2.035(0.078)	-6.330(0.399)
2005cg	SS ^a
2005hj	SS	-79.666(12.424)	13.579(1.428)	4.419(0.724)	-1.992(1.501)
2006gz	SS ^a
Mean Values	SS	-51.606(13.420)	10.876(2.023)	2.785(1.279)	-6.825(4.918)
1997br	KP	-27.590(0.870)	9.341(0.093)	0.853(0.066)	-18.325(0.774)
2001ay	KP ^a
2002cx	KP	-91.571(-0.000)	20.205(-0.000)	0.078(0.005)	-21.816(0.802)
2004S	KP	-56.908(11.259)	11.959(1.151)	6.307(1.496)	-5.768(3.760)
2005hk	KP ^a

^aThose SNe without fit parameters were not fit well by the function because the data was too sparse for a good fit.

The X_{6150} evolution (as shown in Figure 3.6) shows the least scatter for all SNe, particularly around the time of maximum light. Due to their broader line profiles, the BL SNe show much stronger values for X_{6150} but their evolution still parallels the CN mean fit. These broader lines are thought to be due to a wider spatial range of silicon in the ejecta (Benetti et al. 2005; Blondin et al. 2012; Branch et al. 2006, 2009; Wang, X. et al. 2009). Being nearly consistent with the CN mean fit, the CL SNe are slightly weaker around maximum and become much stronger after transitions. As with X_{5750} , this spectral index has a smaller transition for the CL SNe. The SS SNe evolve very nearly the same as the CN mean fit with more scatter before 5 days before maximum and after transition. There is only a hint of transition in the KP SNe causing them to begin weaker and become stronger after transition.

$$X_{6150}(t) = \frac{\alpha}{1 + e^{\frac{\beta-t}{\gamma}}} + \epsilon, \quad -10days \leq t \leq +25days \quad (3.5)$$

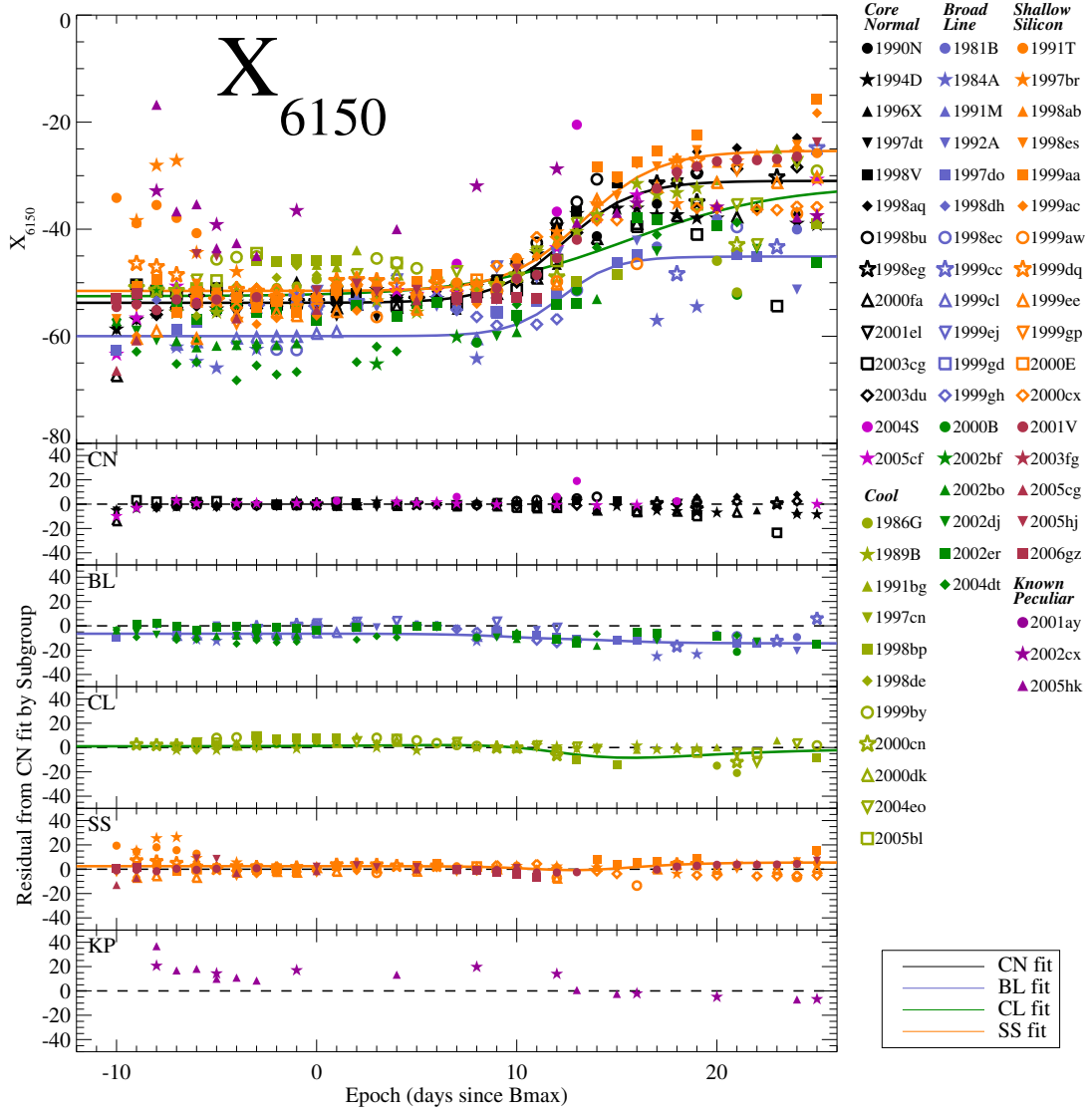


Fig. 3.6. X_{6150} Evolution. The evolution of the X_{6150} spectral index. The top panel shows measurements between 10 days before maximum to 25 days after maximum. The solid lines are average fits of each SNe subgroups as defined in Branch et al. (2009) using a simple fit given by Equation 3.5 and the mean values given in Table 3.5. The mean values were determined by fitting the function from 10 days pre-maximum to 25 days post-maximum. The 5 panels below show the residuals of the data with the fit. Each panel represents a different subgroup: “Core Normal” (CN), “Broad Line” (BL), “Cool” (CL), “Shallow Silicon” (SS), and “Known Peculiar” (KP) respectively.

Table 3.5: Evolution Fit Parameters for X_{6150}

SN	Branch Subtype	α	β	γ	ϵ
1990N	CN	20.168(1.939)	13.232(0.223)	1.453(0.558)	-54.011(0.373)
1994D	CN	17.170(0.139)	9.775(0.068)	1.519(0.051)	-54.406(0.082)
1996X	CN ^a
1997dt	CN ^a
1998V	CN	24.723(2.385)	12.077(0.270)	1.633(0.425)	-52.571(0.216)
1998aq	CN	31.395(0.463)	13.186(0.292)	2.831(0.122)	-53.785(0.148)
1998bu	CN	25.550(0.296)	11.184(0.053)	1.429(0.042)	-54.423(0.113)
1998eg	CN	23.074(0.608)	11.717(1.101)	1.756(0.349)	-53.596(0.397)
2000fa	CN	18.038(0.635)	12.080(0.208)	1.860(0.163)	-55.199(0.256)
2001el	CN	42.240(0.785)	18.000(0.000)	3.566(0.211)	-52.620(0.214)
2003cg	CN ^a
2003du	CN	26.017(0.215)	12.891(0.083)	1.982(0.061)	-54.386(0.080)
2004S	CN	22.609(0.530)	9.978(0.166)	1.865(0.109)	-50.696(0.331)
2005cf	CN	24.053(0.276)	12.217(0.108)	2.517(0.084)	-54.215(0.109)
Mean Values	CN	22.773(8.734)	12.187(2.102)	1.739(0.951)	-53.517(1.170)
1981B	BL ^a
1984A	BL	12.727(4.994)	16.331(1.647)	2.101(1.566)	-64.418(0.246)
1991M	BL ^a
1992A	BL	10.576(0.236)	10.971(0.229)	0.932(0.154)	-54.445(0.144)
1997do	BL	14.792(0.297)	11.957(0.110)	1.817(0.103)	-59.057(0.184)
1998dh	BL	27.650(0.000)	16.626(0.000)	0.688(0.000)	-54.209(0.110)
1998ec	BL ^a
1999cc	BL	...) ^a
1999cl	BL ^a
1999ej	BL ^a
1999gd	BL ^a
1999gh	BL	26.278(0.000)	21.087(0.000)	0.315(0.000)	-55.461(0.083)
2000B	BL ^a
2002bf	BL ^a
2002bo	BL ^a
2002dj	BL	17.101(0.225)	12.746(0.077)	1.483(0.072)	-60.508(0.102)
2002er	BL ^a
2004dt	BL	26.605(0.355)	10.400(0.159)	2.391(0.110)	-65.443(0.111)
Mean Values	BL	14.873(5.985)	12.284(2.071)	1.307(0.885)	-59.979(4.207)
1986G	CL	2.840(0.380)	-1.149(0.322)	0.623(0.280)	-52.045(0.218)
1989B	CL	23.582(0.586)	11.496(0.167)	1.862(0.136)	-55.087(0.186)
1991bg	CL ^a
1998bp	CL ^a
1998de	CL ^a
1999by	CL ^a
2000cn	CL ^a
2000dk	CL	3.342(0.914)	0.043(1.200)	1.390(1.091)	-51.735(0.745)
2004eo	CL	15.185(0.419)	10.495(0.295)	3.313(0.304)	-50.940(0.212)
2005bl	CL	11.980(1.020)	14.234(2.877)	1.052(1.304)	-47.214(0.454)
1997cn	CL ^a
Mean Values	CL	20.841(4.899)	15.526(7.864)	3.851(2.307)	-52.529(2.237)
1991T	SS	21.332(0.337)	13.592(0.184)	1.171(0.132)	-46.836(0.236)
1998ab	SS ^a
1998es	SS	28.755(0.530)	13.583(0.206)	2.199(0.225)	-52.308(0.181)
1999aa	SS	28.657(0.417)	13.896(0.094)	2.400(0.124)	-46.411(0.144)
1999ac	SS	39.508(0.458)	13.311(0.103)	2.572(0.074)	-57.270(0.129)
1999aw	SS ^a
1999dq	SS	24.178(1.449)	12.485(1.493)	1.875(0.437)	-50.510(0.190)
1999ee	SS	23.252(0.271)	12.910(0.068)	0.615(0.041)	-54.459(0.146)
1999gp	SS ^a
2000E	SS ^a

Table 3.5 – Continued

SN	Branch Subtype	α	β	γ	ϵ
2000cx	SS	15.076(0.253)	10.623(0.093)	1.442(0.088)	-51.597(0.159)
2001V	SS	27.739(0.333)	13.860(0.102)	2.247(0.075)	-53.843(0.211)
2005cg	SS ^a
2005hj	SS	27.062(0.991)	15.382(0.488)	2.321(0.299)	-50.513(0.311)
2006gz	SS	20.793(0.000)	29.059(0.000)	0.408(0.000)	-52.804(0.176)
Mean Values	SS	25.823(6.360)	13.666(1.687)	1.961(0.683)	-51.026(3.658)
1997br	KP	22.668(1.080)	17.014(0.290)	2.766(0.243)	-46.513(0.345)
2001ay	KP ^a
2002cx	KP	-5.506(1.110)	18.081(1.305)	1.962(1.263)	-32.070(0.730)
2004S	KP	22.609(0.530)	9.978(0.166)	1.865(0.109)	-50.696(0.331)
2005hk	KP ^a

^aThose SNe without fit parameters were not fit well by the function because the data was too sparse for a good fit.

3.3 Correlation Evolution

At B-band maximum there are several features that correlate with $\Delta m_{15}(B)$ as hinted in Chapter 2. A more detailed table of the calculated Pearson’s correlation coefficients is given in Table 3.6. The first line of each row in Table 3.6 shows correlations calculated using all SNe in our sample that were spectroscopically observed at the time of B-band maximum. The second line in each row show the correlations excluding any “Broad Line” and “Known Peculiar” SNe with spectra at maximum. At maximum there are 23 SNe with spectra in our sample this implies that a Pearson’s correlation coefficient of 0.3961 has a 5% chance of occurring in purely random data. Of these 23 SNe only 2, SN 1999cl and SN 2001ay, are within the BL or KP subgroup. For 21 data points a Pearson’s correlation coefficient of 0.4132 has a 5% probability. The last column of Table 3.6 indicates that most features correlate significantly with $\Delta m_{15}(B)$ at the time of B-band maximum. Those that do not correlate significantly with $\Delta m_{15}(B)$ — X_{4570} and X_{5485} — still correlate with X_{5750} , which in turn strongly correlates with $\Delta m_{15}(B)$. These correlations become stronger when we exclude any “Broad Line” and “Known Peculiar” SNe, with a few exceptions. Most strongly affected by the removal of the 2 SNe are correlations relating each of

Table 3.6. Correlations between Spectral Indexes*

	X_{4570}	X_{5150}	X_{5485}	X_{5750}	X_{6150}	$\Delta m_{15}(B)$
X_{4570}	1	-0.23(0.08) -0.27(0.12)	0.46(0.10) 0.38(0.14)	-0.49(0.10) -0.76(0.03)	-0.10(0.15) 0.33(0.09)	0.38(0.15) 0.75(0.03)
X_{5150}		1	-0.51(0.08) -0.55(0.10)	0.65(0.07) 0.67(0.07)	-0.52(0.10) -0.67(0.10)	-0.62(0.07) -0.70(0.07)
X_{5485}			1	-0.47(0.09) -0.61(0.08)	0.34(0.14) 0.78(0.03)	0.39(0.11) 0.61(0.08)
X_{5750}				1	-0.68(0.05) -0.68(0.06)	-0.93(0.01) -0.95(0.01)
X_{6150}					1	0.65(0.07) 0.58(0.09)
$\Delta m_{15}(B)$						1

*The correlations between spectral indexes and each other as well as $\Delta m_{15}(B)$ are shown for all 23 spectra taken at B_{max} (top line in each row) and for 21 spectra (on the bottom line, excluding SN 2001ay the only KP SN and SN 1999cl the only BL SN). Correlations of 0.3961 (for the top line) and 0.4132 (for the bottom line) have a 5% probability of occurring by a random distribution. Only the previously classified SNe were used to find the correlations.

the Si II lines and $\Delta m_{15}(B)$ with both X_{4570} and X_{5485} . There were 2 correlations that decreased, the X_{4570} vs. X_{5485} and the X_{6150} vs. $\Delta m_{15}(B)$, but both changes were not significant since the standard deviations (from a jack knife test) associated with these Pearson's correlation coefficients were larger than the change.

Following from the simple fits used to describe the evolution of the spectral index values it should be expected that the correlations between spectral indexes would evolve similarly. The evolution of the correlations with $\Delta m_{15}(B)$ are shown in Figure 3.7. There are noticeably strong correlations within a week of maximum, particularly between 5 days prior and 6 days after maximum as shown by the shaded region. There are also some significant correlations around 2–3 weeks post maximum. It appears that the correlations do not hold during the period from 1–2 weeks after maximum when the spectral indexes associated with the absorption features make their transitions. The most notable feature is the strong anti-correlation between X_{5750} and $\Delta m_{15}(B)$ which begins at 9 days pre-maximum and continues until 12 days post-maximum. The two emission humps also have strong wide correlations/anti-

correlations with $\Delta m_{15}(B)$ around maximum. At late time the X_{5485} switches from absorption to emission due to line blending such that the S II ‘w’ is lost so it is no longer very reliable which explains its lack of significant correlations in the later epochs. Similar results are shown when the spectral indexes are correlated with each other.

There is a noticeable switch from anti-correlation to correlation of the X_{5750} feature from near maximum to 2–3 weeks post-maximum. A main reason for this transition is that the Si II $\lambda 5750$ feature is overtaken by a Na ID feature (Branch et al. 2005; Doull & Baron 2011)see, and references above. However, this is explanation is still debated (Leibundgut et al. 1993; Mazzali et al. 1997). If Na ID is the source of this absorption, than why does it correlate with Δm_{15} ? If it is not Na ID than what is the source of this absorption? It should be noted that this is clearly not the CSM Na I, the line is too broad and the velocity of the line corresponds to the ejecta velocity (Garnavich et al. 2004).

3.4 PCA Evolution

From the strong correlations of each spectral index with each other and $\Delta m_{15}(B)$ this naturally leads to the conclusion that there may be a single main parameter driving the evolution of spectral features. To this end, principal components analysis (PCA) is employed to determine the dependence of the principal component on each X_λ and $\Delta m_{15}(B)$. The coefficients associated with each measurement for the 1st (PC1) and 2nd (PC2) principal components are shown in Figure 3.8. The left two panels in Figure 3.8 show the coefficients for PC1 and PC2 for all SNe in our sample, while the right two panels show PC1 and PC2 for our sample without the BL and KP SNe. The most striking characteristic of Figures 3.8(a) and 3.8(b) is the epochs from 5 days before maximum to 8 days after maximum, where all coefficients have similar absolute values. This characteristic suggests that these features are all influenced by one main parameter nearly equally during these epochs. The next two sections

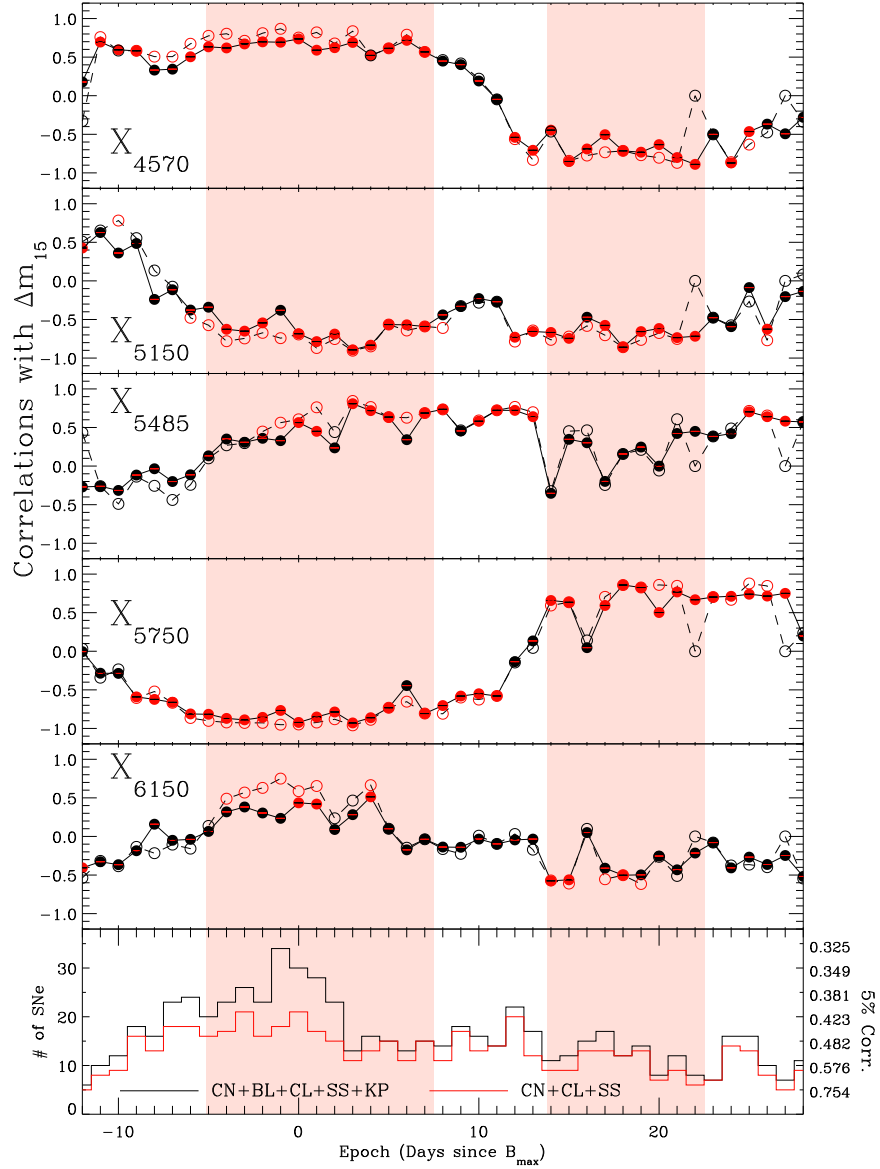


Fig. 3.7. Δm_{15} Correlation Evolution. The evolution of correlation with $\Delta m_{15}(B)$ for all 5 spectral indexes. The red points have a probability of 5% or less to occur randomly. The solid points are the correlations for all SNe with spectra at that epoch while the open circles are the correlations with “Broad Line” and “Known Peculiar” SNe removed. The shaded regions highlight the epochs of greatest correlation. Similar results are seen when the spectral indexes are correlated with each other.

use this strong dependence on PC1 for two purposes: 1) predict light curve decline rate ($\Delta m_{15}(B)$) from spectral features, and 2) correct the Hubble diagram. Figures 3.8(c) and 3.8(d) show PC2 for the complete set of spectra and the set with BL and KP SNe removed. PC2 shows much more scatter than PC1 and higher principal components show more scatter. This confirms that the majority of variation within our SNe sample is captured by PC1.

Principal component analysis provides a straight forward method to determine the percentage of variation contained in each principal component. The evolution of these percentages is shown in Figure 3.9. It can easily be seen that the first principal component contains the most variation during the epochs that correspond to the greatest correlation between the spectral index measurements. Within 5 days of maximum, PC1 is the strongest and then from +18 to +22 days. There is a large spike in the percentage of variation contained in PC1 at +21 days after maximum but this is likely due to a small number of SNe with spectra on that day. From Figure 3.9 it could be argued that the best epochs during which to obtain spectra for a SNe Ia would be ± 5 days and between +18 and +22 days from maximum with the earlier epoch range being the better of the two. The worst epochs would be between +8 days and +14 days from maximum with day 11 being the absolute worst since there is only a few percent difference in the amount of variation contained in PC1 and PC2. This time also corresponds to the epochs when SNe Ia are the most homogeneous.

3.5 Predicting Light Curve Decline Rate from Spectral Features Using WSIM

The correlations between all 5 spectral indexes and $\Delta m_{15}(B)$ as well as their equal weight to PC1 allow for a straight forward method to predict $\Delta m_{15}(B)$, a light curve characteristic, from a single spectrum or even a single spectral feature. The procedure to predict $\Delta m_{15}(B)$ is as follows:

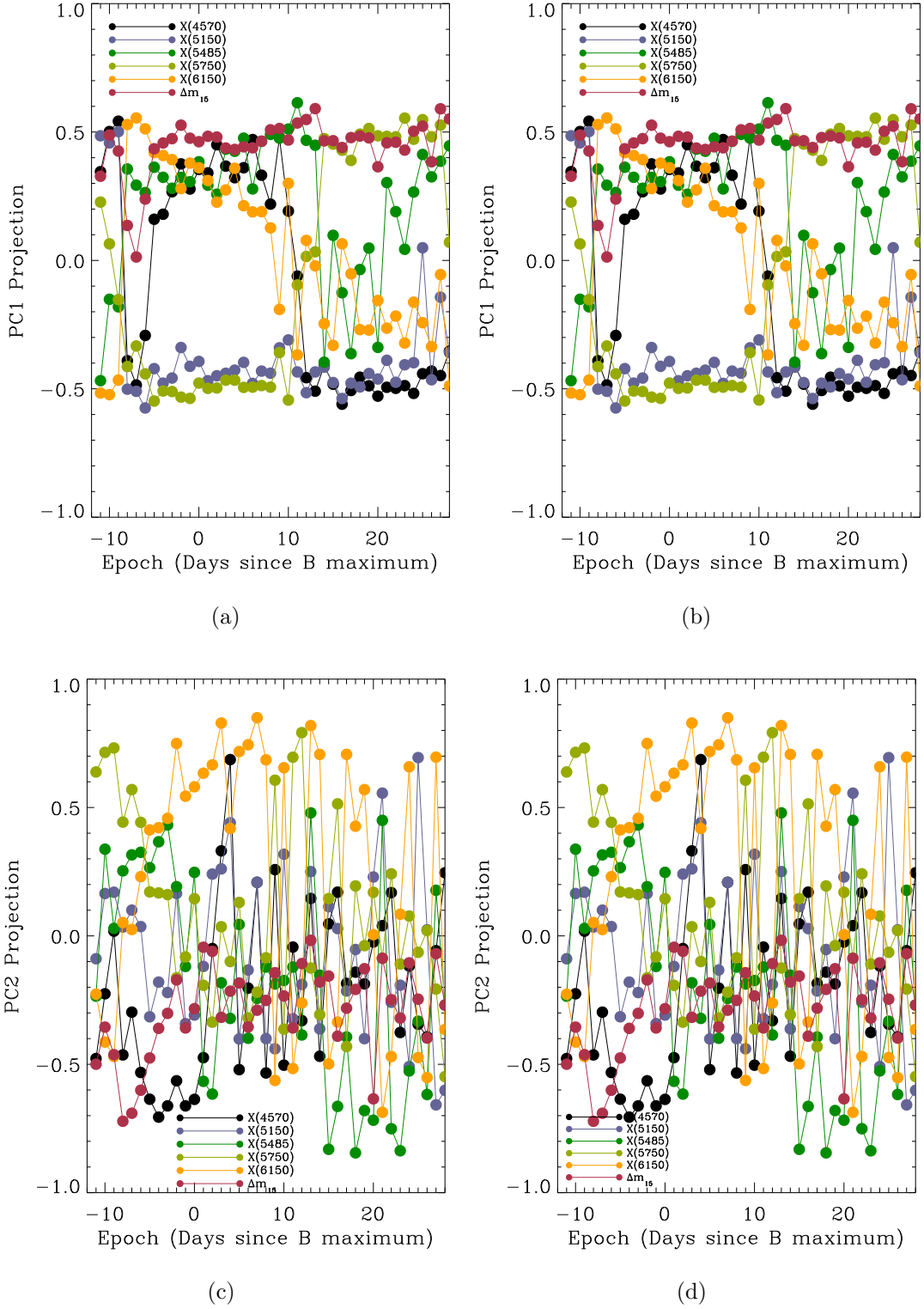


Fig. 3.8. PC1 & PC2 Evolution. The evolution of the coefficients of the first and second principle components. The colors represent the coefficients for each measurement at that epoch. The plots on the left are for all spectra, and the plots on the right are for the spectra without Broad Line SNe spectra.

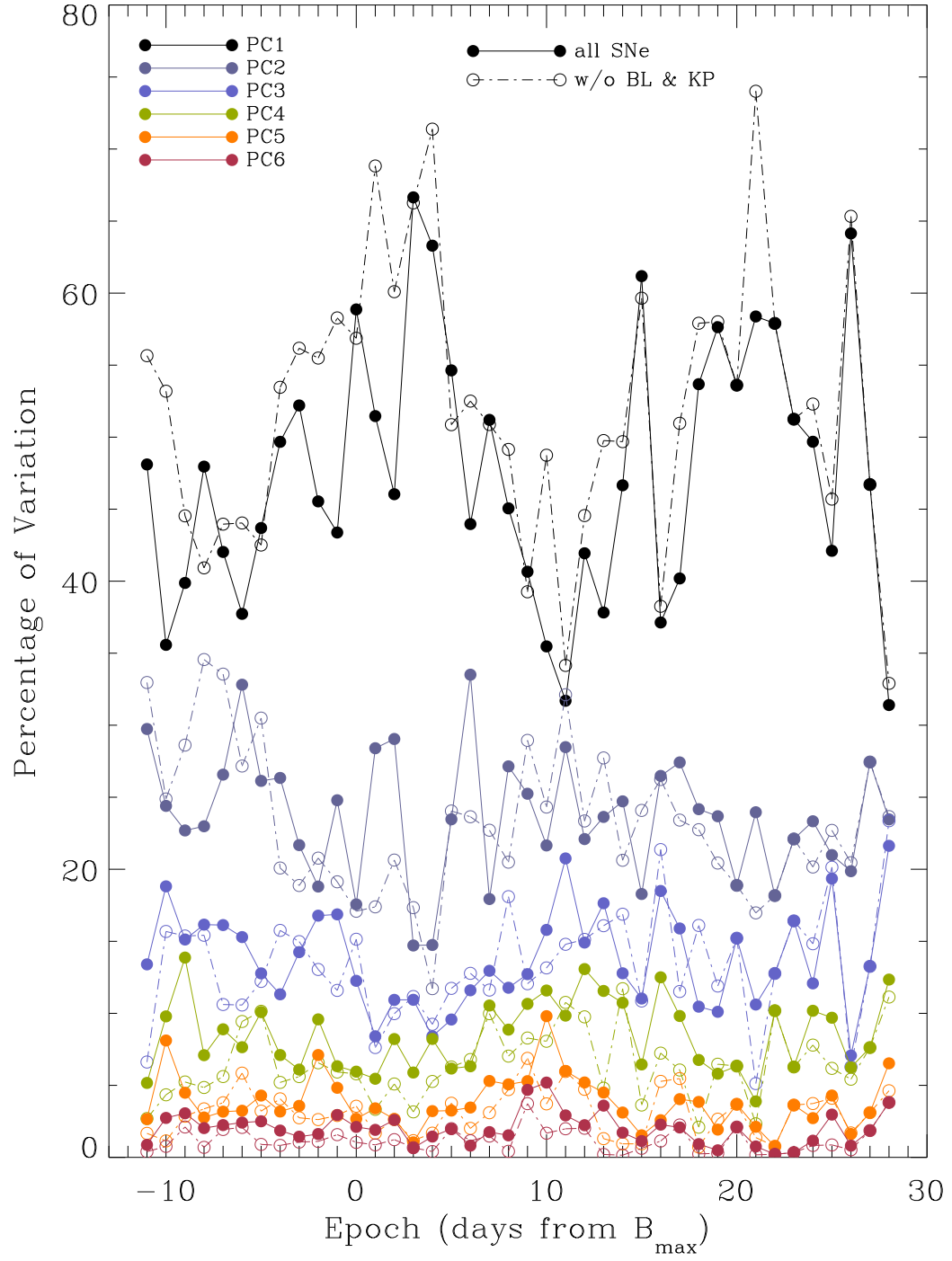


Fig. 3.9. Percent Variation Evolution. The percentage of variation contained in each principal component as a function of epoch.

1. Use all data to determine the Principal Components.
2. Collapse data to only the average first principal component (PC1) (averaged over epochs within a week of B_{max}).
3. Expand back into the X'_λ 's and $\Delta m_{15}(B)'$. This gives the relationship described by:

$$\Delta m_{15}(B)' = \frac{PC1 \hat{e}_{\Delta m_{15}(B)} PC1 \hat{e}_{X_\lambda}'}{X_\lambda} \quad (3.6)$$

4. Using Equation 3.6 to estimate $\Delta m_{15}(B)$ from the original X_λ 's. Then the estimates from each X_λ is averaged.

This procedure is used to estimate $\Delta m_{15}(B)$ for each individual spectral feature (solid colored circles) then these were averaged for each epoch (larger black open circles). Five SNe are used as examples in Figure 3.10 to illustrate the results of the above procedure. Steps 3 and 4 are necessary when we do not know the decline rate for the SNe because we will not be able to calculate PC1 without it. With the data at hand we can make a stronger estimate using multiple epochs shown by the open circles on the left-hand side of Figure 3.10. The open black circle shows the average of all epochs indiscriminately. Only reasonable $\Delta m_{15}(B)$ values ($0.5 \leq \Delta m_{15}(B) \leq 2.0$) are used to calculate the average shown by the open violet squares. The open blue-gray diamonds are the average of reasonable values as was done for the violet square but also, the average was restricted to epochs within 6 days of maximum and between 18 and 26 days after maximum. These three averages for all SNe are shown in Figure 3.11. An average of all epochs systematically underestimates $\Delta m_{15}(B)$ while the averages with cuts do better. This method can estimate $\Delta m_{15}(B)$ but with low precision and may be useful for SNe with very sparse data.

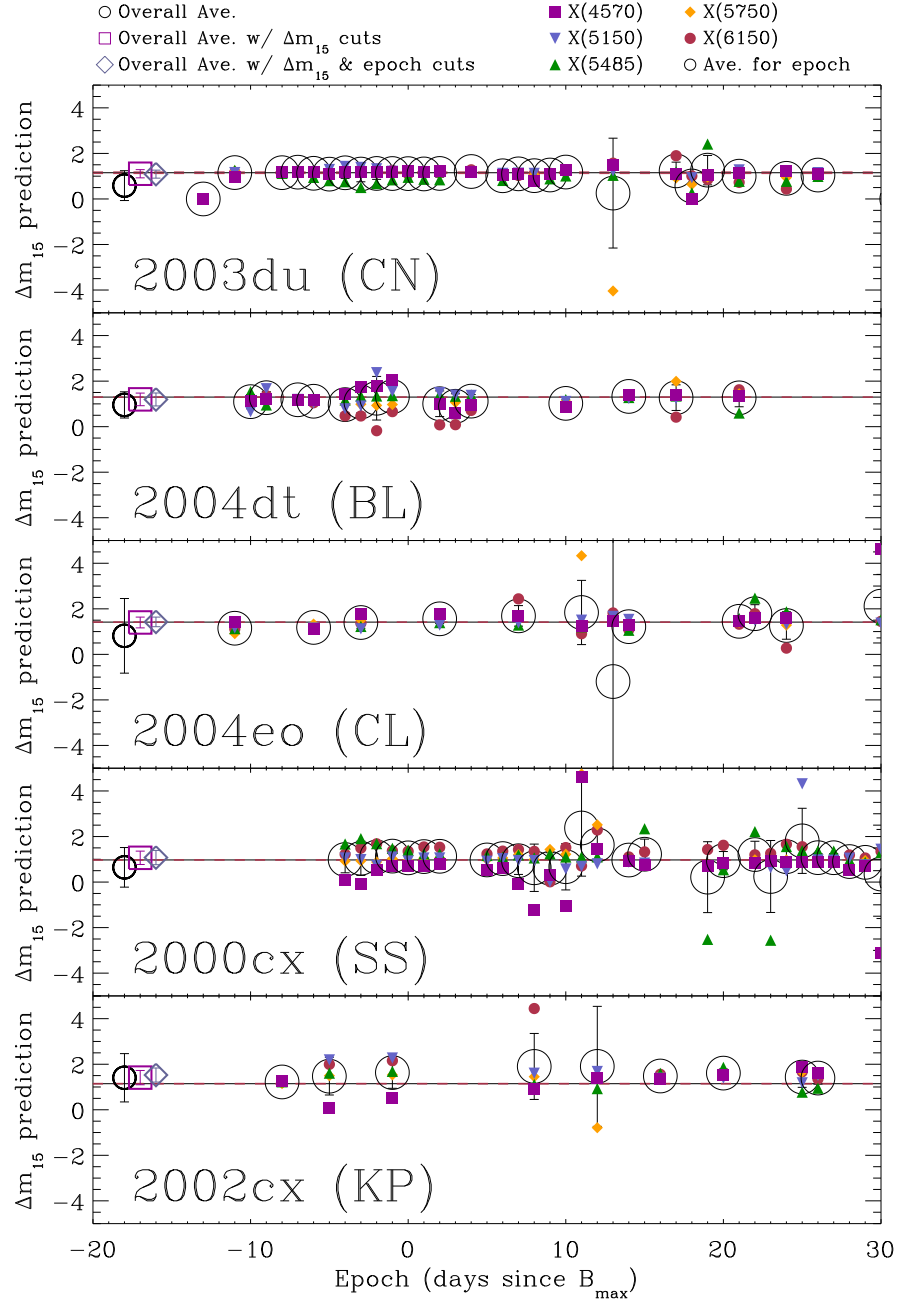


Fig. 3.10. Δm_{15} Prediction Examples. The simple relationship from Equation 3.6 is used to estimate $\Delta m_{15}(B)$ for all SNe in our sample. Five examples are shown in this figure. The filled symbols at each epoch represent the estimated $\Delta m_{15}(B)$ based on an individual spectral feature (magenta square - X_{4570} , blue upside down triangle - X_{5150} , green triangle - X_{5485} , orange diamond - X_{5750} , and red circle - X_{6150}) while the large, black, open circle is the average of these 5 estimates for that epoch. Three points on the far left of each plot represent the average of all data for that SNe (black open circle), the average of all measurements with $0.5 \leq \Delta m_{15}(B) \leq 2.0$ as “reasonable” estimates (violet open square), and the average with the same $\Delta m_{15}(B)$ cuts for epochs within 6 days of maximum and epochs between 18 days and 26 days after maximum to correspond with epochs of greatest correlations (blue-gray open diamond).

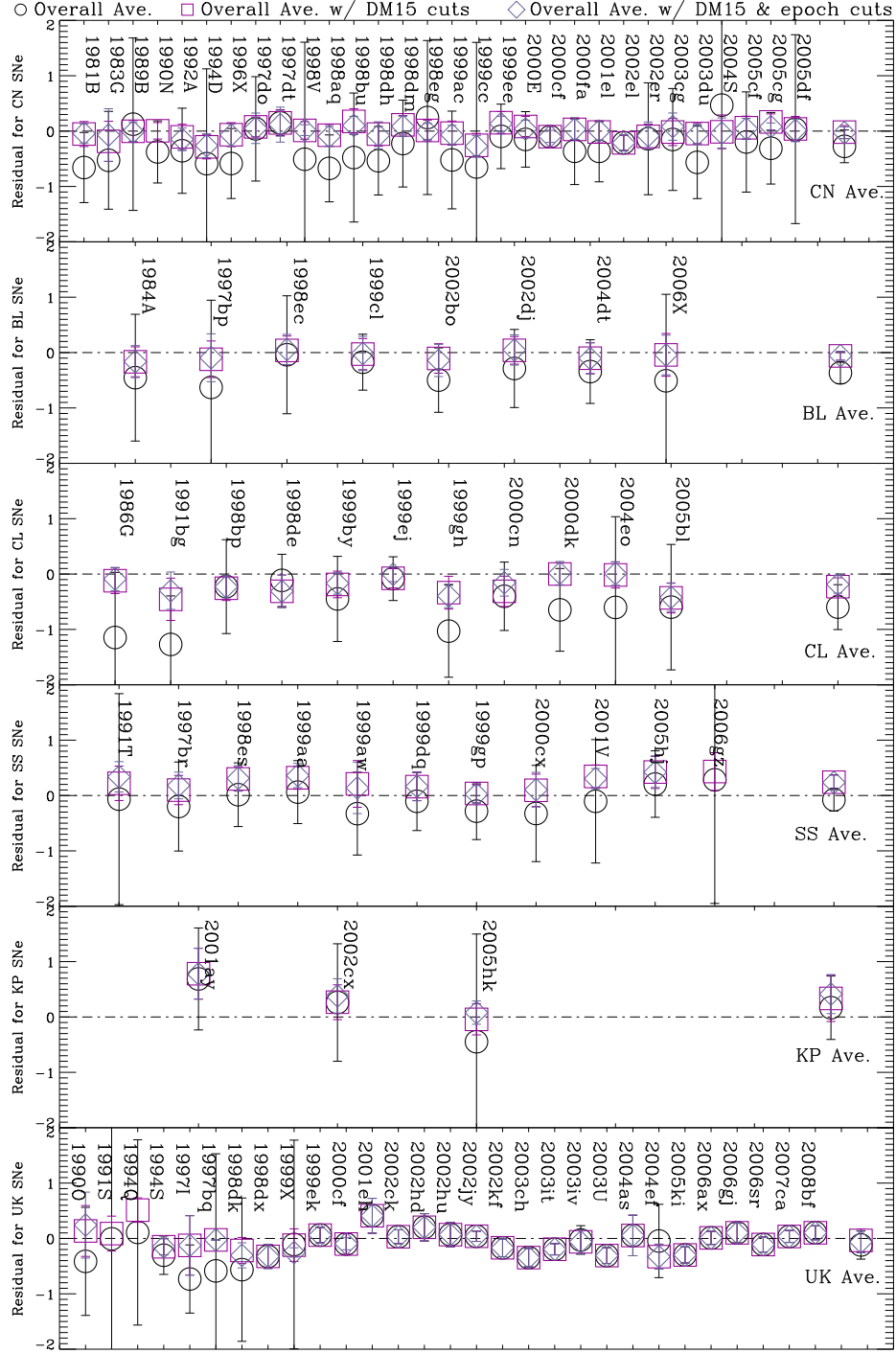


Fig. 3.11. Δm_{15} Predictions for the Entire Dataset. Estimates of $\Delta m_{15}(B)$ are made here for the SNe in our sample. These estimates are made from the averages as shown in Figure 3.10. The black open circles show the average estimate for all features over all epochs available. A cut to “reasonable” $\Delta m_{15}(B)$ values ($0.5 \leq \Delta m_{15}(B) \leq 2.0$) is made and the resulting average is represented by the violet open squares. The same Δm_{15} cuts are made for the blue-gray open diamonds with additional cuts to epochs within 6 days of maximum and between 18 and 26 days past maximum. Table 3.7 lists the estimated values alongside the Δm_{15} values found in the literature.

Table 3.7: Estimates of $\Delta m_{15}(B)$ from WSIM and PCA

SN	Branch Subtype	$\langle \Delta m_{15}(B) \rangle$ (All) ^a	$\langle \Delta m_{15}(B) \rangle$ (first cut) ^b	$\langle \Delta m_{15}(B) \rangle$ (sec- ond cut) ^c	$\Delta m_{15}(B)$	Source
1990N	CN	0.76(0.56)	1.14(0.15)	...	1.138(0.050)	Wang, L. et al. (2006a)
1994D	CN	1.03(0.95)	1.27(0.22)	1.29(0.22)	1.558(0.050)	Wang, L. et al. (2006a)
1996X	CN	0.71(0.63)	1.23(0.22)	1.23(0.20)	1.299(0.009)	Wang, L. et al. (2006a)
1997dt	CN	1.19(0.23)	1.19(0.23)	1.16(0.32)	1.04(0.15)	Jha et al. (2006a)
1998V	CN	0.82(1.09)	1.16(0.16)	1.17(0.10)	1.150(0.025)	Wang, L. et al. (2006a)
1998aq	CN	0.51(0.60)	1.11(0.19)	1.09(0.18)	1.185(0.008)	Wang, L. et al. (2006a)
1998bu	CN	0.57(0.83)	1.19(0.23)	1.12(0.16)	1.014(0.008)	Wang, L. et al. (2006a)
1998eg	CN	1.40(1.39)	1.16(0.19)	1.15(0.14)	1.15(0.09)	Jha et al. (2006a)
2000fa	CN	0.77(0.62)	1.16(0.20)	1.17(0.18)	1.140(0.027)	Wang, L. et al. (2006a)
2001el	CN	0.80(0.55)	1.15(0.20)	1.17(0.16)	1.166(0.004)	Wang, L. et al. (2006a)
2003cg	CN	1.10(0.95)	1.23(0.25)	1.33(0.25)	1.25(0.05)	Elias-Rosa et al. (2006)
2003du	CN	0.60(0.59)	1.11(0.18)	1.09(0.18)	1.151(0.037)	Wang, L. et al. (2006a)
2004S	CN	1.30(2.17)	1.19(0.31)	1.17(0.28)	1.210(0.016)	Wang, L. et al. (2006a)
2005cf	CN	0.97(0.91)	1.22(0.22)	1.21(0.19)	1.161(0.003)	Wang, L. et al. (2006a)
1981B	BL	0.47(0.63)	1.07(0.23)	1.08(0.17)	1.125(0.070)	Wang, L. et al. (2006a)
1984A	BL	0.84(1.14)	1.13(0.27)	1.13(0.29)	1.294(0.100)	Wang, L. et al. (2006a)
1991M	BL	0.95(0.80)	1.33(0.43)	1.06(0.22)	1.510(0.100)	Wang, L. et al. (2006a)
1992A	BL	0.94(0.76)	1.21(0.23)	1.17(0.20)	1.320(0.050)	Wang, L. et al. (2006a)
1997do	BL	1.12(0.66)	1.17(0.18)	1.15(0.27)	1.099(0.238)	Wang, L. et al. (2006a)
1998dh	BL	0.72(0.62)	1.20(0.22)	1.18(0.24)	1.258(0.038)	Wang, L. et al. (2006a)
1998ec	BL	0.95(0.70)	1.11(0.26)	1.13(0.27)	1.074(0.028)	Wang, L. et al. (2006a)
1999cc	BL	0.91(2.26)	1.31(0.22)	1.29(0.20)	1.567(0.102)	Wang, L. et al. (2006a)
1999cl	BL	1.07(0.50)	1.22(0.28)	1.23(0.31)	1.243(0.043)	Wang, L. et al. (2006a)
1999ej	BL	1.36(0.40)	1.37(0.17)	1.44(0.13)	1.446(0.018)	Wang, L. et al. (2006a)
1999gd	BL	0.78(0.79)	1.27(0.24)	1.25(0.16)	1.170(0.041)	Wang, L. et al. (2006a)
1999gh	BL	0.69(0.83)	1.39(0.30)	1.33(0.21)	1.721(0.008)	Wang, L. et al. (2006a)
2000B	BL	0.75(1.82)	1.19(0.33)	1.32(0.09)	1.089(0.407)	Wang, L. et al. (2006a)
2002bo	BL	0.76(0.58)	1.15(0.27)	1.12(0.29)	1.260(0.007)	Wang, L. et al. (2006a)
2002dj	BL	0.79(0.70)	1.12(0.25)	1.13(0.27)	1.08(0.05)	Pignata et al. (2008)
2002er	BL	1.12(0.66)	1.20(0.22)	1.22(0.25)	1.301(0.010)	Wang, L. et al. (2006a)
2004dt	BL	0.96(0.58)	1.20(0.28)	1.19(0.28)	1.299(0.002)	Wang, L. et al. (2006a)
2006X	BL	0.57(0.99)	1.13(0.39)	1.12(0.36)	1.17(0.04)	Wang, X. et al. (2008)
1986G	CL	0.50(1.18)	1.52(0.23)	1.55(0.21)	1.643(0.070)	Wang, L. et al. (2006a)
1989B	CL	1.45(1.38)	1.27(0.21)	1.25(0.17)	1.262(0.070)	Wang, L. et al. (2006a)
1991bg	CL	0.58(0.88)	1.40(0.39)	1.56(0.34)	1.857(0.100)	Wang, L. et al. (2006a)
1997cn	CL	1.19(1.03)	1.48(0.47)	1.86(0.07)	1.86(0.10)	Hachinger et al. (2006)

Table 3.7 – Continued

SN	Branch Subtype	$\langle \Delta m_{15}(B) \rangle$ (All) ^a	$\langle \Delta m_{15}(B) \rangle$ (first cut) ^b	$\langle \Delta m_{15}(B) \rangle$ (sec- ond cut) ^c	$\Delta m_{15}(B)$	Source
1998bp	CL	1.63(0.66)	1.64(0.22)	1.67(0.20)	1.903(0.036)	Wang, L. et al. (2006a)
1998de	CL	1.77(0.47)	1.57(0.29)	1.57(0.29)	1.881(0.031)	Wang, L. et al. (2006a)
1999by	CL	1.34(0.77)	1.61(0.25)	1.63(0.21)	1.796(0.008)	Wang, L. et al. (2006a)
2000cn	CL	1.27(0.62)	1.36(0.27)	1.52(0.24)	1.675(0.027)	Wang, L. et al. (2006a)
2000dk	CL	0.81(0.75)	1.46(0.20)	1.47(0.21)	1.457(0.033)	Wang, L. et al. (2006a)
2004eo	CL	0.88(1.03)	1.40(0.24)	1.42(0.21)	1.417(0.005)	Wang, L. et al. (2006a)
2005bl	CL	1.33(1.13)	1.50(0.27)	1.51(0.25)	1.93(0.10)	Taubenberger et al. (2008)
1991T	SS	0.87(1.91)	1.16(0.31)	1.28(0.28)	0.940(0.050)	Wang, L. et al. (2006a)
1997br	SS	0.95(0.82)	1.24(0.26)	1.32(0.24)	1.141(0.011)	Wang, L. et al. (2006a)
1998es	SS	0.76(0.57)	1.04(0.22)	1.06(0.23)	0.745(0.013)	Wang, L. et al. (2006a)
1999aa	SS	0.88(0.59)	1.13(0.21)	1.17(0.22)	0.811(0.004)	Wang, L. et al. (2006a)
1999ac	SS	0.71(0.91)	1.20(0.21)	1.17(0.18)	1.241(0.030)	Wang, L. et al. (2006a)
1999aw	SS	0.47(0.77)	1.02(0.42)	0.95(0.46)	0.814(0.006)	Wang, L. et al. (2006a)
1999dq	SS	0.87(0.53)	1.13(0.25)	1.14(0.26)	0.973(0.013)	Wang, L. et al. (2006a)
1999ee	SS	0.85(0.58)	1.09(0.21)	1.06(0.15)	0.944(0.006)	Wang, L. et al. (2006a)
1999gp	SS	0.75(0.51)	1.07(0.17)	1.05(0.16)	1.029(0.135)	Wang, L. et al. (2006a)
2000E	SS	0.93(0.50)	1.16(0.18)	1.12(0.16)	1.079(0.021)	Wang, L. et al. (2006a)
2000cx	SS	0.65(0.88)	1.06(0.30)	1.07(0.32)	0.971(0.006)	Wang, L. et al. (2006a)
2001V	SS	0.66(1.07)	1.09(0.21)	1.05(0.18)	0.743(0.035)	Wang, L. et al. (2006a)
2005cg	SS	0.63(0.65)	1.11(0.14)	1.02(0.06)	0.94(0.05)	Quimby et al. (2006)
2005hj	SS	0.94(0.61)	1.16(0.29)	1.15(0.30)	0.74(0.17)	Quimby et al. (2007)
2006gz	SS	1.07(2.01)	1.12(0.34)	...	0.69(0.04)	Hicken et al. (2007)
2001ay	KP	1.23(0.92)	1.32(0.46)	1.32(0.46)	0.543(0.006)	Wang, L. et al. (2006a)
2002cx	KP	1.41(1.05)	1.41(0.32)	1.52(0.32)	1.145(0.016)	Wang, L. et al. (2006a)
2005hk	KP	1.01(1.16)	1.52(0.28)	1.64(0.21)	1.56(0.09)	Phillips et al. (2007)
1983G	UK	0.84(0.88)	1.18(0.36)	1.29(0.47)	1.37(0.01)	Hachinger et al. (2006)
1990O	UK	0.30(1.47)	1.11(0.47)	1.20(0.61)	0.96(0.10)	Hamuy et al. (1996b)
1991S	UK	1.03(2.20)	1.13(0.32)	...	1.04(0.10)	Hamuy et al. (1996b)
1994Q	UK	0.98(1.67)	1.39(0.22)	...	0.8750(...)	Bronder et al. (2008) ^d
1994S	UK	0.80(0.35)	0.95(0.15)	0.95(0.15)	1.10(0.10)	Blondin et al. (2006)
1997I	UK	0.40(0.62)	1.01(0.54)	1.01(0.54)	1.137(0.026)	Knop et al. (2003) ^d
1997bp	UK	0.71(1.17)	1.11(0.33)	1.14(0.43)	1.231(0.013)	Wang, L. et al. (2006a)
1997bq	UK	0.59(2.11)	1.15(0.00)	1.15(0.00)	1.174(0.022)	Wang, L. et al. (2006a)
1998ab	UK	0.60(0.80)	1.12(0.22)	1.12(0.23)	1.053(0.009)	Wang, L. et al. (2006a)
1998dk	UK	0.74(0.98)	1.13(0.24)	1.04(0.23)	1.344(0.077)	Wang, L. et al. (2006a)

^dfrom stretch using the conversion equation found in Perlmutter et al. (1997)

Table 3.7 – Continued

SN	Branch Subtype	$\langle \Delta m_{15}(B) \rangle$ (All) ^a	$\langle \Delta m_{15}(B) \rangle$ (first cut) ^b	$\langle \Delta m_{15}(B) \rangle$ (sec- ond cut) ^c	$\Delta m_{15}(B)$	Source
1998dm	UK	0.83(0.52)	1.08(0.20)	1.07(0.21)	0.983(0.339)	Wang, L. et al. (2006a)
1998dx	UK	1.23(0.22)	1.23(0.22)	1.23(0.22)	1.55(...)	Reindl et al. (2005)
1999X	UK	1.09(1.14)	1.29(0.25)	1.12(0.08)	1.377(0.058)	Wang, L. et al. (2006a)
1999ek	UK	1.27(0.14)	1.27(0.14)	1.27(0.14)	1.21(...)	Hicken et al. (2009a)
2000cf	UK	1.26(0.19)	1.26(0.19)	1.27(0.11)	1.364(0.043)	Wang, L. et al. (2006a)
2001eh	UK	1.24(0.32)	1.24(0.32)	1.24(0.32)	0.830(0.104)	Foley et al. (2008)
2002el	UK	1.21(0.14)	1.21(0.14)	1.21(0.14)	1.424(0.018)	Wang, L. et al. (2006a)
2002ck	UK	1.15(0.12)	1.15(0.12)	1.15(0.12)	1.120(0.024)	Blondin et al. (2011) ^e
2002hd	UK	1.42(0.25)	1.42(0.25)	1.42(0.25)	1.217(0.076)	Blondin et al. (2011) ^e
2002hu	UK	1.11(0.22)	1.11(0.22)	1.11(0.22)	1.04(0.07)	Hicken et al. (2009a)
2002jy	UK	1.03(0.09)	1.03(0.09)	1.03(0.09)	0.990(0.035)	Blondin et al. (2011) ^e
2002kf	UK	1.19(0.16)	1.19(0.16)	1.19(0.16)	1.355(0.031)	Blondin et al. (2011) ^e
2003ch	UK	1.22(0.17)	1.22(0.17)	1.22(0.17)	1.561(0.094)	Blondin et al. (2011) ^e
2003it	UK	1.19(0.10)	1.19(0.10)	1.19(0.10)	1.386(0.049)	Blondin et al. (2011) ^e
2003iv	UK	1.39(0.26)	1.36(0.21)	1.36(0.21)	1.417(0.060)	Blondin et al. (2011) ^e
2003U	UK	1.24(0.14)	1.24(0.14)	1.24(0.14)	1.548(0.081)	Blondin et al. (2011) ^e
2004as	UK	1.15(0.37)	1.15(0.37)	1.15(0.37)	1.093(0.034)	Blondin et al. (2011) ^e
2004ef	UK	1.45(0.66)	1.17(0.22)	1.17(0.22)	1.496(0.003)	Wang, L. et al. (2006a)
2005df	UK	1.15(1.71)	1.16(0.23)	1.13(0.20)	1.116(0.013)	Wang, L. et al. (2006a)
2005ki	UK	1.18(0.15)	1.18(0.15)	1.18(0.15)	1.478(0.025)	Blondin et al. (2011) ^e
2006ax	UK	1.09(0.12)	1.09(0.12)	1.09(0.12)	1.08(0.05)	Hicken et al. (2009a)
2006gj	UK	1.49(0.18)	1.49(0.18)	1.49(0.18)	1.39(0.17)	Hicken et al. (2009a)
2006sr	UK	1.15(0.14)	1.15(0.14)	1.15(0.14)	1.26(0.09)	Hicken et al. (2009a)
2007ca	UK	1.08(0.11)	1.08(0.11)	1.08(0.11)	1.045(0.020)	Blondin et al. (2011) ^e
2008bf	UK	1.11(0.13)	1.11(0.13)	1.11(0.13)	1.01(...)	Hicken et al. (2009a)

^ecalculated from SALT2 x_1 ^aThe average of all $\Delta m_{15}(B)$ estimates over all spectral indexes over all epochs.^bThe average of $\Delta m_{15}(B)$ estimates were made over all spectral indexes over all epochs with a spectrum including only reasonable $\Delta m_{15}(B)$ values ($0.5 \leq \Delta m_{15}(B) \leq 2.0$).^cThe average of $\Delta m_{15}(B)$ estimates were made over all spectral indexes from epochs within 6 days of maximum and from 18 to 26 days after maximum including only reasonable $\Delta m_{15}(B)$ values ($0.5 \leq \Delta m_{15}(B) \leq 2.0$).

4. FUTURE WORK

4.1 WSIM in NIR and UV Spectra

One of the most straight forward extensions of this work would be to develop the WSIM for other spectral ranges. In particular, the near-infrared (NIR) SNe Ia spectra have been shown to be particularly useful by Marion et al. (2009). Results using the pseudo-equivalent width measurements have shown a correlation of NIR features with Δm_{15} . The initial application of WSIM, however did not show a similar correlation. This may be due in part to different normalization and error corrections required for the new spectral range. New Monte Carlo simulations need to be run in order to characterize the effects of noise on WSIM at these wavelengths. Another area of interest for SNe Ia spectra is the ultra-violet (UV) range. This range is particularly useful for distant supernovae because the UV spectra will be redshifted into the visible range. Characterizing UV spectra for nearby SNe will be crucial in understanding the spectra of distant SNe (see, Foley et al. 2008).

4.2 Flux Ratios Applied to Wavelet Decomposed Spectra

Bailey et al. (2009) developed a systematic test of spectral flux ratios. They were successful in finding ratios that correlated well for their sample and reduced the residual of SNe Ia peak magnitudes. It was suggested by Blondin et al. (2011) that the WSIM should be used in conjunction with Bailey's method. The advantage of using WSIM for Bailey's method would be that the affects from noise and the overall shape of the spectra on the flux ratios would be reduced.

4.3 Photometric Redshifts and Template Spectra

One of the main initial motivations for developing WSIM was to build an algorithm to generate template spectra for the testing the method of determining redshift from photometric data (photo-z). There have been two proposed methods of determining photometric redshifts for SNe Ia (Asztalos et al. 2010; Wang, Y. 2007; Wang, Y. et al. 2007). The proposed template generator will use the PCA data from WSIM as a lever by which new heterogeneous spectra can be generated by a small number of parameters.

4.4 WSIM Applied to K-corrections

The ability to separate spectra into different wavelet scales has the potential to be useful to characterize not only the scales relevant to spectral features but it also gives the advantage of being able to characterize the large scale structure of the spectra. Some work in this direction has been pursued by Arsenijevic (2011) where the Daubechies wavelet coefficient for scale 15 was correlated to SALT2 color, c . Another possibility would be to remove the scales related to the spectral features and test the effects of spectral features on the calculation of K corrections (Hsiao et al. 2007; Nugent et al. 2002).

5. SUMMARY AND DISCUSSION

The study of Type Ia supernovae has been crucial in our understanding of the universe as a whole and was the tool that led to the concept of dark energy. SNe Ia are uniformly bright which makes them ideal cosmological probes. Theory explains this as being due to the uniform composition and mass of their progenitors. The progenitor of a SN Ia is thought to be a C-O white dwarf which accretes matter from a companion until, as it approaches the Chandrasakar limit ($\sim 1.4M_{\odot}$), a runaway thermonuclear explosion takes place and the WD is completely obliterated. An alternate theory says that two WDs coalesce and overcome the Chandrasakar limit. Whatever the progenitor is, it has been observed that SNe Ia are a highly homogeneous set of events.

However, it has been seen that SNe Ia do show variations that can be corrected for, making them a ‘standardizable candle.’ Currently, SNe Ia can be corrected for the variations related to decline rate (parameterized as Δm_{15} in this work) and color. It has also been shown that the peak magnitude correlates with host galaxy properties, namely morphology, age, and possibly metallicity. Some of this work is directed towards expanding the search for spectral luminosity indicators using a new technique of measuring line strengths, the Wavelet Spectral Index Method (WSIM). Previous work has shown relationships between peak magnitude and ratios of spectral flux or pseudo-equivalent width. The correlations that are found center around the two Si II features at 5750 Å and 6150 Å.

In this work, WSIM has been introduced using à trous wavelet decomposition. The power of the Wavelet Spectral Index Method is in the fact that it decomposes the spectra into different wavelet scales. The smallest scales correspond to electronic noise and the largest scales correspond to the overall shape of the spectra leaving the medium scales to contain the most information about the spectral features themselves. WSIM can use lower resolution spectra since all spectra are set to 5 Å bins,

in this work spectra with resolution as low as 8–9 Å has been used alongside spectra with ≥ 1 Å resolution. Not only can WSIM isolate the important scales from the noise, it is also able to use the noise scales to correct for bias in the measurements. And the noise that cannot be corrected for can still be easily characterized. Another advantage of the WSIM over previous work that has been done using the pseudo-equivalent widths is that the wavelet spectral indexes are normalized in such a way that the features can be measured from an objective zero level without having to approximate a continuum.

Previous work which classified SNe Ia into separate subgroups using pseudo-equivalent width has been reproduced using the WSIM. It is clearly shown that the sub-groupings are not distinct but part of a continuous variation among SNe Ia. The wavelet spectral indexes were also used to trace the evolution of spectral features during the course of the weeks surrounding the light curve maximum. The correlations between features are seen to be significant within a week of maximum and from 2–3 weeks post-maximum (more data needs to be collected to better establish the late time correlations). These correlations are seen between spectral indexes and other spectral indexes and also between spectral indexes and Δm_{15} . The X_{5750} corresponds possibly to two different absorption features over the course of the evolution, Si II near maximum and Na ID 2–3 weeks after maximum. This change is due most likely to a change in the abundance of one or both of the ions or a change in the excitation of these two ions. Si II anti-correlates with Δm_{15} and Na ID correlates with Δm_{15} . The late time identification of this line has been uncertain but the strong correlation with Δm_{15} shows that this feature should provide clues to the underlying physics of the explosion.

These correlations were exploited using principal components analysis (PCA). It is found that the most variation is contained in the first principal component (PC1) near maximum peaking at B-band maximum and a few days past maximum. A secondary maximum in the variation contained in PC1 occurs 2–3 weeks past

maximum. From this result the best time to obtain a spectrum of a SNe Ia is within 5 days of maximum and from +18 days to +22 days from maximum, with the earlier epochs being the overall best epochs. The worst epochs to obtain a spectrum would be +11 days after maximum (± 3 days). During the best epochs only 2 PCs are needed to describe $\sim 80\text{--}90\%$ of the variation and ~ 4 PCs are necessary to describe the same percentage of the variation on the worst epochs.

Near maximum, all spectral indexes and Δm_{15} are shown to contribute equally to PC1. The PCA results allow the decline rate (Δm_{15}) to be estimated from a single spectra, and even a single spectral feature through the use of PC1. The statistics on which these predictions are based are small and leave much room for improvement but this could be a useful tool in understanding the relationship between spectra and progenitors as well as generating heterogeneous spectral templates. This process should be reversible so that a Δm_{15} value could be used to estimate the spectral indexes. It is one of the future goals of this work to develop such an algorithm to generate a set of heterogeneous template spectra in order to test photometric redshift methods for SNe Ia.

The future of the wavelet spectral index method as a tool for studying Type Ia supernovae looks promising. The recent publication of new data could help to given these calculations more statistically solid foundations. It is the hope of the author to develop a publicly available GUI so that the community at large will be able to perform the WSIM calculations. Possible avenues of future work include using principal components to develop heterogeneous spectral templates, and develop new spectral luminosity indicators to improve SNe Ia as standardizable candles. The WSIM could easily be extended beyond the optical portion of SNe spectra, particularly into the NIR and UV. Other optical features could be added to the set of spectral indexes also. Building off previous work, flux ratios could be tested on decomposed spectra similar to the method of Bailey et al. (2009) but now without the continuum-like background after wavelet decomposition has been performed. The

ability to separate out the continuum-like background wavelet scales could be used to constrain the effects of spectral features on K-corrections. The higher wavelet scales have also been shown to correlate with SNe colors (Arsenijevic 2011). And the principal components analysis could be extended to include other SNe properties such as host galaxy morphology as well as more light curve measurements. Overall, the work has only begun for the WSIM.

REFERENCES

- Altavilla, G., Stehle, M., Ruiz-Lapuente, P., Mazzali, P., Pignata, G., et al. 2007, *A&A*, 475, 585
- Altavilla, G., Ruiz-Lapuente, P., Balastegui, A., Méndez, J., Irwin, M., et al. 2009, *ApJ*, 695, 135
- Anupama, G. C. 1997, *AJ*, 114, 2054
- Anupama, G. C., Sahu, D. K., & Jose, J. 2005, *A&A*, 429, 667
- Arsenijevic, V., Fabbro, S., Mourão, A. M., & Rica da Silva, A. J. 2008, *A&A*, 492, 535
- Arsenijevic, V. 2011, *MNRAS*, 414, 1617
- Asztalos, S., Nikolaev, S., de Vries, W., Olivier, S., Cook, K., & Wang, L. 2010, *ApJ*, 713, 1167
- Baade, W. 1926, *Astronomische Nachrichten*, 228, 359
- Baade, W. 1936, *PASP*, 48, 226
- Baade, W., & Zwicky, F. 1934a, in *Proc. Natl. Acad. Sci.*, 20, 254
- Baade, W., & Zwicky, F. 1934b, in *Proc. Natl. Acad. Sci.*, 20, 259
- Bailey, S., Aldering, G., Antilogus, P., Aragon, C., Baltay, C., et al. 2009, *A&A*, 500, L17
- Barbon, R., Rosino, L., & Iijima, T. 1989, *A&A*, 220, 83
- Barbon, R., Benetti, S., Rosino, L., Cappellaro, E., & Turatto, M. 1990, *A&A*, 237, 79

- Baron, E., & Hauschildt, P. H. 1998, *ApJ*, 495, 370
- Benetti, S., Meikle, P., Stehle, M., Altavilla, G., Desidera, S., et al. 2004, *MNRAS*, 348, 261
- Benetti, S., Cappellaro, E., Mazzali, P. A., Turatto, M., Altavilla, G., et al. 2005, *ApJ*, 623, 1011
- Blondin, S., Dessart, L., Leibundgut, B., Branch, D., Höflich, P., et al. 2006, *AJ*, 131, 1648
- Blondin, S., Mandel, K. S., & Kirshner, R. P. 2011, *A&A*, 526, A81
- Blondin, S., Matheson, T., Kirshner, R. P., Mandel, K. S., Berlind, P., et al. 2012, *AJ*, 143, 126
- Bongard, S., Baron, E., Smadja, G., Branch, D., & Hauschildt, P. H. 2006, *ApJ*, 647, 513
- Bongard, S., Baron, E., Smadja, G., Branch, D., & Hauschildt, P. H. 2008, *ApJ*, 687, 456
- Boroson, T. A., & Green, R. F. 1992, *ApJS*, 80, 109
- Branch, D. 1972, *A&A*, 16, 247
- Branch, D., & Patchett, B. 1973, *MNRAS*, 161, 71
- Branch, D., Lacy, C. H., McCall, M. L., Sutherland, P. G., Uomoto, A., Wheeler, J. C., & Wills, B. J. 1983, *ApJ*, 270, 123
- Branch, D., Doggett, J. B., Nomoto, K., & Thielemann, F.-K. 1985, *ApJ*, 294, 619
- Branch, D. 1990, in *Supernovae*, ed. A. G. Petschek, (New York Springer-Verlag), 30

- Branch, D., Fisher, A., & Nugent, P. 1993, *AJ*, 106, 2383
- Branch, D., & van den Bergh, S. 1993, *AJ*, 105, 2231
- Branch, D., Romanishin, W., & Baron, E. 1996, *ApJ*, 465, 73
- Branch, D., Garnavich, P., Matheson, T., Baron, E., Thomas, R. C., et al. 2003a, *AJ*, 126, 1489
- Branch, D., Baron, E. A., & Jeffery, D. J. 2003b, in *Lecture Notes in Physics Vol. 598, Supernovae and Gamma-Ray Bursters*, ed. K. Weiler (Berlin: Springer), 47
- Branch, D., Baron, E., Thomas, R. C., Kasen, D., Li, W., & Filippenko, A. V. 2004, *PASP*, 116, 903
- Branch, D., Baron, E., Hall, N., Melakayil, M., & Parrent, J. 2005, *PASP*, 117, 545
- Branch, D., Dang, L. C., Hall, N., Ketchum, W., Melakayil, M., et al. 2006, *PASP*, 118, 560
- Branch, D., Jeffery, D. J., Parrent, J., Baron, E., Troxel, M. A., et al. 2008, *PASP*, 120, 135
- Branch, D., Dang, L. C., & Baron, E. 2009, *PASP*, 121, 238
- Bronder, T. J., Hook, I., Howell, D. A., Sullivan, M., Perrett, K., et al. 2007, in *AIP Conf. Proc. 924, The Multicolored Landscape of Compact Objects and Their Explosive Origins*, ed. L. A. Antonelli, L. Piersanti, A. Tornambe, L. Burderi, T. Di Salvo, et al. (Cefalu, Sicily: AIP), 415
- Bronder, T. J., Hook, I. M., Astier, P., Balam, D., Balland, C., et al. 2008, *A&A*, 477, 717
- Budavári, T. 2009, *ApJ*, 695, 747
- Commins, E. D. 2004, *New A Rev.*, 48, 567

- Connolly, A. J., Csabai, I., Szalay, A. S., Koo, D. C., Kron, R. G., Munn, J. A. 1995, *AJ*, 110, 2655
- Cormier, D., & Davis, T. M. 2011, *MNRAS*, 410, 2137
- Davis, T. M., James, J. B., Schmidt, B. P., & Kim, A. G. 2007, in *AIP Conf. Proc.* 924, *The Multicolored Landscape of Compact Objects and Their Explosive Origins*, ed. L. A. Antonelli, L. Piersanti, A. Tornambe, L. Burderi, T. Di Salvo, et al. (Cefalu, Sicily: AIP), 330
- Di Stefano, R. 2010, *ApJ*, 719, 474
- Di Stefano, R., Voss, R., & Claeys, J. S. W. 2011, *ApJ*, 738, L1
- Doull, B. A., & Baron, E. 2011, *PASP*, 123, 765
- Elias, J. H., Matthews, K., Neugebauer, G., & Persson, S. E. 1985, *ApJ*, 296, 379
- Elias-Rosa, N., Benetti, S., Cappellaro, E., Turatto, M., Mazzali, P. A., et al. 2006, *MNRAS*, 369, 1880
- Filippenko, A. V., Richmond, M. W., Matheson, T., Shields, J. C., Burbidge, E., et al. 1992a, *ApJ*, 384, L15
- Filippenko, A. V., Richmond, M. W., Branch, D., Gaskell, M., Herbst, W., et al. 1992b, *AJ*, 104, 1543
- Fisher, A. K. 2000, *Direct Analysis of Type Ia Supernovae Spectra*, Ph.D. Thesis, The University of Oklahoma
- Folatelli, G. 2004, *New A Rev.*, 48, 623
- Folatelli, G., Phillips, M. M., Morrell, N., Tanaka, M., Maeda, K., et al. 2012, *ApJ*, 745, 74
- Foley, R. J., Filippenko, A. V., & Jha, S. W. 2008, *ApJ*, 686, 117

- Foley, R. J., & Kasen, D. 2011, *ApJ*, 729, 55
- Foley, R. J., Filippenko, A. V., Kessler, R., Bassett, B., Frieman, J. A., et al. 2012, *AJ*, 143, 113
- Francis, P. J., Hewett, P. C., Foltz, C. B., & Chaffee, F. H. 1992, *ApJ*, 398, 476
- Francis, P. J., & Wills, B. J. 1999, *ASP Conf. Ser.* 162, *Quasars and Cosmology*, ed. G. Ferland & J. Baldwin (San Francisco: ASP), 363
- Gallagher, J. S., Garnavich, P. M., Berlind, P., Challis, P., Jha, S., et al. 2005, *ApJ*, 634, 210
- Gallagher, J. S., Garnavich, P. M., Caldwell, N., Kirshner, R. P., Jha, S. W., et al. 2008, *ApJ*, 685, 752
- Garavini, G., Folatelli, G., Goobar, A., Nobili, S., Aldering, G., et al. 2004, *AJ*, 128, 387
- Garavini, G., Aldering, G., Amadon, A., Amanullah, R., Astier, P., et al. 2005, *AJ*, 130, 2278
- Garavini, G., Folatelli, G., Nobili, S., Aldering, G., Amanullah, R., et al. 2007a, *A&A*, 470, 411
- Garavini, G., Nobili, S., Taubenberger, S., Pastorello, A., Elias-Rosa, N., et al. 2007b, *A&A*, 471, 527
- Garnavich, P. M., Bonanos, A. Z., Krisciunas, K., Jha, S., Kirshner, R. P., et al. 2004, *ApJ*, 613, 1120
- Gilfanov, M., & Bogdán, Á. 2010, *Nature*, 463, 924
- Guy, J., Astier, P., Nobili, S., Regnault, N., & Pain, R. 2005, *A&A*, 443, 781
- Guy, J., Astier, P., Baumont, S., Hardin, D., Pain, R., et al. 2007, *A&A*, 466, 11

- Hachinger, S., Mazzali, P. A., & Benetti, S. 2006, MNRAS, 370, 299
- Hachinger, S., Mazzali, P. A., Tanaka, M., Hillebrandt, W., & Benetti, S. 2008, MNRAS, 389, 1087
- Hachisu, I., Kato, M., Saio, H., & Nomoto, K. 2012, ApJ, 744, 69
- Hamuy, M., Phillips, M. M., Maza, J., Suntzeff, N. B., Schommer, R. A., et al. 1995, AJ, 109, 1
- Hamuy, M., Phillips, M. M., Suntzeff, N. B., Schommer, R. A., Maza, J., & Aviles, R. 1996a, AJ, 112, 2398
- Hamuy, M., Phillips, M. M., Suntzeff, N. B., Schommer, R. A., Maza, J., et al. 1996b, AJ, 112, 2408
- Hamuy, M., Trager, S. C., Pinto, P. A., Phillips, M. M., Schommer, R. A., et al. 2000, AJ, 120, 1479
- Hamuy, M., Trager, S. C., Pinto, P. A., Phillips, M. M., Schommer, R. A., et al. 2001, AJ, 122, 3506
- Hamuy, M., Maza, J., Pinto, P. A., Phillips, M. M., Suntzeff, N. B., et al. 2002, AJ, 124, 417
- Harkness, R. P., Wheeler, J. C., Margon, B., Downes, R. A., Kirshner, R. P., et al. 1987, ApJ, 317, 355
- Harris, G. L. H., Hesser, J. E., Massey, P., Peterson, C. J., & Yamanaka, J. M. 1983, PASP, 95, 607
- Hatano, K., Branch, D., & Deaton, J. 1998, ApJ, 502, 177
- Hauschildt, P. H. 1992, J. Quant. Spec. Radiat. Transf., 47, 433

- Hernandez, M., Meikle, W. P. S., Aparicio, A., Benn, C. R., Burleigh, M. R., et al. 2000, MNRAS, 319, 223
- Hicken, M., Garnavich, P. M., Prieto, J. L., Blondin, S., DePoy, D. L., Kirshner, R. P., & Parrent, J. 2007, ApJ, 669, L17
- Hicken, M., Challis, P., Jha, S., Kirshner, R. P., Matheson, T., et al. 2009a, ApJ, 700, 331
- Hicken, M., Wood-Vasey, W. M., Blondin, S., Challis, P., Jha, S., et al. 2009b, ApJ, 700, 1097
- Hillebrandt, W., Sim, S. A., & Röpke, F. K. 2007, A&A, 465, L17
- Hoefflich, P., & Khokhlov, A. 1996, ApJ, 457, 500
- Holschneider, M., Kronland-Martinet, R., Morlet, J., Tchamitchian. P., 1989, in Wavelets, Time-Frequency Methods and Phase Space, ed. J.-M. Combes, A. Grossmann & P. Tchamitchian (Berlin: Springer-Verlag), 289
- Howell, D. A. 2001, ApJ, 554, L193
- Howell, A., & Nugent, P. 2004, in Cosmic Explosions in Three Dimensions, ed. P. Hoefflich, P. Kumar & J. C. Wheeler (Cambridge, UK: Cambridge University Press), 151
- Howell, D. A., Sullivan, M., Nugent, P. E., Ellis, R. S., Conley, A. J., et al. 2006, Nature, 443, 308
- Howell, D. A., Sullivan, M., Brown, E. F., Conley, A., Le Borgne, D., et al. 2009, ApJ, 691, 661
- Howell, D. A. 2011, Nature Communications, 2,

- Hsiao, E. Y., Conley, A., Howell, D. A., Sullivan, M., Pritchett, C. J., et al. 2007, *ApJ*, 663, 1187
- Hubble, E. P. 1929a, *ApJ*, 69, 103
- Hubble, E. 1929b, in *Proc. Natl. Acad. Sci.*, 15, 168
- Humason, M. L. 1936, *PASP*, 48, 110
- Hyvärinen, A., J. Karhunen, and E. Oja 2001, *Independent Component Analysis*,
- Iben, I., Jr., & Tutukov, A. V. 1984, *ApJS*, 54, 335
- Ivanov, V. D., Hamuy, M., & Pinto, P. A. 2000, *ApJ*, 542, 588
- James, J. B., Davis, T. M., Schmidt, B. P., & Kim, A. G. 2006, *MNRAS*, 370, 933
- Jha, S., Garnavich, P. M., Kirshner, R. P., Challis, P., Soderberg, A. M., et al. 1999, *ApJS*, 125, 73
- Jha, S., Kirshner, R. P., Challis, P., Garnavich, P. M., Matheson, T., et al. 2006a, *AJ*, 131, 527
- Jha, S., Branch, D., Chornock, R., Foley, R. J., Li, W., Swift, B. J., Casebeer, D., & Filippenko, A. V. 2006b, *AJ*, 132, 189
- Jha, S., Riess, A. G., & Kirshner, R. P. 2007, *ApJ*, 659, 122
- LSST Science Collaborations, Abell, P. A., Allison, J., Anderson, S. F., Andrew, J. R., Angel, J. R. P., et al. 2009, *arXiv:0912.0201*
- Kasen, D., Nugent, P., Wang, L., Howell, D. A., Wheeler, J. C., et al. 2003, *ApJ*, 593, 788
- Kelly, P. L., Hicken, M., Burke, D. L., Mandel, K. S., & Kirshner, R. P. 2010, *ApJ*, 715, 743

- Kessler, R., Becker, A. C., Cinabro, D., Vanderplas, J., Fieman, J. A., et al. 2009, *ApJS*, 185, 32
- Khokhlov, A. M. 1991, *A&A*, 245, 114
- Khokhlov, A., Mueller, E., & Hoefflich, P. 1993, *A&A*, 270, 223
- Kirshner, R. P., Oke, J. B., Penston, M. V., & Searle, L. 1973, *ApJ*, 185, 303
- Kirshner, R. P., Jeffery, D. J., Leibundgut, B., Challis, P. M., Sonneborn, G., et al. 1993, *ApJ*, 415, 589
- Knop, R. A., Aldering, G., Amanullah, R., Astier, P., Blanc, G., et al. 2003, *ApJ*, 598, 102
- Koenig, T. 2005, in *ASP Conf. Ser. 342, 1604-2004: Supernovae as Cosmological Lighthouses*, ed. M. Turatto, S. Benetti, L. Zampieri, & W. Shea (San Francisco : ASP), 53
- Kotak, R., Meikle, W. P. S., Pirnata, G., Stehle, M., Smartt, S. J., et al. 2005, *A&A*, 436, 1021
- Kowal, C. T. 1968, *AJ*, 73, 1021
- Krisciunas, K., Garnavich, P. M., Stanishev, V., Suntzeff, N. B., Prieto, J. L., et al. 2007, *AJ*, 133, 58
- Lampeitl, H., Smith, M., Nichol, R. C., Bassett, B., Cinabro, D., et al. 2010, *ApJ*, 722, 566
- Leavitt, H. S., & Pickering, E. C. 1912, *Harvard College Observatory Circular*, 173, 1
- Lepo, K., & van Kerkwijk, M. 2011, *arXiv:1109.4394*

- Leibundgut, B., Kirshner, R. P., Filippenko, A. V., Shields, J. C., Foltz, C. B., Phillips, M. M., & Sonneborn, G. 1991, *ApJ*, 371, L23
- Leibundgut, B., Kirshner, R. P., Phillips, M. M., Wells, L. A., Suntzeff, N. B., et al. 1993, *AJ*, 105, 301
- Leonard, D. C., Li, W., Filippenko, A. V., Foley, R. J., & Chornock, R. 2005, *ApJ*, 632, 450
- Li, I. H., & Yee, H. K. C. 2008, *AJ*, 135, 809
- Li, W. D., Qiu, Y. L., Qiao, Q. Y., Zhu, X. H., Hu, J. Y., et al. 1999, *AJ*, 117, 2709
- Li, W., Filippenko, A. V., Gates, E., Chornock, R., Gal-Yam, A., et al. 2001, *PASP*, 113, 1178
- Li, W., Filippenko, A. V., Chornock, R., Berger, E., Berlind, P., et al. 2003, *PASP*, 115, 453
- Macri, L. M., Calzetti, D., Freedman, W. L., Gibson, B. K., Graham, J. A., et al. 2001, *ApJ*, 549, 721
- Maeda, K., & Iwamoto, K. 2009, *MNRAS*, 394, 239
- Mardia, K. V., Kent, J. T., & Bibby, J. M. 1979, *Multivariate Analysis*, (London: Academic Press)
- Marion, G. H., Höflich, P., Wheeler, J. C., Robinson, E. L., Gerardy, C. L., et al. 2006, *ApJ*, 645, 1392
- Marion, G. H., Höflich, P., Gerardy, C. L., Vacca, W. D., Wheeler, J. C., et al. 2009, *AJ*, 138, 727
- Marschall, L. A. 1988, *Supernova Story*, (New York: Plenum Press)

- Matheson, T., Kirshner, R., Challis, P., Jha, S., Garnavich, P. M., et al. 2008, *AJ*, 135, 1598
- Mazzali, P. A., Lucy, L. B., Danziger, I. J., Gouiffes, C., Cappellaro, E., & Turatto, M. 1993, *A&A*, 269, 423
- Mazzali, P. A., Chugai, N., Turatto, M., Lucy, L. B., Danziger, I. J., et al. 1997, *MNRAS*, 284, 151
- Mazzali, P. A., Sauer, D. N., Pastorello, A., Benetti, S., & Hillebrandt, W. 2008, *MNRAS*, 386, 1897
- McCall, M. L. 1985, *Lecture Notes in Physics Vol. 224, Supernovae as Distance Indicators*, ed. N. Bartel (Berlin: Springer-Verlag), 48
- McLaughlin, D. B. 1963, *PASP*, 75, 133
- Meikle, W. P. S., Cumming, R. J., Geballe, T. R., Lewis, J. R., Walton, N. A., et al. 1996, *MNRAS*, 281, 263
- Meikle, P., & Hernandez, M. 2000, *Memorie della Societa Astronomica Italiana*, 71, 299
- Mihalas, D. 1978, *Stellar Atmospheres*, (San Francisco: W. H. Freeman and Co.)
- Minkowski, R. 1939, *ApJ*, 89, 156
- Minkowski, R. 1941, *PASP*, 53, 224
- Mittaz, J. P. D., Penston, M. V., & Snijders, M. A. J. 1990, *MNRAS*, 242, 370
- Murtagh, F., & Heck, A. 1987, *Multivariate Data Analysis*, (Dordrecht: D. Reidel)
- Neill, J. D., Sullivan, M., Howell, D. A., Conley, A., Seibert, M., et al. 2009, *ApJ*, 707, 1449

- Nugent, P., Phillips, M., Baron, E., Branch, D., & Hauschildt, P. 1995, *ApJ*, 455, L147
- Nugent, P., Baron, E., Branch, D., Fisher, A., & Hauschildt, P. H. 1997, *ApJ*, 485, 812
- Nugent, P., Kim, A., & Perlmutter, S. 2002, *PASP*, 114, 803
- Oke, J. B., & Searle, L. 1974, *ARA&A*, 12, 315
- Pakmor, R., Fink, M., Hillebrandt, W., Kromer, M., Roepke, F., et al. 2010a, in *Proc. 25th Texas Symp. on Relativistic Astrophysics*, ed. F. M. Rieger, C. van Eldik, & W. Hofmann, (Heidelberg, Germany: PoS), <http://pos.sissa.it/cgi-bin/reader/conf.cgi?confid=123>, 74
- Pakmor, R., Kromer, M., Röpke, F. K., Friedrich, K., Sim, S. A., et al. 2010b, *Nature*, 463, 61
- Pastorello, A., Taubenberger, S., Elias-Rosa, N., Mazzali, P. A., Pignata, G., et al. 2007, *MNRAS*, 377, 1531
- Patat, F., Benetti, S., Cappellaro, E., Danziger, I. J., della Valle, M., Mazzali, P. A., & Turatto, M. 1996, *MNRAS*, 278, 111
- Payne-Gaposchkin, C., & Whipple, F. L. 1940, in *Proc. Natl. Acad. Sci.*, 26, 264
- Pennypacker, C., Tilquin, A., Melchior, A.-L., Combes, F., & Pain, R. 2004, *New A Rev.*, 48, 577
- Perlmutter, S., Gabi, S., Goldhaber, G., Goobar, A., Groom, D. E., et al. 1997, *ApJ*, 483, 565
- Perlmutter, S., Aldering, G., Goldhaber, G., Knop, R. A., Nugent, P., et al. 1999, *ApJ*, 517, 565

- Phillips, M. M., Phillips, A. C., Heathcote, S. R., Blanco, V. M., Geisler, D., et al. 1987, *PASP*, 99, 592
- Phillips, M. M., Wells, L. A., Suntzeff, N. B., Hamuy, M., Leibundgut, B., Kirshner, R. P., & Foltz, C. B. 1992, *AJ*, 103, 1632
- Phillips, M. M. 1993, *ApJ*, 413, L105
- Phillips, M. M., Lira, P., Suntzeff, N. B., Schommer, R. A., Hamuy, M., & Maza, José 1999, *AJ*, 118, 1766
- Phillips, M. M., Li, W., Frieman, J. A., Blinnikov, S. I., DePoy, D., et al. 2007, *PASP*, 119, 360
- Pignata, G., Benetti, S., Mazzali, P. A., Kotak, R., Patat, F., et al. 2008, *MNRAS*, 388, 971
- Prieto, J. L., Rest, A., & Suntzeff, N. B. 2006, *ApJ*, 647, 501
- Prieto, J. L., Stanek, K. Z., & Beacom, J. F. 2008, *ApJ*, 673, 999
- Pskovskii, Y. P. 1969, *Soviet Ast.*, 12, 750
- Quimby, R., Höflich, P., Kannappan, S. J., Rykoff, E., Rujopakarn, W., Akerlof, C. W., Gerardy, C. L., & Wheeler, J. C. 2006, *ApJ*, 636, 400
- Quimby, R., Höflich, P., & Wheeler, J. C. 2007, *ApJ*, 666, 1083
- Raskin, C., Scannapieco, E., Rockefeller, G., Fryer, C., Diehl, S., et al. 2010, *ApJ*, 724, 111
- Reindl, B., Tammann, G. A., Sandage, A., & Saha, A. 2005, *ApJ*, 624, 532
- Riess, A. G., Press, W. H., & Kirshner, R. P. 1996, *ApJ*, 473, 88
- Riess, A. G., Filippenko, A. V., Challis, P., Clocchiatti, A., Diercks, A., et al. 1998a, *AJ*, 116, 1009

- Riess, A. G., Nugent, P., Filippenko, A. V., Kirshner, R. P., & Perlmutter, S. 1998b, *ApJ*, 504, 935
- Riess, A. G., Kirshner, R. P., Schmidt, B. P., Jha, S., Challis, P., et al. 1999, *AJ*, 117, 707
- Riess, A. G., Fliri, J., & Valls-Gabaud, D. 2012, *ApJ*, 745, 156
- Ruiz-Lapuente, P., Cappellaro, E., Turatto, M., Gouiffes, C., Danziger, I. J., della Valle, M., & Lucy, L. B. 1992, *ApJ*, 387, L33
- Sahu, D. K., Tanaka, M., Anupama, G. C., Kawabata, K. S., Maeda, K., et al. 2008, *ApJ*, 680, 580
- Saio, H., & Nomoto, K. 1985, *A&A*, 150, L21
- Salvo, M. E., Cappellaro, E., Mazzali, P. A., Benetti, S., Danziger, I. J., Patat, F., & Turatto, M. 2001, *MNRAS*, 321, 254
- Sandage, A., & Tammann, G. A. 1993, *ApJ*, 415, 1
- Scalzo, R. A., Aldering, G., Antilogus, P., Aragon, C., Bailey, S., et al. 2010, *ApJ*, 713, 1073
- Seitenzahl, I. R., Ciaraldi-Schoolmann, F., & Röpke, F. K. 2011, *MNRAS*, 414, 2709
- Shapley, H., & Hearn, A. B. 1952, in *Proc. Natl. Acad. Sci.*, 38, 839
- Shaw, R. L. 1979, *A&A*, 76, 188
- Shen, K. J., Kasen, D., Weinberg, N. N., Bildsten, L., & Scannapieco, E. 2010, *ApJ*, 715, 767
- Shensa, M. J. 1992, *Proc. IEEE Transactions on Signal Processing*, 40, 2464
- Silverman, J. M., Ganeshalingam, M., Li, W., Filippenko, A. V., Miller, A. A., et al. 2011, *MNRAS*, 410, 585

- Sim, S. A., Röpke, F. K., Hillebrandt, W., Kromer, M., Pakmor, R., et al. 2010, *ApJ*, 714, L52
- Starck, J.-L., Murtagh, F., & Bijaoui, A. 1995, *Astronomical Data Analysis Software and Systems IV*, 77, 279
- Starck, J.-L., Siebenmorgen, R., & Gredel, R. 1997, *ApJ*, 482, 1011
- Stanishev, V., Goobar, A., Benetti, S., Kotak, R., Pignata, G., et al. 2007, *A&A*, 469, 645
- Stephenson, F. R., & Green, D. A. 2002, *Historical Supernovae and Their Remnants*, (Oxford: Clarendon Press)
- Stritzinger, M., Mazzali, P. A., Sollerman, J., & Benetti, S. 2006, *A&A*, 460, 793
- Strolger, L.-G., Smith, R. C., Suntzeff, N. B., Phillips, M. M., Aldering, G., et al. 2002, *AJ*, 124, 2905
- Sullivan, M., Ellis, R. S., Aldering, G., Amanullah, R., Astier, P., et al. 2003, *MNRAS*, 340, 1057
- Sullivan, M., Le Borgne, D., Pritchett, C. J., Hodsman, A., Neill, J. D., et al. 2006, *ApJ*, 648, 868
- Sullivan, M., Conley, A., Howell, D. A., Neill, J. D., Astier, P., et al. 2010, *MNRAS*, 406, 782
- Tanaka, M., Mazzali, P. A., Benetti, S., Nomoto, K., Elias-Rosa, N., et al. 2008, *ApJ*, 677, 448
- Tanaka, M., Kawabata, K. S., Yamanaka, M., Maeda, K., Hattori, T., et al. 2010, *ApJ*, 714, 1209

- Taubenberger, S., Hachinger, S., Pignata, G., Mazzali, P. A., Contreras, C., et al. 2008, MNRAS, 385, 75
- Taubenberger, S., Benetti, S., Childress, M., Pakmor, R., Hachinger, S., et al. 2011, MNRAS, 412, 2735
- Thomas, R. C., Aldering, G., Antilogus, P., Aragon, C., Bailey, S., et al. 2007, ApJ, 654, L53
- Turatto, M., Benetti, S., Cappellaro, E., Danziger, I. J., Della Valle, M., Gouiffes, C., Mazzali, P. A., & Patat, F. 1996, MNRAS, 283, 1
- Tutukov, A. V., & Yungelson, L. R. 1994, MNRAS, 268, 871
- Valentini, G., Di Carlo, E., Massi, F., Dolci, M., Arkharov, A. A., et al. 2003, ApJ, 595, 779
- van den Bergh, S., & Pazder, J. 1992, ApJ, 390, 34
- van Kerkwijk, M. H., Chang, P., & Justham, S. 2010, ApJ, 722, L157
- Wagers, A., Wang, L., & Asztalos, S. 2010, ApJ, 711, 711
- Wang, L., Wheeler, J. C., & Hoefflich, P. 1997a, ApJ, 476, L27
- Wang, L., Hoefflich, P., & Wheeler, J. C. 1997b, ApJ, 483, L29
- Wang, L., Baade, D., Höflich, P., Khokhlov, A., Wheeler, J. C., et al. 2003, ApJ, 591, 1110
- Wang, L., Strovink, M., Conley, A., Goldhaber, G., Kowalski, M., Perlmutter, S., & Siegrist, J. 2006, ApJ, 641, 50
- Wang, L., Baade, D., Höflich, P., Wheeler, J. C., Kawabata, K., Khokhlov, A., Nomoto, K., & Patat, F. 2006, ApJ, 653, 490

- Wang, L., Baade, D., & Patat, F. 2007, *Science*, 315, 212
- Wang, L., & Wheeler, J. C. 2008, *ARA&A*, 46, 433
- Wang, X., Wang, L., Zhou, X., Lou, Y.-Q., & Li, Z. 2005, *ApJ*, 620, L87
- Wang, X., Li, W., Filippenko, A. V., Krisciunas, K., Suntzeff, N. B., et al. 2008, *ApJ*, 675, 626
- Wang, X., Filippenko, A. V., Ganeshalingam, M., Li, W., Silverman, J. M., et al. 2009, *ApJ*, 699, L139
- Wang, Y. 2007, *ApJ*, 654, L123
- Wang, Y., Narayan, G., & Wood-Vasey, M. 2007, *MNRAS*, 382, 377
- Webbink, R. F. 1984, *ApJ*, 277, 355
- Wells, L. A., Phillips, M. M., Suntzeff, B., Heathcote, S. R., Hamuy, M., et al. 1994, *AJ*, 108, 2233
- Wheeler, J. C., & Harkness, R. P. 1986, in *NATO ASIC Proc. 180, Galaxy Distances and Deviations from Universal Expansion*, (Dordrecht: D. Reidel Publishing Co.), 45
- Wheeler, J. C., Harkness, R. P., Barker, E. S., Cochran, A. L., & Wills, D. 1987, *ApJ*, 313, L69
- Wheeler, J. C., & Harkness, R. P. 1990, *Reports on Progress in Physics*, 53, 1467
- Whelan, J., & Iben, I., Jr. 1973, *ApJ*, 186, 1007
- Whitney, C. A. 1983, *A&AS*, 51, 443
- Woosley, S. E., & Weaver, T. A. 1986, *ARA&A*, 24, 205

- Yamanaka, M., Kawabata, K. S., Kinugasa, K., Tanaka, M., Imada, A., et al. 2009, *ApJ*, 707, L118
- Yoon, S.-C., & Langer, N. 2005, *A&A*, 435, 967
- Yuan, F., Quimby, R. M., Wheeler, J. C., Vinkó, J., Chatzopoulos, E., et al. 2010, *ApJ*, 715, 1338
- Zwicky, F. 1965, in *Stellar Structure - Stars and Stellar Systems Vol. VIII*, ed. L. Hugh Aller & D. Benjamin (Chicago: University of Chicago Press), 367
- Zwicky, F., & Karpowicz, M. 1965, *AJ*, 70, 564

APPENDIX A

INTRODUCTION TO PCA AND ICA

A.1 Principal Components Analysis

Principal Components Analysis (PCA) is a statistical tool to characterize multidimensional data. PCA accomplishes this by transforming the data into a new, uncorrelated coordinate system. In order to make the appropriate transformation, PCA seeks to find correlations between measured variables. This also makes PCA an ideal tool for reducing the dimensionality of data without reducing their variation. The transformation matrix is calculated using the correlation matrix.

The original data can now be transformed into the new, uncorrelated variables by the linear transformation given in Equation A.1:

$$\vec{y} = \mathbb{P} \vec{x} \quad (\text{A.1})$$

Where \vec{x} is the series of variable values for one object expressed as a vector, \mathbb{P} is the transformation matrix, and \vec{y} is the data expressed in the new coordinate system, as values in the principal components. Or, to express it a little differently:

$$y_i = \sum_{j=0}^n p_{ij} x_j \quad (\text{A.2})$$

The resultant factor y_i is one of the principal components, and the principal component with the largest variance is called the first principal component (PC1).

To make sure that one parameter does not dominate the analysis due to a simple difference in magnitude, all the data are standardized. Standardization is a process where the data are first mean subtracted (giving a zero mean) and then normalized by the standard deviation giving a variance of 1. Now all the data is equally weighted regardless of the units being used. A covariance matrix, \mathbb{C}_x is then constructed for all the data vectors. It is the unit length eigenvectors of \mathbb{C}_x that become the weight vectors for each principal component and indicate the direction of each component. The eigenvalues of \mathbb{C}_x (d_1, d_2, \dots, d_n) are measures of the amount of variance characterized by each principal components. Which means that p_{1j} is the unit vector in the direction of the first principal component for all of the data vectors \vec{x} . An example of what this looks like in three dimensions is given in Figure A.1 showing the principal component of two spectral indexes and Δm_{15} from the data discussed earlier in the text.

The results of PCA can be used to reduce the dimensionality of the data. To do this only the necessary principal components, y_i , are used and Equation A.1 is solved for \vec{x} as in Equation A.3.

$$\vec{x}_j = \sum_{i=0}^m y_i p_{ji} \quad (\text{A.3})$$

where m is the total number of principal components used to reconstruct the data.

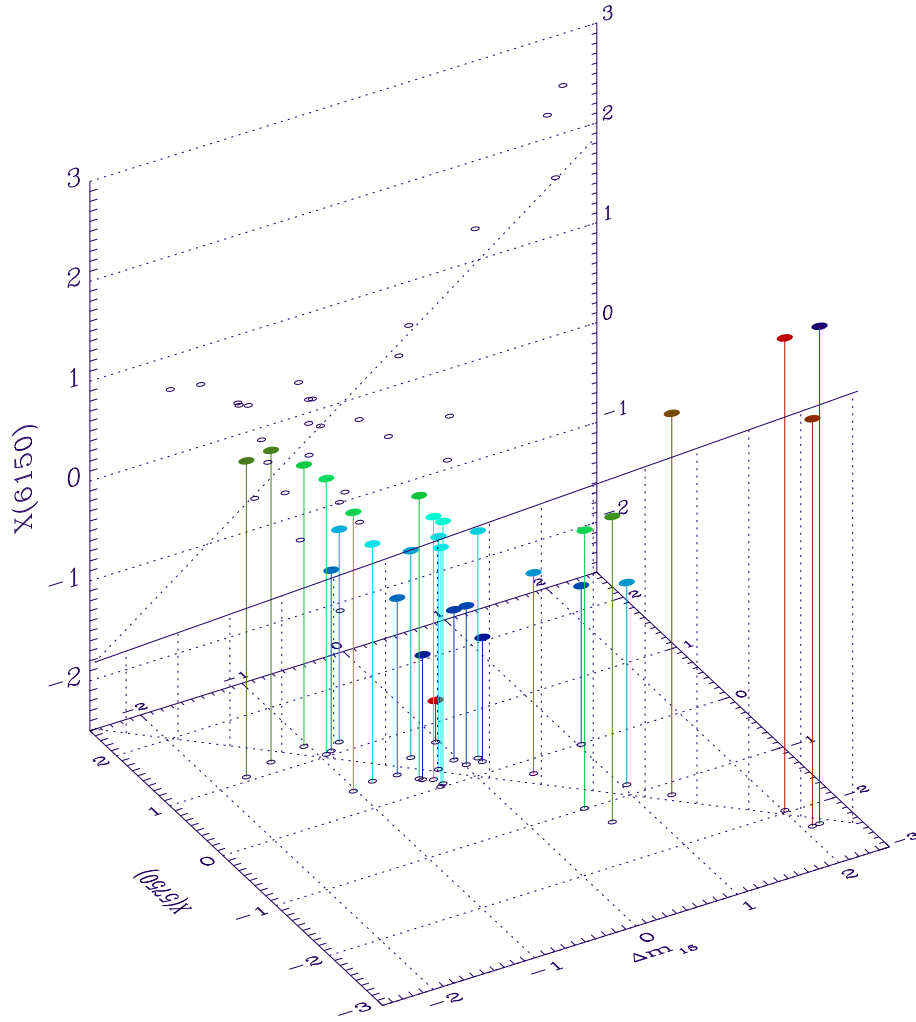


Fig. A.1. Here is an example of PCA being applied to three variables, Δm_{15} , X_{5750} , and X_{6150} . The first principal component clearly points along the direction of greatest variance.

For more detailed mathematical treatment of PCA see Hyvärinen, Karhunen, & Oja (2001), Mardia et al. (1979), and Murtagh & Heck (1987). For some applications to other astronomical data sets see Boroson & Green (1992), Francis et al. (1992), Francis & Wills (1999), Cormier & Davis (2011); Davis et al. (2007); James et al. (2006), Mittaz et al. (1990), Whitney (1983).

VITA

Permanent Address

Andrew J. Wagers
Cedarville University
Department of Science & Mathematics
251 N. Main St
Cedarville, OH 45314

Education

- B.A. Physics, Berea College, September 2002.
- M.S. Physics, Stephen F. Austin State University, August 2005.
- Ph.D. Physics, Texas A& M University, August 2012.

Employment

- Assistant Professor of Physics, Cedarville University, Cedarville, OH, 2011 - present.
- Part-time Professor of Physics, Blinn College, Bryan, TX, Spring 2007.

Publications

- Wagers, A. J., Wang, L., & Asztalos, S., 2010, Quantifying Spectral Features of Type Ia Supernovae, *Astrophysical Journal*, 711, 711-730